Alexey Koshkin

Bachelor Degree in Mathematics

Application of metabolic systems biology to the production of cell- and virus-based therapeutics

Dissertation to obtain Master Degree in
Biochemistry

Supervisors:
Dr. Ana Margarida Palma Teixeira,
IBET/ITQB-NOVA
Dr. Maria Margarida de Carvalho Negrão Serra,
IBET/ITQB-NOVA

Jury:
Presidente: Prof. Dr. Carlos Alberto Gomes Salgueiro
Examiner: Prof. Dr. Moritz von Stosch
Supervisor: Prof. Dr. Ana Margarida Palma Teixeira

November, 2015

FACULDADE DE
CIÊNCIAS E TECNOLOGIA
UNIVERSIDADE NOVA DE LISBOA

Alexey Koshkin

Bachelor Degree in Mathematics

Application of metabolic systems biology to the production of cell- and virus-based therapeutics

Dissertation to obtain Master Degree in
Biochemistry

Supervisors:
Dr. Ana Margarida Palma Teixeira,
IBET/ITQB-NOVA
Dr. Maria Margarida de Carvalho Negrão Serra,
IBET/ITQB-NOVA

Jury:
Presidente: Prof. Dr. Carlos Alberto Gomes Salgueiro
Examiner: Prof. Dr. Moritz von Stosch
Supervisor: Prof. Dr. Ana Margarida Palma Teixeira

November, 2015

FACULDADE DE
CIÊNCIAS E TECNOLOGIA
UNIVERSIDADE NOVA DE LISBOA

Copyright

Application of metabolic systems biology to the production of cell- and virus-based therapeutics

Alexey Koshkin FCT-UNL

Acknowledgements

I would like to acknowledge all the people directly or indirectly involved in this thesis.

To Dr. Paula Alves, for giving me the opportunity to do my master thesis at the Animal Cell Technology Unit at ITQB/IBET, for the good working conditions offered and for being a strong example of leadership and professionalism.

To Dr. Ana Teixeira, for her professionalism, for inviting me to Animal Cell Technology Unit, for giving me a chance to apply my mathematical background to crucial branch of human knowledge – biology. Especially for the opportunity to do my master thesis in two exceptionally interesting fields: stem cell biology and adenoviruses.

To Dr. Margarida Serra, for warmly receiving me in stem cell lab. For her professionalism, kindness, encouragement, constant support and trust.

To Dr. Nuno Carinhas, for his professionalism and his knowledge of metabolism and matlab.

To Daniel Pais to friend, who showed me the interesting world of adenovirus, metabolomics, GC-MS, and especially for his positive mood and good companionship.

To Daniela Sequeira, for showing me traditional Portuguese food, juice, for let the "F = d(mv)/dt" and for being a good friend during this year.

To Dr. Mada Carido, for being my company on coffee break every morning. For her sense of humor, support and for being a good friend.

To Marcos, for his constant good mood. To Ricardo, for the good music and companionship on weekends. To Ana Margarida, for being a friend and for her interest in GC-MS, even during the summer. To all stem lab folks. To Bàrbara, for showing me what is downstream. To all my friends and colleagues in TCA, for the good working environment, friendship, interesting discussion topics and good mood.

To professor Pedro Tavares, Alice Pereira and Ricardo Franco.

Especialmente, quero agradecer, à Cláudia Correia, quem me ensinou quase tudo que conheço sobre stem. Por ser uma bom amiga. Por me sempre dar força, motivação, e por me sempre ajudar a estar animado. Obrigado por apoio e confiança em mim. Esta tese não podia ter sido feita sem ti.

Queria agradecer meus pais. Por toda a apoio, por sempre me ajudar e acreditarem em mim. Хотел воспользоваться этой возможностью для того, чтобы искренне поблагодарить Вас за всё тепло и заботу. За то что помогли мне добиться всего в этой жизни. Этот тезис такой же Ваш как и мой. Спасибо.

À minha Família
e
À minha M

Preface

The current master thesis was performed at the Animal Cell Technology Unit (ACTU), IBET / ITQB-NOVA, within the scope of the projects "Probing adenovirus-host cell interactions: a systems biotechnology approach to improve production of gene delivery vectors" (Ref. PTDC/EBB-BIO/119501/2010, funded by Fundação para a Ciência e a Tecnologia (FCT)), "CAREMI - Cardio Repair European Multidisciplinary Initiative" (Ref. HEALTH-F5-2010-242038, funded by the European Union) and "CARDIOSTEM-Engineered cardiac tissues and stem cell-based therapies for cardiovascular applications" (Ref. MITP-TB/ECE/0013/2013, funded by FCT).

Part of the work of this thesis has been submitted for publication and presented as oral and poster communications at national and international conferences.

Submitted Articles:

- Nuno Carinhas[#], Daniel AM Pais[#], Alexey Koshkin, Paulo Fernandes, Ana S Coroadinha, Manuel JT Carrondo, Paula M Alves, Ana P Teixeira. "Parallel 13C labeling and isotopic nonstationary metabolic flux analysis of MDCK cells during growth and canine adenovirus vector production" (submitted to Biotechnology and Bioengineering, October, 2015)
- Cláudia Correia, Madalena Carido, Alexey Koshkin, Nuno Espinha, Tomo Saric, Pedro A. Lima, Margarida Serra, Paula M. Alves. "Effective Hypothermic storage of human pluripotent stem cell derived cardiomyocytes compatible with global distribution of cells for clinical applications and toxicology testing" (submitted to STEM CELLS Translational Medicine, September, 2015)

Oral Presentation:

- Cláudia Correia, Alexey Koshkin, Madalena Carido, Marcos Sousa, Ana Teixeira, Margarida Serra, Paula M Alves. Integrated strategies for the production, maturation and storage of functional cardiomyocytes derived from human pluripotent stem cells. 9th International Meeting of the Portuguese Society for Stem Cells and Cell therapies, October 2015. Oeiras, Portugal.

Poster Presentations:

- Daniel AM Pais, Alexey Koshkin, Paulo Fernandes, Carina Silva, Ana S Coroadinha, Paula M Alves, Ana P Teixeira. Studying the impact of adenovirus infection on cell metabolism using 13C-labelled glucose and glutamine. ESACT 24th, June 2015. Barcelona, Spain.
- Cláudia Correia, Alexey Koshkin, Nuno Espinha, Madalena Carido, Marcos Sousa, Catarina Brito, Manuel Carrondo, Tomo Saric, Ana Teixeira, Margarida Serra, Paula M Alves. Integrated strategies

for the production and storage of functional cardiomyocytes derived from human pluripotent stem cells. ESACT 24th, June 2015. Barcelona, Spain.

- Cláudia Correia, Alexey Koshkin, Nuno Espinha, Madalena Carido, Marcos Sousa, Catarina Brito, Manuel Carrondo, Tomo Saric, Ana Teixeira, Margarida Serra, Paula M Alves. Integrated strategies for the production and storage of functional cardiomyocytes derived from human pluripotent stem cells. ISSCR Annual Meeting, June 2015. Stockholm, Sweden.

Abstract

The main aim of this thesis was to apply systems biology tools, namely metabolomics, ^{13}C-MFA and gene expression profiling, to study the production processes of two promising advanced-therapy medicinal products: i) adenovirus vectors (AdVs) for gene delivery and ii) human induced pluripotent stem cell-derived cardiomyocytes (hiPSC-CMs) for cardiac cell-based therapy.

To deliver improved yields of adenoviral vectors, deeper knowledge on how they manipulate the metabolic network of the host cell to supply energy and macromolecule components for their replication is needed. In this thesis, the metabolism of a human amniocyte-derived cell line (1G3) was studied in non-infected and AdV infected cultures through parallel labeling experiments with [1,2-^{13}C]glucose and [U-^{13}C]glutamine.^{13}C data revealed a greater percentage of labeled TCA cycle metabolites from glutamine, highlighting the anaplerotic role of this amino acid. Upon infection, glucose consumption and lactate production rates were significantly increased, as well as the majority of amino acid rates. Arresting cell growth before infection significantly lowered AdV replication compared to infection of exponentially growing cells, while triggering an even more pronounced stimulation of metabolism. These results portray a metabolic blueprint of human adenovirus infection and highlight the requirement of a favorable cellular environment for its replication.

Improved knowledge on the complex cellular metabolic programs involved in cardiomyogenesis and CM maturation is needed to bring hiPSC-CMs closer to the clinic/industry. The second part of the thesis focused on the identification of phenotypic, structural and metabolic alterations during CM differentiation and maturation, using different culture medium compositions. Our results show that the metabolism of early differentiated hiPSC-CMs do not significantly differ from hiPSC when cultured in glucose-rich medium, both relying on glycolysis. Nonetheless, hiPSC-CMs displayed metabolic plasticity being able to consume not only glucose but also lactate and fatty acids. Noteworthy, when cultured in glucose-depleted medium supplemented with fatty acids, hiPSC-CMs showed a more mature structure and gene expression profiles and used fatty acid as energy source, a typical feature of adult CMs.

Collectively, the generated knowledge may be applied for bioprocess optimization of AdV production and for improving CM differentiation and maturation processes.

Key Words: System biology, metabolomics, metabolic flux analysis, adenovirus vector, viral infection, human induced pluripotent stem cells, human induced pluripotent stem cells derived cardiomyocytes, cardiomyocyte differentiation, human cardiomyocyte maturation.

Resumo

O principal objectivo desta tese consistiu na utilização de ferramentas de biologia dos sistemas, tais como metabolómica, ^{13}C-MFA e perfil de expressão génica para estudar os processos de produção de dois produtos com relevância terapêutica: i) vectores de adenovírus (ADVS) para entrega de genes em terapia génica e ii) cardiomiócitos derivados de células estaminais pluripotentes humanas induzidas (hiPSC-CM) para aplicação em terapia celular cardíaca.

De modo a melhorar os rendimentos da produção de vectores adenovirais é necessário aprofundar o conhecimento sobre o modo como estes vectores manipulam a rede metabólica da célula hospedeira para obter energia e macromoléculas necessárias para sua replicação. Nesta tese, o metabolismo de uma linha celular humana derivada de amniócitos (1G3) foi estudado em culturas não-infectadas e infectados por AdV, usando experiências paralelas com dois substratos marcados: [1,2-^{13}C]glucose e [U-^{13}C]glutamine. Estas experiências demonstraram que a glutamina apresenta uma maior contribuição na formação de intermediários do TCA em comparação com a glucose, destacando assim o papel anaplerotic da glutamina. Após a infecção, as taxas de consumo de glucose e produção de lactato aumentaram significativamente/consideravelmente, assim como as taxas de consumo da maioria dos aminoácidos. A paragem no crescimento celular antes da infecção reduziu consideravelmente a replicação de AdV em comparação com a infecção das células em crescimento exponencial e provocou uma estimulação mais pronunciada do metabolismo. A combinação destes resultados originou um modelo metabólico de infecção por adenovírus humano que evidencia as condições de um ambiente celular mais favorável para a sua replicação.

Um conhecimento mais aprofundado sobre os mapas metabólicos envolvidos na diferenciação de hiPSCs em CMs bem como na maturação dos hiPSC-CMs produzidos é essencial para acelerar a utilização de hiPSC-CMs na clinica e industria. A segunda parte da tese focou-se na caracterização fenotipica, estrutural e metabólica durante o processo de diferenciação em CMs assim como durante a maturação dos hiPSC-CMs quando cultivados em meios com composições distintas. Os nossos resultados demostraram que o metabolismo dos hiPSC-CMs, logo após o processo de diferenciação, e depois de 20 dias em cultura em meio rico em glucose, não é significativamente diferente do metabolismo das hiPSCs, apresentando um metabolismo preferencialmente glicolitico. No entanto, foi demonstrado que os hiPSC-CMs apresentam plasticidade metabólica sendo capazes de consumir não apenas glucose, mas também outros substratos, nomeadamente ácidos gordos e lactato. De notar que quando cultivados em meio sem glucose suplementado com ácidos gordos, os hiPSC-CMs apresentaram uma estrutura, perfil de expressão genética e metabolismo mais próximo de CMs adultos.

Coletivamente, o conhecimento gerado pode ser aplicado para a otimização de bioprocessos de produção AdV e para a melhoria dos processos de diferenciação e maturação CM.

Abbreviation list

ACL ATP citrate lyase
ACTC1 encodes cardiac muscle alpha actin.
Ad2 adenovirus type 2
Ad5 adenovirus type5
AKG alpha-ketoglutarate
AKGDH aKG dehydrogenase
ALT alanine aminotransferase
BMC bone marrow-derived cells
BMP bone morphogenic protein
Bry T T brachyury transcription factor
BSA bovine serum albumin
CACNA1C gene encoding Calcium channel, voltage-dependent, L type, alpha 1C subunit protein
CAR coxscackie and adenovirus receptor
CHD coronary heart diseases
CMs cardiomyocytes
c-Myc Myc
CPC cardiac progenitor cells
CVD cardiovascular diseases
DKK1 dickkopf homolog 1
DMEM Dulbecco modified Eagle medium
DMSO Dimythyl sulfoxide
EDP Entner-Doudoroff pathway
EMP Embden-Meyrhof-Parnas
EMU elementary metabolic unit
FBS fetal bovine serum
FGF fibroblast growth factors
FSG fish skin gelatin
G6P glucose-6-phosphate
GAPDH Glyceraldehyde-3-Phosphate Dehydrogenase
GATA4 Transcription factor GATA-4
GC-MS Gas chromatography–mass spectrometry
GDH glutamate dehydrogenase
GFP green fluorescent protein
GLUT1 Glucose transporter 1
GLUT3 Glucose transporter 3
hCMs human cardiomyocytes
HCN4 hyperpolarization activated cyclic nucleotide-gated potassium channel 4
hESCs human embryonic stem cells
hESC-CMs human emrionic pluripotent stem cell derived cariomyocytes
hiPSCs human induced pluripotent stem cells
hiPSC-CMs human induced pluripotent stem cell derived cardiomyocytes
ICM inner cell mass
IDH isocitrate dehydrogenase
IgG immunoglobulin G
IgM immunoglobulin G
ISL-1 Insulin gene enhancer protein ISL-1
ITRs inverted terminal repeat

IWR inhibitors of Wnt response
KDR Kinase insert domain receptor
KLF 4 Kruppel-like factor 4
LDH lactate dehydrogenase
Lin28 Lin-28 homolog A
MDH malate dehydrogenase
MEF mouse embryonic fibroblast
MFA metabolic flux analysis
MI myocardial infraction
MLP major late promoter
MSCs mesenchymal stem cells
MYH6 gene encoding myosin heavy chain, α isoform protein
MYH7 myosin, heavy chain 7
MYL2 myosin light chain 2 (myosin regulatory light chain 2, ventricular/cardiac muscle isoform)
MYL7 myosin regulatory light chain 2 (myosin regulatory light chain 2, atrial isoform (MLC2a))
NANOG transcription factor critically involved with self-renewal of undifferentiated embryonic stem cells
NKX-2.5 Homeobox protein Nkx-2.5
NMR Nuclear magnetic resonance
NPC nuclear pore complex
Oct4 transcription factor octamer 4
OXPHOS oxidative phosphorylation
PC pyruvate carboxylase
PDGFRα platelet-derived growth factor receptor α
PDH pyruvate dehydrogenase
PFA paraformaldehyde
PK pyruvate kinase
PPP pentose phosphate pathway
R5P ribose-5-phosphate
RCA replication complement adenovirus
ROS reactive oxygen species
RT-qPCR real time-quantitative polymerase chain reaction
SIRPα/β signal-regulatory protein alpha/betta
SMs skeletal myoblast
Sox2 SRY (sex determining region Y)-box 2
SSEA-1 stage-specific embryonic antigen-1
SSEA-4 stage-specific embryonic antigen-4
TCA citric acid cycle
TGF-β transcription growth factor β
TNNT2 Cardiac muscle troponin T
TRA-1-60 the human embryonal carcinoma marker antigen
TP terminal protein
VCAM1 vascular cell adhesion molecule 1
VEGF vascular endothelial growth factor
WNT Wnt signaling pathways

Contents

List of Figures

List of Tables

1. INTRODUCTION

There is significant pressure to bring the next generation of cell culture-derived therapies (virus- and stem cell-based products) to market at lower costs. The "black-box" approach currently prevailing during early stage development of cell culture-based products can be reduced in the era of omics technologies. More efficient production requires deeper understanding of cellular metabolism and its regulation, which provides the building blocks and energy for cell growth and virus production, and is known to play a pivotal role in dictating cell fate with key metabolic pathways differently activated in stem cells as compared to restricted progenitor and differentiated cells. A metabolic systems biology approach was pursued in this thesis to gain insights on the production processes of two biomedical relevant products: i) replication of adenoviral vectors in human cell lines, with applications on gene therapy and vaccination and ii) cardiomyocytes differentiation from pluripotent stem cells.

1.1 Metabolism and metabolic flux analysis

1.1.1 Metabolism

Metabolism (from the Greek μεταβολή, i.e., transition, transformation) is the sum of all chemical processes occurring within living cells and organisms, and consists of two main types of reactions, catabolic and anabolic. Catabolic reactions involve the breaking down of organic substrates (metabolites) by their oxidation to provide energy (e.g. ATP) (de Bolster, 1997a). Anabolism is the process of synthesizing macromolecules from low molecular weight precursors using the energy generated in catabolism (de Bolster, 1997b).

Most metabolic studies involving estimation of fluxes in different cells and culture conditions are focused on central carbon metabolism, i.e. glycolysis, tricarboxylic acids (TCA) cycle, oxidative phosphorylation (OXPHOS), pentose phosphate pathway (PPP) and amino acids metabolism (Figure 1.1) (Vacanti and Metallo, 2013). Glycolysis is a series of reactions that catabolize one glucose molecule into two molecules of pyruvate or lactate, generating ATP. The TCA (or Krebs) cycle is a set of oxidation, decarboxlation, isomerization and condensation reactions that take place in the mitochondria with the purpose of energy generation in the form of reducing equivalents (NADH, $FADH_2$), while releasing CO_2. OXPHOS is a set of electron transport reactions occurring in the inner mitochondrial membrane that generate a proton gradient that is channeled to produce ATP by phosphorylation of ADP in the presence of O_2. The proton donors for the gradient formation are the NADH and $FADH_2$ moieties generated in the TCA cycle and potentially glycolysis. PPP converts glycolytic intermediates (glucose-6-phosphate (G6P)) into pentose phosphates that are used as precursors for nucleotide synthesis, while simultaneously generating NADPH, a form of reducing power used in anabolic processes.

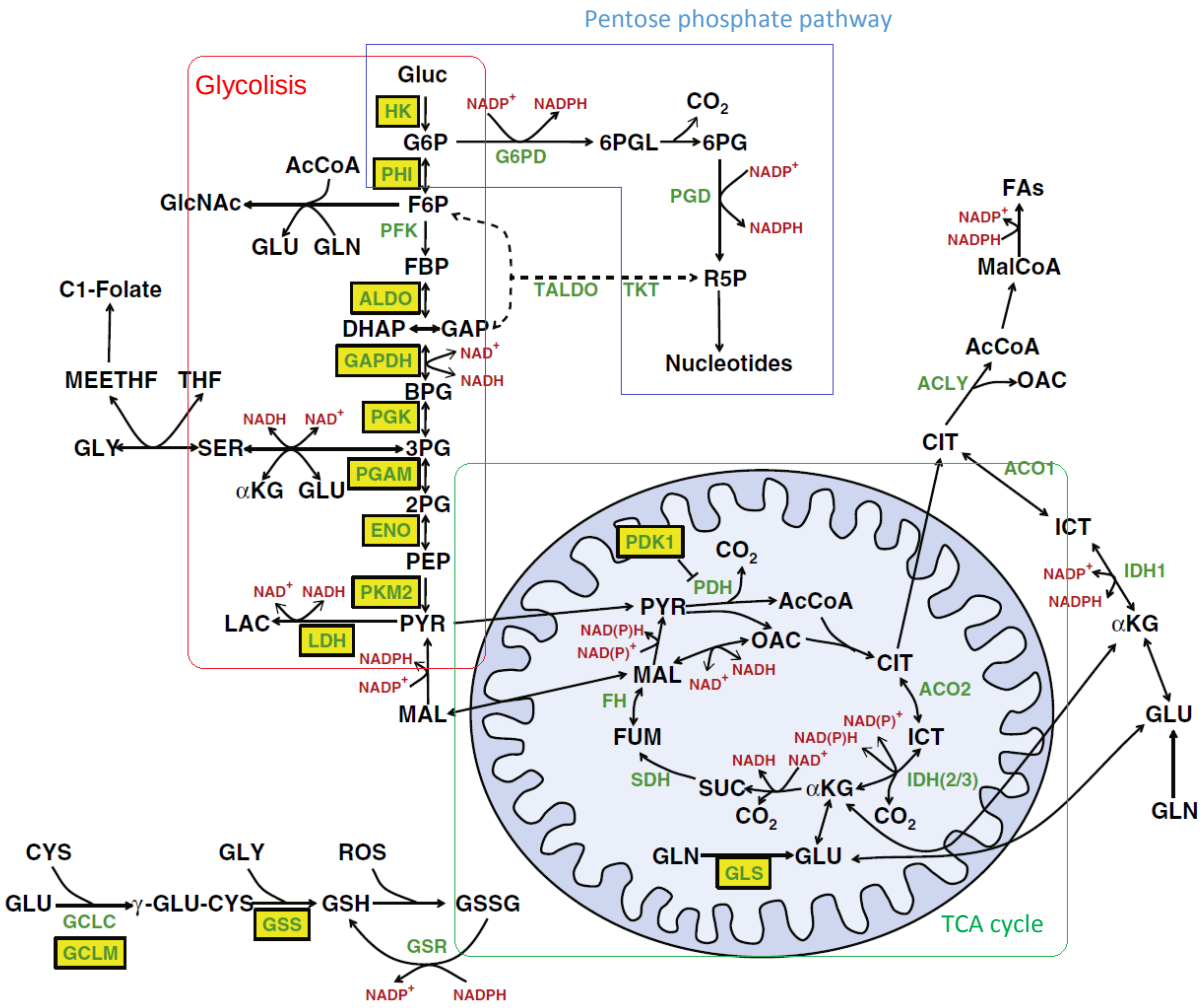

Figure 1.1: Map of central metabolic pathways occurring in mammalian cells (adapted from (Vacanti and Metallo, 2013)).

1.1.2 Metabolomics, isotopic studies and metabolic flux analysis (MFA)

The metabolites involved in biochemical reactions and processes can be identified and quantified using new metabolomic technologies (Smith et al., 2006; Sreekumar et al., 2009). Analysis of the metabolome, the complete set of small-molecule chemicals, can provide information on the metabolic flux distributions occurring in the cell, which by turn are a function of gene expression, protein modifications and interactions at different levels (Nielsen, 2003; Nöh and Wiechert, 2011). Comparing with regulatory networks composed of protein-DNA and protein-protein interactions, where there are still many unknown components, metabolic networks consisting of all metabolic reactions occurring in cellular metabolism can be described and predicted using mathematical models (Price et al., 2003). However, accurate estimation of metabolic fluxes can only be presently achieved in representative networks of central metabolism using a combination of computational, intra-metobolomic (intracellular metabolites) and extra-metabolomic (extracellular metabolites, that is, present in the cell culture medium) techniques, including isotopic tracing studies (using

substrate molecules in which one or more of the atoms is replaced by a different isotope) (Kelleher, 2004; Oldiges et al., 2007).

Isotopic tracers have been used since the inception of metabolism investigation in the 20th century. These were firstly radioactive species (e.g. ^{14}C, ^{3}H) administered to cells in small quantities followed by the measurement of radioactivity in end products and other metabolites (Gibbs et al., 1954; Kelleher, 2001). The use of parallel radioisotope experiments allowed the determination of structures, precursors and activities of pathways such as PPP, TCA cycle, anaplerosis, gluconeogenesis and fatty acid metabolism (Table 1.1).

Table 1.1: Radioisotope studies with parallel labeling experiments. Notes: [1]gluc denotes[1-14C]gluc, unless stated otherwise. The semicolon‘‘;’’ denotes parallel experiments (Crown and Antoniewicz, 2013).

Organism	Tracers	Measurements	Major achievements
Rat liver slices	[1]ac; [2]ac	Gluc, $^{14}CO_2$ activity	Quantified isotopic dilution in TCA cycle
Rat liver	[1]r5p; [2,3]p5p	Activity of h6p carbons	Determined structure of non-oxPPP
Yeast	[1]; [2]; [6]; [U]gluc	$^{14}CO_2$ activity	Estimated oxPPP, EMP and pyruvate fixation fluxes
n/a	[2]; [3]gluc	Activity of h6p carbons	Accounted for h6p recycling in estimation of oxPPP
Rat liver slices	[1]; [2]prop; [1]; [2]pyr; bicarb	Gluc, glycogen, FA, lact, $^{14}CO_2$ activities	Elucidated pyruvate and propionate conversion to glucose and label shuffling in TCA cycle
Rat adipose tissue	[1]; [6]gluc	Lipid, $^{14}CO_2$ activities	Evaluated methods for oxPPP estimation
Tissue slices	[1]; [6]gluc; [1]; [6]fruc	Glycerol, $^{14}CO_2$ yields	Estimated oxPPP flux and hexose isomerization
Isolated rat liver	[2]; [5]glu	Gluc, $^{14}CO_2$, FA, glycogen activities	Identified metabolism of akg to citrate via reductive carboxylation
Rat liver	[1]; [2]ac; [1]; [16]palm; [18]stear; [10]ole	Activity of glycogen carbons	Examined relative contribution of α, β, and ω-oxidation of FA
Rat adipose tissue	[1]; [2]; [3]pyr; bicarb	Glycogen, glyc, FA, lact, $^{14}CO_2$ activities	Probed pyruvate metabolism and glyceroneogenesis
Rat adipose tissue	[1-^{3}H,^{14}C]; [2-^{3}H,^{14}C]; [3-^{3}H,^{14}C]; [6-^{3}H,^{14}C]gluc	^{3}H in gluc, H_2O; ^{3}H:^{14}C ratio in FA, glyc, lact	Investigated isotope discrimination and H-exchange by isomerization reactions
Kidney cortex slices	[2]; [3]lact; [2]; [3]pyr	Activity of gluc, lact, ala, glu carbons	Estimated TCA cycle and gluconeogenesis fluxes
Tetrahymena	Gluc, fruc, ribose, glyc tracers	Glycogen, glyc, RNA, $^{14}CO_2$ activities	Estimated glycolysis and PPP fluxes
Rat liver	[1]; [2]lact; [1]; [2]pyr; [1]oct; bicarb	Activity of carbons, fragments and molecules	Extensive study on various gluconeogenic precursors
Rat liver and kidney	Variety of palm tracers	Activity of hydroxy-butyric acid carbons	Probed multiple pathways for acetoacetate formation
Rat liver	[1,4]; [2,3]succinate	$^{14}CO_2$ yields	Determined pyruvate carboxylation/decarboxylation fluxes into TCA cycle

More recently, advances in stable isotope (e.g. ^{13}C, ^{2}H, ^{15}N) measurement through nuclear magnetic resonance (NMR) and mass spectrometry (MS) have replaced the use of radioactive isotopes in metabolic studies, owing to easier experimental implementation and greater information generated (Bier, 1987) (Table 1.2). Stable isotope experiments, when combined with metabolic flux analysis (MFA), allow the greatest quantitative resolution of metabolic flux distributions in cultured cells. MFA relies on an “inverse problem” in which fluxes are calculated by fitting measured metabolite labeling distributions while being constrained by the material balances around a metabolic network. Both mammalian and bacterial cells have a complex

metabolic network described by high dimensional system of differential equations; thus, fitting of simulated data requires significant computational power, which until has hindered the application of these tools. Fortunately, increasing computational resources combined with algorithms for metabolic network decomposition, namely the elementary metabolic unit (EMU) method (Antoniewicz et al., 2007), have allowed deeper characterization of cellular metabolism in different biological systems and under different conditions.

Table 1.2: Stable-isotope studies with parallel labeling experiments. Notes: [1]gluc denotes [1-13C]gluc, unless stated otherwise. A semicolon ‘‘;’’denotes parallel experiments, and plus-sign ‘‘þ’’ denotes multiple tracers used in a single experiment; int-intracellular; ext-extracellular (Crown and Antoniewicz, 2013).

Organism	Tracers	Measurements	Major achievements
Isolated rat hepatocytes	$^{15}NH_4^+$; [5–^{15}N]gln	MS - uracil	Related mass isotopomers to precursor enrichments and pyrimidine biosynthesis
Rat hearts	[3]pyr; [2]ac; [2]ac+[3]prop; [1,2]ac+[3]pyr	NMR - glutamate	Analyzed ^{13}C-NMR spectra and modeled flux of TCA cycle
3T3-L1 adipocytes	[1]ac; [1,2]acac	MS - fatty acids	First ISA study on fatty acid synthesis
Hep-G2	[1]ac; [U]acac; [4,5]MVA; [1,2,3,4]oct	MS - cholesterol	Examined cholesterol synthesis as a polymerization of MVA precursors
Sprague-Dawley rats	[3]; [1]lact; [2]glyc; [6-^{3}H]gluc	MS - glucose	First MIDA study on gluconeogenesis pathway
Rat hearts	[1]oct; [U]lact+[U]pyr; [1]oct+[U]lact+[U]pyr; [U]glu; [U]ac	MS - citrate and its fragments	Estimated relative rates of PC/PDH/CS/FA oxidation
C. glutamicum	[1]gluc; 40% [U]gluc	MS - ext. ala, lys, trehalose	Performed ^{13}C-MFA using parallel data sets and ratios of M+*x*/M+0 isotopomers
E. coli	[1]gluc; 20% [U]gluc	MS - biomass AA	Developed metabolic flux ratio analysis (MetaFor)
E. coli	[1]gluc; 20% [U]gluc	MS - biomass AA	Demonstrated improved flux observability with PLE's
C. glutamicum	[1]gluc; 50% [U]gluc or fruc	MS - ext. lys, trehalose	^{13}C-MFA with only external metabolite measurements
Brown adipocytes	[U]gluc; [U]gln; [U]ac; [U]acac	MS - fatty acids	Utilized ISA to quantify carbon sources for *de novo* lipogenesis
Various bacteria	[1]gluc; 20% [U]gluc	MS - biomass AA	Quantified glucose metabolism via EMP/ED/oxPPP in several bacteria using MetaFor
B. napus	[1,2]gluc+[U]gluc; [U]ala; 50% [U]gln	MS - biomass AA, FA, gluc, glyc	Integrated ^{13}C-MFA: utilized [^{15}N]-tracers to assess protein synthesis and turnover
Isolated hepatocytes	[$^2H_5$]glyc; [U]glyc; ^2H_2O	MS - glucose	Integrated ^{13}C-MFA: quantified net and reversible fluxes in gluconeogenesis pathway
C. glutamicum	[1]; [6]; [1,6]gluc	MS - CO_2	^{13}C-MFA with CO_2 as the only labeling measurement
Maize root tips	[1]; [2]gluc	NMR - int. sugars, AA	Integrated ^{13}C-MFA: estimated fluxes from ^{13}C-enrichments
Soybean seedlings	[U]gluc; [U]gln	MS - biomass AA, int. sugars, organic acids	Integrated ^{13}C-MFA: utilized two labeled substrates to improve flux resolution
D. ethenogenes	[1]; [2]ac; bicarb	MS - biomass AA	Elucidated pathways for ile, leu, thr biosynthesis, and identified *Re*-CS
C. acetobutylicum	[U]gluc; [U]glu; [U]asp; others	MS - int. metabolites	Demonstrated bifurcated TCA cycle and identified *Re*-CS
P. falciparum	[U]gluc; [*U*-^{13}C,^{15}N]asp; [*U*-^{13}C,^{15}N]gln	MS - int. metabolites	Demonstrated bifurcation of TCA cycle and reductive carboxylation
HEK-293	[1]; [6]; [U]gluc; [U]gln	MS - ext. lactate	^{13}C-MFA with lactate as the only labeling measurement
E. coli	20, 40, 60, 80, 100% [U]gluc	MS - biomass AA	Integrated ^{13}C-MFA: identified exchange of CO_2 and validated *E. coli* model for ^{13}C-MFA

1.2 Gene therapy

Gene therapy can be defined as the transfer of nucleic acid to the somatic cells of a patient with resulting therapeutic effect (Ylä-Herttuala S, 2003). It is based on the modification of the genetic material of living

cells, by correcting genetic defects or overexpressing therapeutic proteins and is able to modify the biology and phenotype of target cells, tissues and organs (Coura and Nardi, 2008). Gene therapy is a promising method to cure a number of diseases, such as cancer, autoimmune disorders, cardiovascular and infection diseases (Bouard et al., 2009).

There are two ways of therapeutic gene introduction intro the target cells: *ex vivo* or *in vivo*. The *ex vivo* method consists in removal of target cells from a patient, their transduction with a viral vector and further re-introduction into the patient. This technique limits the cellular target population to be transduced thus increasing vector concentration and minimizing immunogenic responses. Advantages of the *ex vivo* approach include a higher efficiency of gene transfer and the possibility of cell propagation *in vitro*, thus generating a higher cell dose. However, this method is limited by high costs of manufacturing, quality-control difficulties and low number of target cell types and diseases (Aiuti et al., 2002; Bouard et al., 2009; Räty et al., 2008). Alternatively, *in vivo* gene therapy is based on delivering the selected gene directly into target cells in the patient. This approach is less expensive but the major challenge is lack of efficient, non-toxic gene delivery systems capable of transducing only the target cells in the whole organism (Bouard et al., 2009).

Despite recently successful gene therapy applications in clinical trials, further understanding of the molecular basis of how viruses and viral vectors interact and influence the host cells are urgently required (Bouard et al., 2009; Räty et al., 2008).

1.2.1 Vectors for gene therapy

There are two main types of gene-delivery vectors: viral and non-viral. Viruses are highly evolved biological machines that efficiently gain access to host cells and exploit the cellular machinery for their needs, thus being effective candidates for usage as vector for gene therapy (Räty et al., 2008). Viral vectors have also disadvantages, such as limitation on the size of the therapeutic gene inserted in the viral DNA, possible immunological responses by the patient's organism, and difficulties in viral vector production and purification. On the other hand, non-viral vectors (DNA, liposomes, cationic lipids, etc) avoid to a great extent these limitations, but have demonstrated an extremely low efficiency, and hence have not enjoyed widespread use.

Five classes of viral vectors are used today for clinical application: retroviruses, lentiviruses, adenoviruses, adeno-associated viruses (AAVs) and herpes simplex-1 virus (HSV-1s) (Thomas et al., 2003). Advantages and disadvantages of each class as a viral vector delivery system are summarized in Table 1.3. Depending on the purpose, different viral vectors are preferable. However, currently, adenoviruses are the dominant gene delivery system used for gene therapy.

As an example, the first gene therapy products to be developed (SiBiono GeneTech's Gendicine™ in 2003 and Sunway Biotech´s Oncorine™ in 2006) were based on adenoviral vectors (J.K. Raty, J.T . Pikkarainen, 2008).

Table 1.3: Principal deliverly vectors, advantage and limitations. (adapted (Bouard et al., 2009; J.K. Raty, J.T . Pikkarainen, 2008; Thomas et al., 2003)

Vector	Advantages	Limitations
Non-viral vectors	1) Easy preparation 2) Non-pathogenic	1) Limited transduction 2) Bacterial contaminants
Non-enveloped		
Adenovirus	1) High efficiency 2) Transduces quiescent and dividing cells 3) More than 30 kb transgene capacity 4) Easy to produce in high titers	1) Coxsackie adenovirus receptor-dependent transduction 2) Immunogenic 3) Existing humoral response to certain serotypes
Adenoassociated virus (AAV)	1) Tranduces quiescent and dividing cells 2) Very long expression time 3) Non-pathogenic, low immunogenicity 4) Broad tropism	1) Very small transgene capacity 2) Insertional mutagenesis may be a problem
Enveloped		
Retrovirus	1) Persistent gene transfer in dividing cells	1) Only transduces in dividing cells; 2) integration might induce oncogenesis on some application
Lentivirus	1) Low immunogenicity 2) Stable integration to quiescent cells	1) Insertional mutagenesis 2) Potential risk of recombination of pathogenic vector (HIV)
Herpes simplex-1 virus HSV-1	1) Large packaging capacity 2) Strong tropism for neurons	1) Inflammatory; 2) Transient transgene expression in cells other that neurons

1.2.2 Adenoviruses

Adenoviruses are pathogenic, non-enveloped, double-stranded DNA viruses, capable of infecting a wide range of mammalian species, including monkeys, mice, birds and humans (Chen et al., 2011), and can infect the majority of cells, including post-mitotic cells, skeletal muscle, lung, brain and heart (Russell, 2000). In humans, they can induce infection in the eye (acute conjunctivitis) (Jawetz, 1959), in membranes of the respiratory track, intestines or urinary tract. Cytopathic effects in cell cultures derived from human adenoids were firstly observed in 1953 by Rowe and colleagues (Rowe et al., 1953). There have been identified over 50 serotypes, divided into six species (A-F) based on their capacity to agglutinate erythrocytes(Walker and Ditor, 2004). Two serotypes, Ad2 and Ad5, belonging to subgroup C, are the most common used in clinical trials due to low occurrence of severe pathologies in human (Parks et al., 1999) and to the absence of integration into the host cell genome, decreasing the risk of mutagenesis (Gómez-Navarro and Curiel, 2000). The adenovirus genome is well studied and comparatively easily to manipulate (Tatsis and Ertl, 2004). Thus, adenovirus vectors are an attractive tool to study cellular responses to viral infection in parallel to their use for gene delivery and gene therapy (Tatsis and Ertl, 2004).

1.2.3 Viral particles structure

X-ray crystallography and cryoelectron microscopy image reconstruction have provided knowledge the structural composition of adenovirus icosahedral particles. The three principal proteins of the icosahedral capsid are: hexon, penton base and fibre (Figure 1.2). The capsid is covered by 240 hexons and 12 vertices, each comprise one penton base, with one fiber on it (Russell, 2009). In addition, adenoviruses are composed by other structural proteins: 7 proteins are present on the capsid (II, III, IIIa, IV, VI, VIII, IX) and 4 additional proteins are packaged with the linear double-stranded DNA in the core of the viral particle (V, VII, mu and terminal protein).

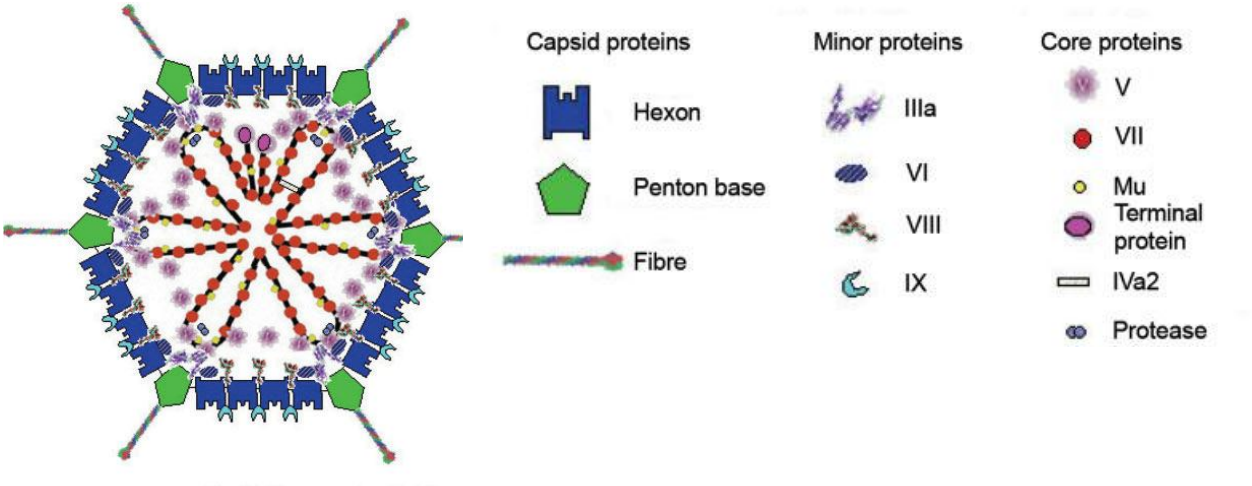

Figure 1.2: Structure of adenovirus. The location of the capsid and minor components are reasonably well defined and are not to scale (adapted from (Russell, 2009))

1.2.4 Viral genome and adenovirus vectors

The adenovirus genome is comprised of a double-stranded, linear DNA molecule with a terminal protein (TP) attached covalently to its 5´termini, which have inverted terminal repeats (ITRs) (Rekosh, 1977). Adenovirus genes can be divided in two groups according to its expression chronology: early (E) and late (L) genes (Figure 1.3). There are eight units for RNA polymerase II-mediated transcription. Early transcriptional units, E1 (E1A, E1B), E2 (E2A, E2B), E3, E4 and E5, are expressed before viral replication. The first region of transcription is E1, producing the protein E1A which changes the host cell's metabolism and genetic expression, facilitating transcription of the viral genome. E1 deregulates cell-cycle control by increasing the stability of p53 and promotes apoptosis through p53-dependent and independent mechanism. However, induction of cellular apoptosis can negatively affect virus replication, so adenovirus should have mechanism to decrease p53 activity. Protein E1B cooperates with protein E1A, providing preservation of cell viability by blocking apoptotic pathways: inhibition of p53 tumor suppressor, TNF and Fas ligand cell death pathways, thus gaining time for successful viral production (Chinnadurai, 1998; Farson et al., 2006). E1B also turns off host cell protein synthesis. DNA-binding proteins and a polymerase are encoded in the

E2 region, being essential for viral replication (Tatsis and Ertl, 2004). The E3 region encodes proteins which inhibit pathways of cell death induced by the host innate immune response to the infected cell. The E4 transcription unit encodes seven proteins affecting viral transcription and cell functions, including cell proliferation and apoptosis, partially by promoting degradation of p53. Two units (IX and IVa2) are expressed with a delay after initiation of viral replication and are essential for nuclear export of viral RNA (Tatsis and Ertl, 2004). The product of the IX gene is a transactivator and increases virion stability, while the IVa2 protein is needed for assembly of adenovirus and packing of viral DNA. The last unit ("Late unit","L") is divided in five genes (L1-L5) that are only expressed after replication of viral DNA. They encode 45 different species of RNA and are involved in the production of different structural components required for viral particle incapsidation and viral capsid formation and maturation (Russell, 2000).

Adenovirus vector construction aims to avoid vector replication during therapy, controlling the genome replication by removing the E1 region (Dormond et al., 2009). The E1 region is responsible for encoding proteins necessary for the expression of the other early and late genes and initiating the virus life cycle (Figure 1.3). Thus, deletion of E1 suppresses the replication properties of adenoviruses. Also, depletion of the E3 region, which is not essential for viral replication in vitro, provides an additional 3.5 kb of space for alternate expression cassettes (Kovesdi and Hedley, 2010). This first generation of adenovirus vectors allows to incorporate a transgene capacity up to 8 kb (Dormond et al., 2009). To increase capacity for transgene incorporation in the viral genome, the third generation adenovirus vectors had the E1, E2A, E4 and E3 regions deleted.

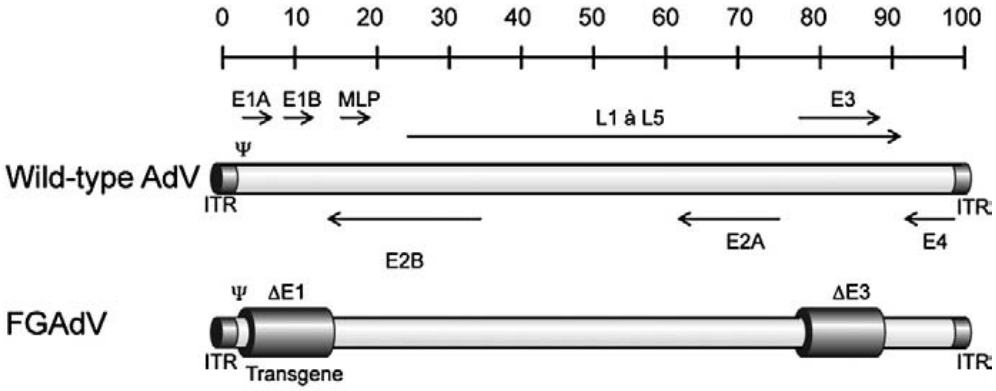

Figure 1.3: Schematic representation of wild-type AdV genome and first generations of AdV. Genomes are divided into 100 map units (28 to 38 kb). E1 to E4: early transcriptunits, L1 to L5: late transcript units, ITR: inverted terminal repeats, MLP: major lateprometer, ψ: packaging signal (adapted from (Dormond et al., 2009))

1.2.5 Infection cycle

AdV5 has a lytic cycle of infection, culminating with the disruption of the host cell and new viral particles release. Firstly, the virus engages with the cell surface through affinity between the protruding domain of the fiber protein and the Coxscackie and Adenovirus Receptor (CAR), which serves as receptor for all adenovirus, except of subgroup B. Effective viral internalization into the host cell requires secondary

interaction between the pentose base protein with cell membrane integrins (Bil-lula and Ussowicz, 2010) (Bil-lula and Ussowicz, 2010). Integrins are heterodimeric transmembrane proteins consisting of α and β subunits and serve important host cell functions, such as cell attachment, migration, growth and differentiation.

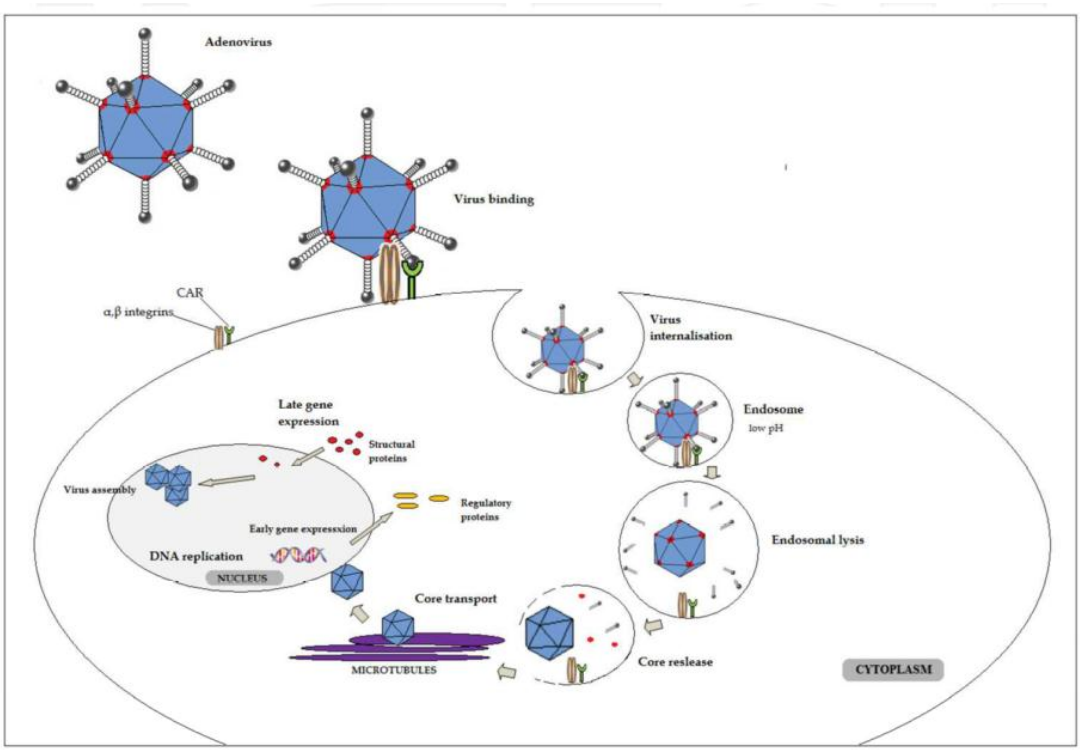

Figure 1.4: AdV infection cycle. An interaction between penton base and integrins induces internalization of viral particle into the host cell. Intra-endosomal mechanisms lead to disintegration of virion shell. Viral DNA is transported into the cell nucleus roviding material for DNA replication. The early phase of replication includes expression of the "early genes" (E1-E4) acting as regulatory factors and facilitating virus replication. Second phase of AdV replication leads to expression of L1-L4 encoding mainly structural proteins determining virus assembly and maturation (Bil-lula and Ussowicz, 2010).

Adenovirus particles enter through the membrane via clathrin-coated pits and vesicles (Patterson and Russell, 1983). Previous investigations of adenovirus internalization, performed on Hella cells showed that clathrin/receptor-mediated endocytosis is the main pathway of AdV5 infection (Wang et al., 1998). After AdV internalization, the next step involves disruption of the early endosome allowing virion release to the cytosol (Meier and Greber, 2003). Different studies show that the release of AdV is triggered by mildly acidic conditions (pH~6) that activate the viral encoded cysteine protease (Blumenthal et al., 1986; Greber et al., 1996). By the time the AdV is delivered to the cytoplasm, it has lost the fiber penton, peripentonal hexon proteins and the capsid stabilizing proteins (proteins IIIa, VIII, and IX) (Figure 1.2) (Saphire et al., 2000). In the cytosol, the virion is transported to the nucleus by microtubules (Suomalainen et al., 1999) in order to deliver its DNA. However, the relatively small size of the nuclear pore complex (25 nM in diameter) indicates that the AdV (90 nM) cannot enter directly into the nucleus. Proteins are imported into the cell

nucleus through aqueous channels that span the nuclear envelope – Nuclear Pore complex (NPC) (Saphire et al., 2000). The nucelocapsid, resulting from rearrangements in the AdV during its transport to the nucleus, docks with NPC where it undergo further disassembly, allowing the DNA to enter the nuclear interior (Saphire et al., 2000). After the viral genome enters the host cell's nucleolus, the cell starts to express viral genes, resulting in the production of viral particles. When the concentration of viral particles reaches a certain level, the host cell membrane disrupts releasing the viral particles (Figure 1.4).

1.2.6 Adenoviral vector production cell lines

First generation AdVs with E1 and E3 deleted regions are replication deficient due to absence of E1A expression (Dormond et al., 2009). Thus, production of AdVs is performed by infection of modified cell lines allowing the complementation *in trans* of genes lacking in the viral genome for its replication. For that purpose, the human embryonic kidney HEK293 cell line is mostly used. HEK293 cells were developed in the 1970's by insertion of E1A and E1B sequences from nucleotides 1 to 4344 (Graham et al., 1977). Since AdVs have a deletion in the E1 region approximately between nucleotides 400 and 3500, overlap between the E1 sequences in the production cell line and AdV can cause homologous recombination between sequences and occurrence of replication-complement adenovirus (RCA) contamination (Hehir et al., 1996). Thus, a strategy to prevent RCA occurrence is to delete the overlap between the E1 sequence in the production cell line and the AdV (Fallaux et al., 1998). Recently, cell lines derived from human amniocytes were proposed as an alternative cell source for recombinant vector production. Absence of sequence overlap between the integrated E1 region and vector DNA excludes the generation of RCA avoiding disadvantages of using HEK293 cells. One of these promising cell lines derived from amniocytes, 1G3, was generated by immortalization of primary human amniocytes with plasmid pSTK146 containing the E1 region of AdV from 505 to 3522nt. To avoid RCA, the E1B intron, the E1B splice acceptor (SA) and the 3' UTR (overlapping with the protein IX gene) were replaced with the corresponding elements from SV40, i.e. intron, SA and polyA signa. The derived cell line had a reduced number of homologous nucleotides and consequently extremely low probability of occurrence of homologous recombination (Silva et al., 2015).

1.3 Stem cell differentiation towards cardiomyocytes

1.3.1 Impact of cardiovascular diseases on humanity

Heart diseases have a huge impact on the human population. According to the World Health Organization report, cardiovascular diseases (CVDs) are the main cause of death worldwide (Heart Federation, 2011). In 2008, more than 17.3 million people died from CVDs, which represent 30% of global mortality (Figure 1.5)

(World Health Organization, 2011). From these, 6.2 million deaths were due to stroke and 7.3 million to coronary heart diseases (CHD) (Heart Federation, 2011).

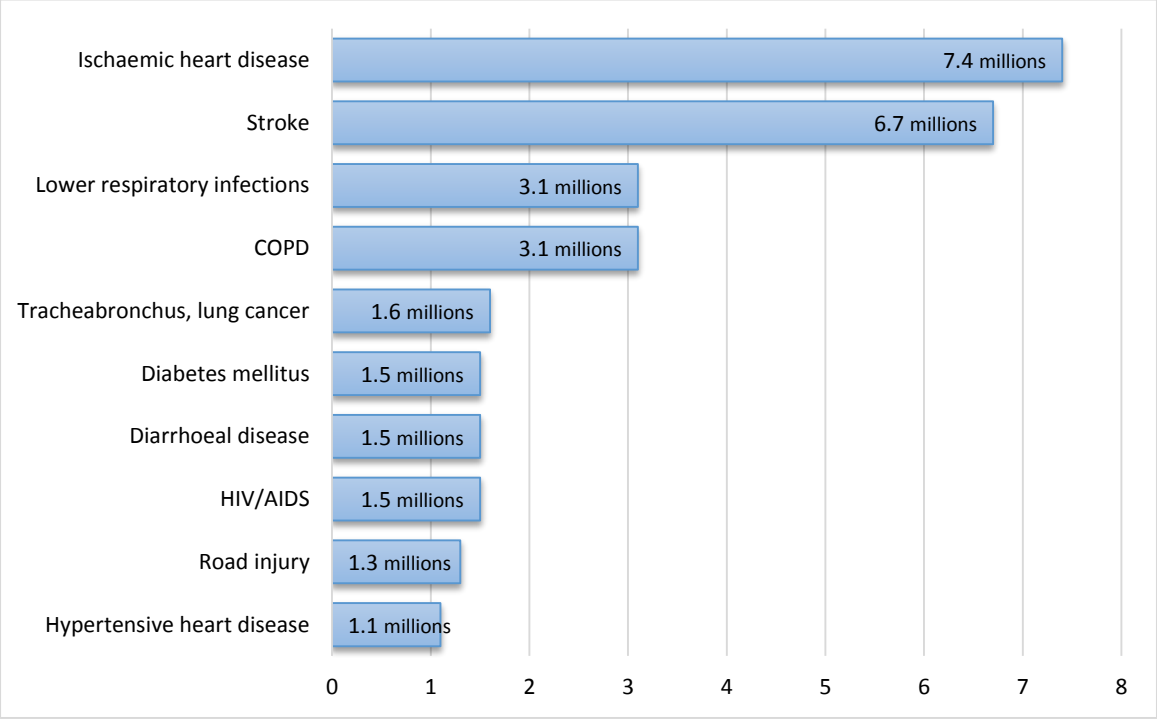

Figure 1.5: The 10 leading causes of death worldwide in 2012 (adapted from World Health Organization, Fact Sheet N 310).

The costs associated to CVD treatments are very high. A report of the World Economic Forum and the Harvard School of Public Health divided the costs of CVD into five groups: screening, primary prevention, secondary prevention, acute hospital care and lost productivity: in 2010, it was about US$ 863 billion (an average per capita cost of US$ 125), and it is estimated to rise to US$ 1,044 billion in 2030 – an increase of 22% (Bloom et al., 2011).

One of the main reasons of the CVD is atherosclerosis, in conjunction with thromboembolism, may result in blood vessels blockage, and consequently in ischemia (Qin et al., 2014). Ischemia represents a restriction of blood supply of the tissue, which cause cells necrosis and apoptosis (Birbrair et al., 2014) by annihilating substrate delivery to cells (infraction)(Baines, 2014; Jennings and Steenbergen, 1985), causing myocardial infraction (MI) better known as "heart attack" (Chang and Towbin, 2006). After acute heart attack, up to 10^9 cardiomyocytes (CMs) died while human heart contain approximately 3 billion CMs (Eefting et al., 2004; Tirziu et al., 2010). Injured heart tissue are then replaced by fibroblasts, which form scar tissue, entailing loss of contractility (Chang and Towbin, 2006) and overload of the surviving myocardium, ultimately resulting in heart failure (Segers and Lee, 2008).

The regenerative capacity of the human myocardium is not adequate to compensate the drastic loss of heart muscle (Segers and Lee, 2008). An experimental approach to regenerate heart tissue may be to utilize the

emerging technologies of stem cells, cell therapy and tissue engineering to repopulate the injured heart with new CMs. Different type of stem cells have been proposed as promising candidates namely: i) human adult stem cells including bone marrow-derived cells (BMCs) (Orlic, 2005), bone marrow-derived mesenchymal stem cells (MSCs) (Zimmermann et al., 2006), skeletal myoblast (SMs) (Dowell et al., 2003) and cardiac progenitor cells (CPC) (Leri et al., 2011) as well as ii) human pluripotent stem cells (hPSC) namely, embryonic (hESCs) and induced pluripotent (iPSCs) stem cells.

Over the last years, PSCs have emerged as an attractive candidate stem cell source for obtaining hCMs. The inherent capacity to grow indefinitely (self-renewal) and to differentiate into all mature cells of the human body (pluripotency), makes hPSCs the only cell source that can provide, *ex-vivo*, an unlimited number of functional hCMs suitable for cell therapy (Améen et al., 2008; Zhang et al., 2009).

1.3.2 Embryonic Stem Cells

ESCs were isolated for the first time in 1981, from mouse embryos, more specifically from the inner cell mass (ICM) of blastocyst (Figure 1.6). Blastocyst is a pre-implantation embryo that develops 5 days after the fertilization. It is composed by the ICM that differentiate into the specialized cell types of the body and the outer cells (trophoblast/trophectoderm) that originate the placenta (Landry and Zucker, 2004). Seventeen years later, Thomson generated the first hESCs, by separation of the ICM, using immunosurgery and by plating the ICM on irradiated mouse embryonic fibroblast (MEF) feeders (Thomson et al., 1998). To maintain hESC colonies, high serum containing Dulbecco´s modified Eagle´s medium was used. hESC colonies originated from ICM were mechanically dissected from old MEFs, and transferred to freshly inactivate MEFs. A hESC line was established by repeated mechanical dissection is subsequent passages (Bongso and Tan, 2005).

Traditionally 1 to 3 day old frozen embryos left after *in vitro* fertilization (UVF) treatment are used for that purpose (Bongso and Tan, 2005). Despite the promising applicability of hESCs in regenerative medicine, there is a set of limitations that hampers their clinical application. These include restrict number of available human embryos, ethical issues and possible immune rejection of hESCs during allogeneic transplantation to patients (Nussbaum et al., 2007).

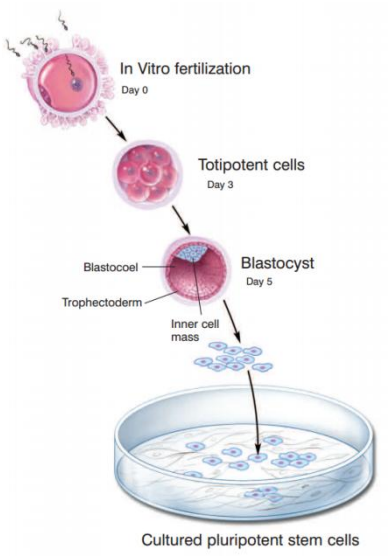

Figure 1.6: Derivation of hESCs (Terese Winslow, 2006).

1.3.3 Induced Pluripotent Stem Cells

In 2006, Yamanaka and co-workers have reprogrammed mature cells to a pluripotent state (O'Malley et al., 2009). The reverted cells were called induced pluripotent stem cells (iPSCs) and were generated by the induced expression of specific reprogramming factors (Nakagawa et al., 2008). In this case, human induced pluripotent stem cells, were derived from human dermal fibroblast, by addition of four transcription factors: Oct4, Sox2, Klf4 and c-Myc, using a retroviral vector (Takahashi et al., 2007). In 2012, Yamanaka was awarded with Nobel Prize in Physiology of Medicine for this discovery. As c-Myc and Klf4 are oncogenes capable to cause tumor formation, other combinations of transcription factors were investigated (Huangfu et al., 2008; Nakagawa et al., 2008). Yu et al showed that the combination of Oct4, Sox2, Nanog and LIN28 transcription factors, delivered by lentivirus vectors, can also efficiently reprogram human somatic cells to pluipotency (Yu et al., 2007). Nevertheless, it was shown that LIN28 can activate endogenous Myc proteins by enhancing translation of insulin-like growth factor-2 (Nakagawa et al., 2008). Consequently, strategies for nuclear reprogramming independent of c-Myc are being explored. There are different methods to introduce transcriptional factors into somatic cells, namely via integrating, excisable, non-integrative vectors, or via DNA-free method (Zwi-Dantsis and Gepstein, 2012). The corresponding advantages and disadvantages are listed in Table 1.4. hiPSCs have shown to be able to circumvent the drawbacks associated to hESCs, allowing for "acceptable" and safe patient-specific (autologous) therapies.

Table 1.4: Methods for reprogramming somatic cells to iPSCs (Robinton and Daley, 2012)**.**

Vector type		Cell types	Factors*	Efficiency (%)	Advantages	Disadvantages
Integrating	Retroviral	Fibroblasts, neural stem cells, stomach cells, liver cells, keratinocytes, amniotic cells, blood cells and adipose cells	OSKM, OSK, OSK + VPA, or OS + VPA	~0.001–1	Reasonably efficient	Genomic integration, incomplete proviral silencing and slow kinetics
	Lentiviral	Fibroblasts and keratinocytes	OSKM or *miR302/367* cluster + VPA	~0.1–1.1	Reasonably efficient and transduces dividing and non-dividing cells	Genomic integration and incomplete proviral silencing
	Inducible lentiviral[23,28]	Fibroblasts, β cells, keratinocytes, blood cells and melanocytes	OSKM or OSKMN	~0.1–2	Reasonably efficient and allows controlled expression of factors	Genomic integration and requirement for transactivator expression
Excisable	Transposon[86]	Fibroblasts	OSKM	~0.1	Reasonably efficient and no genomic integration	Labour-intensive screening of excised lines
	loxP-flanked lentiviral[87]	Fibroblasts	OSK	~0.1–1	Reasonably efficient and no genomic integration	Labour-intensive screening of excised lines, and *loxP* sites retained in the genome
Non-integrating	Adenoviral	Fibroblasts and liver cells	OSKM	~0.001	No genomic integration	Low efficiency
	Plasmid	Fibroblasts	OSNL	~0.001	Only occasional genomic integration	Low efficiency and occasional vector genomic integration
DNA free	Sendai virus	Fibroblasts	OSKM	~1	No genomic integration	Sequence-sensitive RNA replicase, and difficulty in purging cells of replicating virus
	Protein	Fibroblasts	OS	~0.001	No genomic integration, direct delivery of transcription factors and no DNA-related complications	Low efficiency, short half-life, and requirement for large quantities of pure proteins and multiple applications of protein
	Modified mRNA	Fibroblasts	OSKM or OSKML + VPA	~1–4.4	No genomic integration, bypasses innate antiviral response, faster reprogramming kinetics, controllable and high efficiency	Requirement for multiple rounds of transfection
	MicroRNA	Adipose stromal cells and dermal fibroblasts	miR-200c, miR-302s or miR-369s	~0.1	Efficient, faster reprogramming kinetics than commonly used lentiviral or retroviral vectors, no exogenous transcription factors and no risk of integration	Lower efficiency than other commonly used methods

*OSKM and similar factor names represent combinations of reprogramming factors: K, KLF4; L, LIN28; M, c-MYC; N, NANOG; O, OCT4; S, SOX2; and VPA, valproic acid. (Robinton and Daley, 2012).

1.3.3 CM Differentiation - A developmental perspective

During embryonic development, one of the most essential and earliest process is cardiogenesis (Srivastava, 2006). Cardiac development is a dynamic process controlled by sequential expression of multiple signal transduction proteins and transcription factors. Decades of research allowed to understand the main molecular pathways and genes which are responsible for cellular differentiation in mouse model systems, however human heart development is still poorly understood (Musunuru and Domian, 2014). Despite of the differences in the mouse and human heart, investigation on mouse cardiogenesis has provided valuable knowledge/information about key signaling pathways involved in PSC differentiation to CMs (Garbern et al., 2013).

hPSC cardiomyogenesis consists of six major steps i) epithelial to mesodermal transition (day 0); ii) from mesodermal progenitor cells to precardiac mesoderm cells (day 2); iii) specification of the precardiac mesoderm do the cardiac mesoderm (day 3-4); iv) cardiac specification in which the cardiac mesoderm further develops into cardiac progenitor cells (day 5-6); v) from cardiac progenitor cells to immature CM

(day 7); vi) maturation of CMs (extended time in culture). At each stage of differentiation, cells can be characterised, by the expression of a different set of markers (transcriptional factors, surface marker). The steps of hPSC cardiomyogenesis as well as the markers expressed by cells at each differentiation stage are illustrated in Figure 1.7.

The main signalling pathways involved into cardiac induction are: wingless/INT (WNTs) (Marvin et al., 2001), nodal (Brennan et al., 2001)), bone morphogenic proteins (BMPs) (Univer-, 1995) and fibroblast growth factors (FGFs) (Mima and Fischman, 1995). During gastrulation (formation of gastrula in early embryonic development) signals mediated through WNT/β-catenin and transcription growth factor β (TGF-β) family members promote differentiation of PSCs into mesoderm (Murry and Keller, 2008). However, following mesodermal induction, WNT/β-catenin signaling inhibits cardiac differentiation and may redirect cells to alternative mesodermal fates. Therefore, at this stage WNT/β-catenin signaling need to be blocked by specific inhibitors to effectively induce heart development. The biphasic role of the WNT/β-catenin pathway during cardiac differentiation (either promoting or inhibiting cardiogenesis depending on timing), highlights that the concentration and timing of addition of specific growth factors/small molecules are crucial and must be carefully addressed in order to efficiently drive PSCs to a cardiac cell fate.

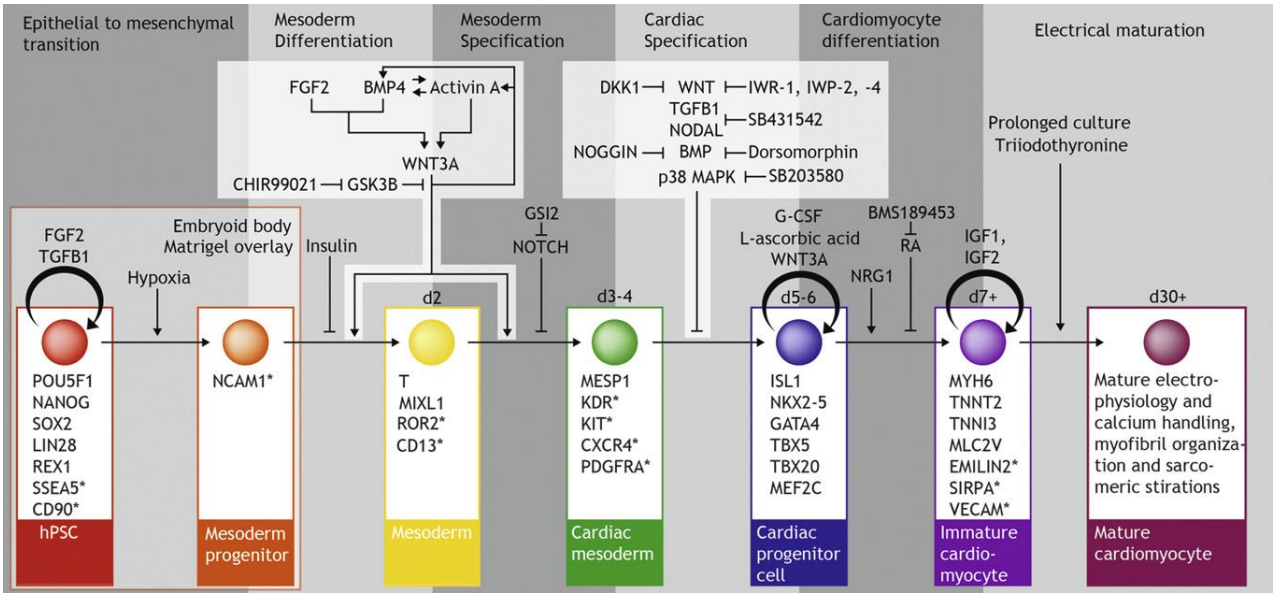

Figure 1.7: Schematic representation of factors involved in hPSCs cardiac differentation (Burridge et al., 2012) Factors that influence the progression through each of the six major steps of hPSC cardiomyogenesis: epithelial to mesenchymal transition, mesoderm differentiation, mesoderm speciation, cardiac specification, cardiomyocyte differentiation, and electrical maturation. Below are the markers associated with each of the seven cell types during differentiation; surface markers are marked with an asterisk.

1.3.4 Current methods for CM differentiation of PSC

Currently, the main approaches for CM differentiation of PSCs are spontaneous differentiation through embryoid body (EB) formation, co-culture with cells presenting cardiac inductive activity and guided

differentiation strategies (induced by growth factors and/or small molecules) (reviewed in (Dierickx et al., 2012)).

Guided/directed differentiation with growth factors and small molecules

Several growth factors/small molecules have been used to induce mesoderm formation and cardiomyogenesis in PSC cultures. Some of these factors are listed in Table 1.5. Activin A, a member of TGF-β family, has been demonstrated to promote cardiomyogenesis in human PSCs (reviewed in (Habib et al., 2008)). BMPs, also members of the TGF-β family, play a key role in promoting mesoderm formation and specifying myocardial lineage commitment during differentiation (Filipczyk et al., 2007; Habib et al., 2008).

Table 1.5: Examples of factors and molecules with observed effects on CM differentiation (adapted from Xu, 2012).

Factor	Known function	Effect on cardiomyocyte differentiation
		Human pluripotent stem cells
Activin A	• Induces endoderm • Induces mesoderm	Positive
BMP4	• Induces mesoderm	Positive
BMP2	• Induces mesoderm	Positive
Dorsomorphin	• Inhibits BMP signaling	Positive
Wnt3A	• Induces endoderm • Induces mesoderm	Positive (at early stage)
DKK1	• Induces cardiac mesoderm	Positive (at late stage) Negative (at early stage)
bFGF	• Induces mesoderm • Mitogen	Positive
SU5402	• Inhibits FGF receptor	Positive
5-Azacytidine	• Demethylates DNA	Positive
DMSO	• Cryoprotectant	Negative
SB203580	• Inhibit P38 MAP kinase	Positive (at low dose)
PD169316		Negative (at high dose)

It has been shown that sequential addition of these two growth factors (at specific concentrations) can generate spontaneous contracting areas within 10 days and 30% of differentiated CMs within three weeks, (Laflamme et al., 2007). The WNT family, namely the WNT/β-catenin pathway, has stage dependent effects on cardiac differentiation. Activation of this pathway at the beginning of differentiation and inhibition at later stages, after mesoderm formation, with IWR/IWP factors enhance cardiomyogenesis (Paige et al., 2010). FGFs have also been described to influence survival and proliferation of cardiac precursors (Mercola et al., 2011). During the last years several directed differentiation protocols have been published, each one using a different combination of growth factors/small molecules added into culture medium at specific time points (Xu, 2012). Table 1.6 highlights some of these protocols as well as the major outcomes obtained in terms of CM yields. For example, the sequential addition of activin A, BMP4, basic fibroblast growth factor (bFGF), Dickkopf homolog 1 (DKK1) and Vascular Endothelial Growth Factor (VEGF) resulted in a population of 40%-50% of cells expressing troponin specific markers (cTnT) (Kattman et al., 2011; Yang

et al., 2008). Despite usually assuring the production of CMs with higher yields and purities, the directed differentiation protocols are normally associated with high costs (e.g. requires the use of expensive inductive factors) that compromises process scalability (Mummery et al., 2012).

Table 1.6: Different approaches for hPSC differentiation towards CMs (Zwi-Dantsis and Gepstein, 2012).

	Differentiation method	Key steps	Serum-free conditions	Yield of cardiomyocytes
Spontaneous differentiation	Suspension (EBs)	hESCs/hiPSCs are detached from the feeder cells and transferred to suspension, where they form three-dimensional aggregates (EBs) After 7–10 days in suspension, EBs are plated on gelatin-coated culture dishes Spontaneous contractions starting 7–8 days after plating	No	1–10 %
Guided differentiation	Monolayer	Undifferentiated hESCs/hiPSCs are treated with bFGF for 6 days Cells are exposed for activin A for 24 h, followed by treatment with BMP4 for another 4 days The cytokines are removed. Beating is observed 12 days after activin treatment	Yes	>30 % (>80 % when including Percoll gradient)
	Suspension (EBs)	hPSCs are guided into the mesodermal lineage by treatment with activin A, BMB4 and bFGF Cardiac induction by treatment with the Wnt inhibitor—DKK1, VEFG and bFGF	Yes	40–50 %
	Co-culture	EBs are continuously cultured in insulin-free medium conditioned with END-2 cells, PGI_2 and MAPK inhibitor Beating foci are observed after 9–12 days in culture	Yes	5–20 %
	Single cells	Undifferentiated hESCs/hiPSCs are treated with BMP2 for 4 (hESCs) and 6 (hiPSCs) days, in the presence of SU5402, a FGF receptor inhibitor BMP2-induced SSEA-1^+ progenitors are plated in a mix of human cardiac fibroblasts and cardiomyocytes to induce their differentiation into cardiomyocytes	Yes	60–80 %
Small molecules	Suspension (EBs)	EBs are cultured with 5-aza-deoxycytidine at days 6–8 after initiating of differentiation Percoll gradient separation may be used in order to further enrich the cardiomyocytes population	No	Two- to threefold induction of cardiac related genes

1.3.5 Metabolic Dynamics during Development

Zygote development to multicellular organism requires higher cell growth, comparing with already formed adult tissue. Though, it is reasonable to expect, that metabolic profiles would differ throughout the embryo development. Figure 1.8 describes the stages of mouse embryo development as well as the main metabolic phenotype associated to each stage. In the first stage of embryo development, from one cell embryo (i.e. zygote) to morula formation, glycolysis rates are very low and pyruvate oxidation is the predominant metabolic process probably due to the presence of abundant maternal mitochondria inherited from the oocyte (Folmes et al., 2012). In the pre-implantation embryo, every cell division, results in the reduction of

the mitochondria number (Folmes et al., 2012). During morula compaction, the first round of differentiation occurs, and cells segregate to trophectoderm, which will originate the placenta, and to the pluripotent ICM (Shyh-Chang et al., 2013). At morula stage of embryogenesis, glucose uptake increases gradually, accompanied by upregulation of GLUT1 and GLUT3 glucose transporters (Pantaleon and Kaye, 1998). At blastocyst stage, glycolysis rates become higher than pyruvate oxidation (Johnson et al., 2003). Mitochondrial segregation among daughter cells occurs until implantation phase (until day 6, Egg Cyclinder, Figure 1.8). Following the implantation, mitochondrial replication increases enabling the transition from glycolysis to a more oxidative metabolism (Johnson et al., 2003).

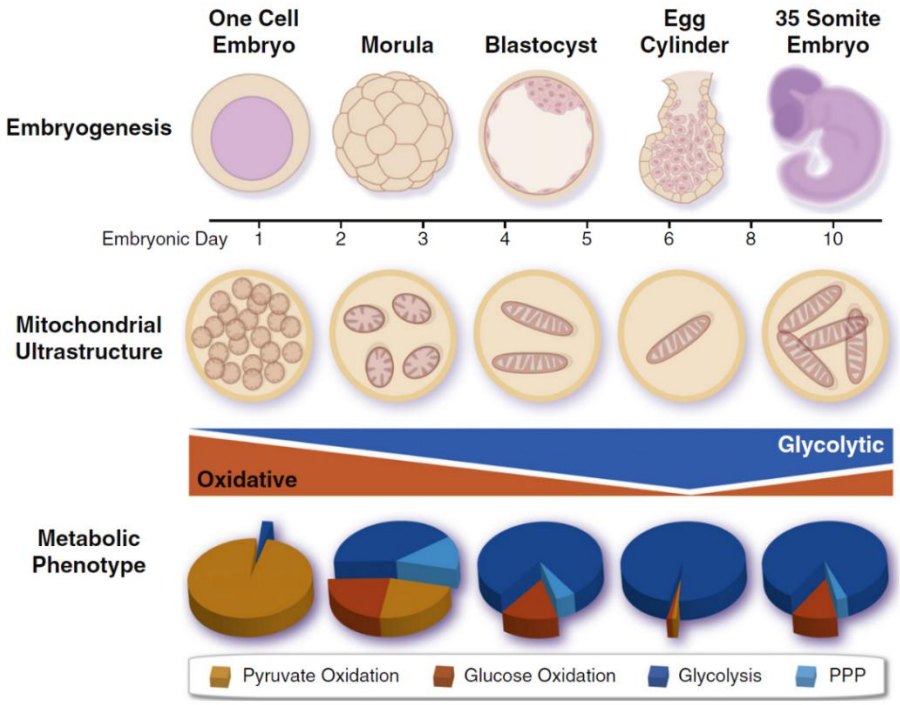

Figure 1.8: Metabolic profile during embryo development (Folmes et al., 2012).

1.3.6 Main metabolic differences between PSC and differentiated cells

Genome integrity is protected in hESCs through maintenance of low level of reactive oxygen species (ROS). This is achieved due to the combination of limited production of ROS molecules and due to increase ROS removal capacity of ESCs (Armstrong et al., 2010). Limited production of reactive oxygen species is a consequence of low number of mitochondria located in embryonic stem cells (Facucho-Oliveira and St John, 2009). Therefore, it was remained unclear if hiPSCs produced from fibroblasts extra mitochondria and possess the same ROS defense mechanism as hESCs. Recent findings suggest that mitochondria morphology in hiPSCs, after cell reprogramming, pass to immature state and mitochondrial gene expression is reduced, which permit hiPSCs having the same ROS properties as hESCs (Armstrong et al., 2010; Prigione et al., 2010). In contrast with hESCs and hiPSCs, which rely mainly on glycolysis (Facucho-

Oliveira and St John, 2009), somatic cells mostly use mitochondrial oxidative phosphorylation to produce energy (ATP's) (Folmes et al., 2011). PSCs have unlimited self-renewal capacity and thus to maintain high level of proliferation, these cells should balance energetic and biosynthetic needs (Zhang et al., 2012). Glycolysis is the main source of energy and biomass precursors required for rapid proliferation of PSCs, while OXPHOS is preferentially used by quiescent cells (Zhang et al., 2012) (Figure 1.9).

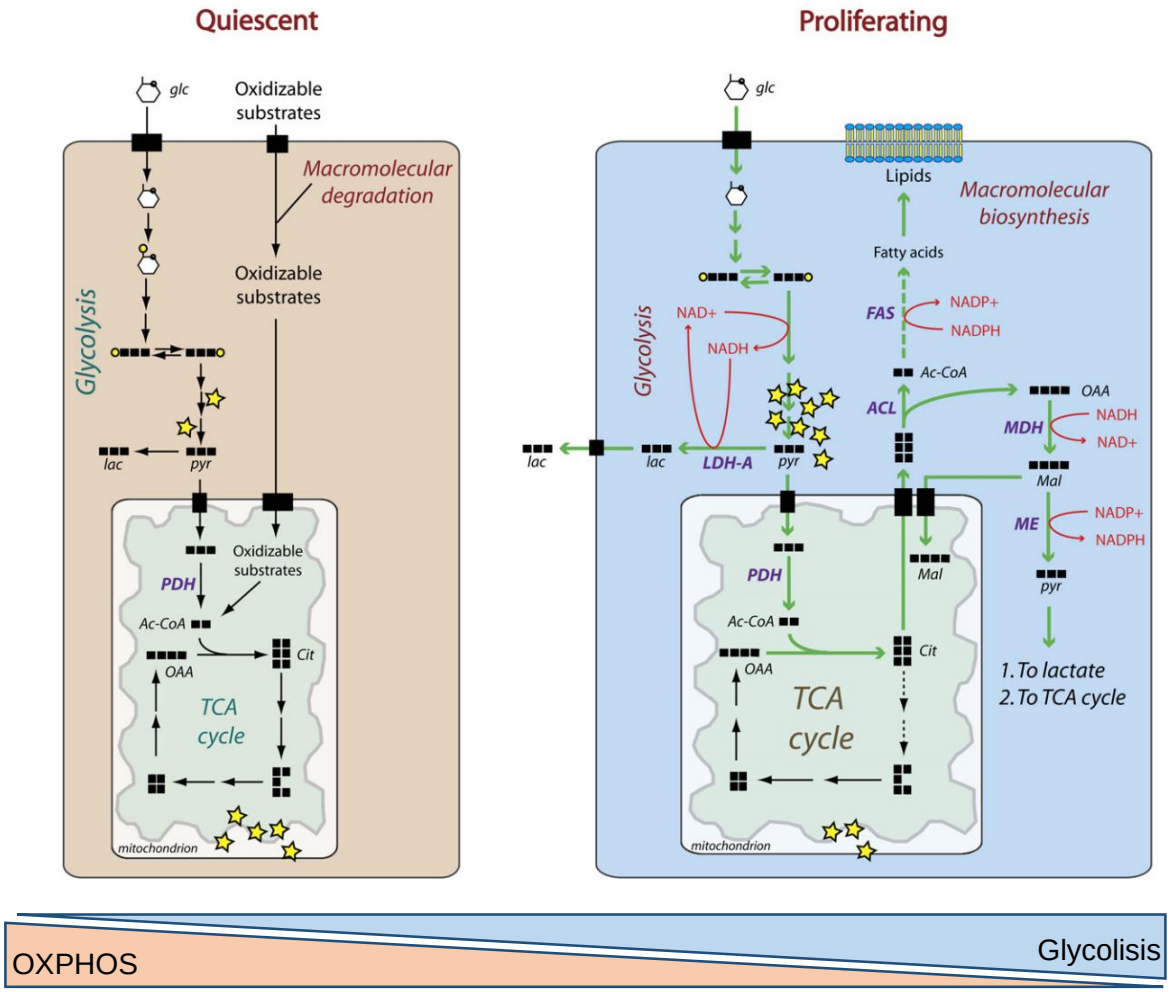

Figure 1.9: Differences between proliferated cells (PSCs) and differentiated/quiescent cells metabolism (adapted from (DeBerardinis et al., 2008)). Energy metabolism shifts from glycolysis to OXPHOS with differentiation or from OXPHOS to glycolysis with reprogramming to pluripotency. Glycolytic flux is elevated in PSCs (right panel) to provide ATP and intermediate metabolites through the pentose phosphate pathway for nucleotide and lipid biosynthesis. Pluripotent cells rely more on glycolysis for energy because respiration is lower and less coupled to energy production than in differentiated cells. The TCA cycle in PSCs provides intermediate metabolites such as citrate and a-ketoglutarate that are siphoned for lipid and amino acid biosynthesis (Zhang et al., 2012).

1.3.7 Human Stem Cell derived Cardiomyocytes: Enrichment by Lactate

Different genetic and non-genetic methods have been applied to purify cardiomyocytes derived from hPSCs, such as percoll separation, flow activated cell sorting using mitochondrial dyes or specific surface markers. One recent and very simple method was to culture the cells in glucose-free lactate-containing media

(Tohyama et al. 2013). It is known that fetal heart can exploit lactate rich environment created by placenta and use lactate as a major source of energy (Fisher et al., 1981). Based on this, Tohyama et al (2013) tested different cell lines under glucose-depletion condition (with or without lactate), and confirmed that CMs survive in this culture medium whereas other cell types, such as primary peripheral lymphatic, primary fetal neurons, primary mouse embryonic fibroblast (MEFs), C2C12 cells, hepatocytes and renal cells (HEK293) died. (Tohyama et al., 2013). With this strategy, CM purity increased up to 98% (Tohyama et al., 2013).

1.3.8 Maturation of CMs derived from hPSC

Several studies have shown that hPSC-derived CMs are immature and display fetal- and, in some cases, embryonic-like phenotype, structural, metabolic and functional properties. Mature hCMs, better reflect the physiology of the adult heart and therefore could be more useful in disease modelling and drug testing. Learning how to mature human CMs may also provide important clues about how our own heart matures in postnatal life. Additionally, since mature CMs present electric and mechanical properties more similar to native myocardium, it is expected that these cells will display less arrhythmic risk and have enhanced contractile performance after transplantation and engraftment (Yang et al., 2014a). CMs maturation can be expressed by changes in cells morphology, metabolism, contractile properties and mitochondrial activities.

1.3.8.1 Morphology

While adult human CMs are rod shaped with lengths in the 100 μm range, hPSC-CMs are smaller in size (10 to 20 μm in diameter) and often round (Yang et al., 2014a). These cells tend to increase in size with prolonged time in culture; however, the shape of these cells remains round or oblong (Robertson et al., 2013; Yang et al., 2014a). Adult CMs have multiple nuclei, large sarcomere area and higher number of mitochondria than hPSC and early and late hPSC-CMs (Figure 1.10).

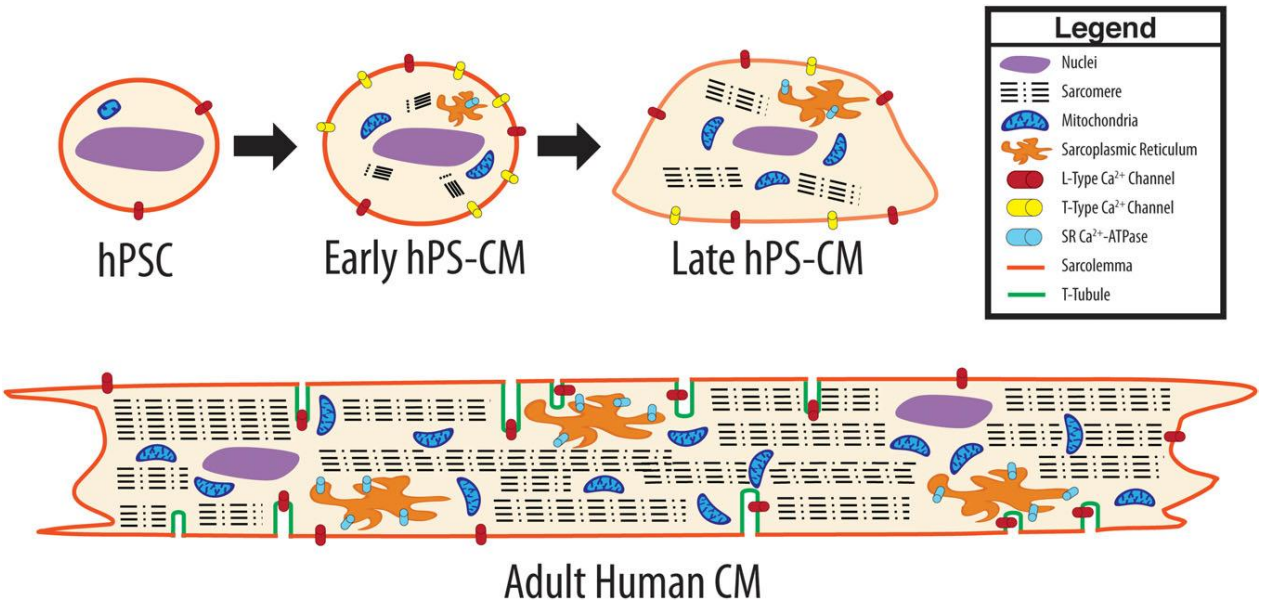

Figure 1.10: **A visual comparison of early hPSC-CM, late hPSC-CM and adult CM morphology.** Early phase hPSC-CM, define the contractile cells, with some proliferative capacity and with embryonic like electrophysiology (i.e., small negative membrane potential and small action potential amplitude), and late phase hPSC-CM define CMs without proliferative capacity and with more adult-like electrophysiology (Robertson et al., 2013).

1.3.8.2 Contractile Apparatus

The sarcomere is the fundamental unit for CM contraction. Tracing of expression levels of sarcomeric proteins, such as cardiac troponin T, cardiac troponin I, α-actinin and β-myosin heavy chain, provides information about hiPSC-CMs assessment of specialization and maturation. Sarcomeric length is also considerably shorter than that found in adult CMs.

1.3.8.3 Mitochondria and metabolic substrate

Mitochondrial structural and functional changes are critical components of maturation during heart development. In immature CMs, mitochondria distribute throughout the cytoplasm in a reticular network and occupy a small fraction of cell volume. Upon the development process, mitochondria are regularly distributed over the cell, develop more mature lamellar crista, and occupy approximately 20% to 40% of the adult myocyte volume. During early cardiac development, glycolysis is a major source of energy. As CMs mature, mitochondrial oxidative capacity increases and β-oxidation becomes the major source of energy (Yang et al., 2014a).

2. AIM OF THE THESIS

The main aim of this thesis was to apply system biology tools to:

i) Comprehensively characterize the metabolism of the 1G3 trans-complementing cell line after adenovirus vector infection;

ii) Elucidate phenotypic, structural and metabolic alterations during hiPSC differentiation towards CMs and maturation, and evaluate the impact of different culture media compositions on hPSC-CM enrichment and maturation.

In the first part of the work, parallel labeling experiments and ^{13}C-MFA were used for determination of intracellular flux distributions in 1G3 cells under exponential growth and growth arrest conditions, both with and without AdV infection. The metabolomics techniques used in this part were YSI, HPLC and GC-MS. In the second part of the thesis, metabolic characterization (including parallel labelling experiments and associated metabolomics techniques) was performed in combination with other tools to fully elucidate phenotypic and functional alterations associated with hiPSC differentiation and CM maturation. Additional analytical techniques were used for phenotypic and structural characterization such as immunofluorescence microscopy, flow cytometry, qRT-PCR and Transmission Electron Microscopy (TEM).

The thesis aims and strategy used are schematically illustrated in Figure 2.1.

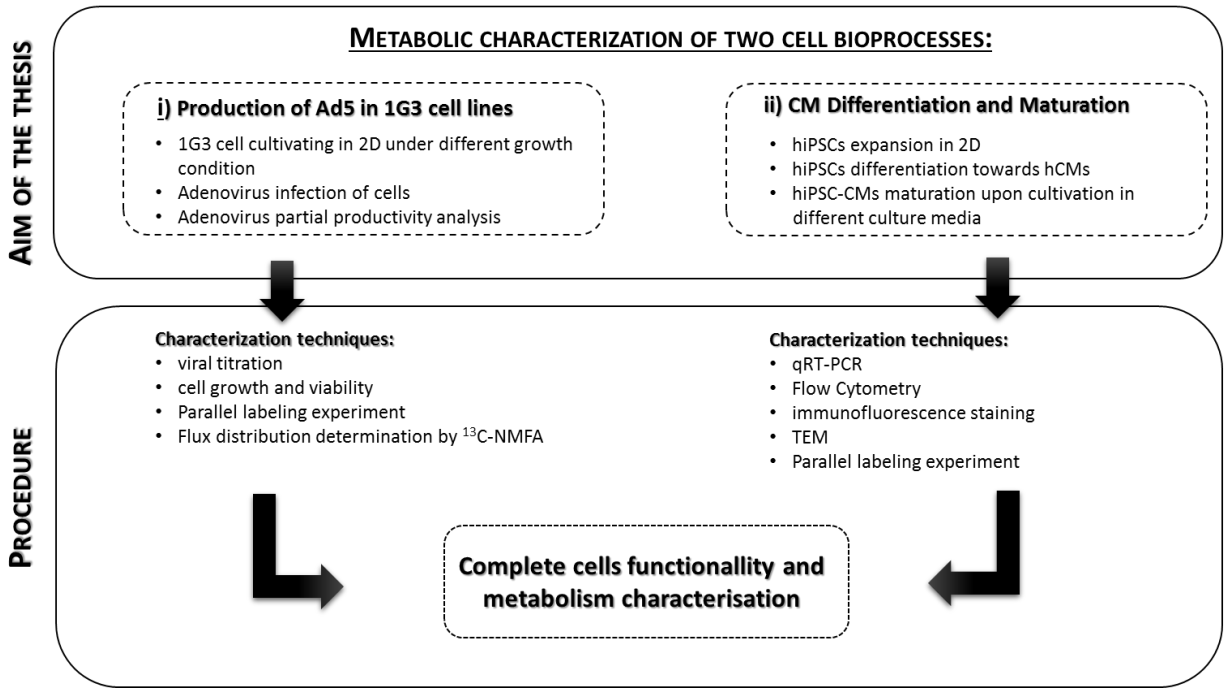

Figure 2.1: Thesis aim and strategies.

3. MATERIALS AND METHODS

3.1 Adenovirus particles production

3.1.1 Cell line and maintenance

The 1G3 cell line has been previously established at our lab (Silva et al., 2015) by immortalization of primary human amniocytes with the plasmid pSTK146UBE2I (Schiedner et al., 2000). Cells were maintained in Dulbecco´s Modified Eagle Medium (DMEM, Gibco, Paisley, UK) supplemented with 1% (v/v) Fetal Bovine Serum (FBS, Gibco), using T-225 flasks in a humidified atmosphere at 37°C with 5% CO_2. Sub-culture was performed twice a week. For cell harvesting, the monolayer was washed with phosphate buffered saline (PBS) and incubated with 0.05% trypsin-EDTA (Invitrogen, UK) until cell detachment.

3.1.2 AdV5 production and titration

The viral vector consisted of an E1-deleted HAdV-5 with an enhanced green fluorescent protein (eGFP) as transgene (HAdV5-GFP). The vector is based on the plasmid pGS66 that contains HAdV-5 sequences from nt 1 to 440 and from nt 3523 to 25935 (Schiedner et al., 2000; Silva et al., 2015). The expression cassette consisting of the hCMV immediate early promoter, a cDNA coding for the eGFP protein and the SV40 polyA signal replace the E1 region in the pGS66 plasmid (Silva et al., 2015). N52.E6 cells were transfected with DNA plasmid, cleaved by SwaI (flanking the adenovirus ITRs), providing production of the HAdV5-GFP vector, which was followed by a purification step with CsCl gradients (Silva et al., 2015).

A viral stock was prepared by infecting HEK293 cells at 80-90% confluence in DMEM with 10% (v/v) FBS. Infection was performed with a multiplicity of infection (MOI) of 5 infection particles per cell. 40 h after infection, cells were trypsin-harvested and the cell pellet was lysed with 0.1% (v/v) Triton X-100 (Sigma-Aldrich, Steinhein, Germany) in 10 mM Tris-HCl buffer at pH=8. Intracellular infectious particles were collected after centrifuging resuspended cells in lysis buffer for 10 min at 3000 g, 4°C. A desalting step was then performed on an AKTA system using a HiPrep 26/10 Desalting Column (GE Healthcare, USA) to change the previous buffer with 10 mM Tris-HCl, 2 mM $MgCl_2$, 0.5 M trehalose, pH=8. Aliquots of viral stock were stored at -85°C.

Quantification of infectious particles was performed by Flow Cytometry as described in (Ferreira et al., 2009). Briefly, HEK293 cells (ATCC CRL-1573) were seeded at 0.25×10^6 cells/well and infected 12 h (hpi) with 1 mL of serial dilutions of the AdV samples in medium (DMEM with 10% FBS). Cells were trypsin-detached at 17-20 hpi and analyzed in a Flow Cytometer (CyFlow Space, Partec, Germany) to evaluate the percentage of GFP-positive cells.

3.1.3 Poly-D-Lysine coating procedure

For the isotopic tracer experiments, a coating procedure was applied to the culture wells, using Poly-D-Lysine (PDL). A working solution of PDL was prepared by diluting a 1mg/mL stock solution 1:100 in sterile water, and filtered with a 0.2 μm filter afterwards.

The day before the experiment, 1.5 mL of the PDL working solution were aseptically pipetted to each well, and left incubating overnight. The next day, PDL solution was removed and plates left to dry in a laminar flow hood for approximately 90 min, with the lids opened. Plates were used for cell inoculation on the same day.

3.1.4 Isotopic tracer experiments and sampling

For the 1G3 cell line, [1,2-^{13}C]glucose (CLM-504-1) and [U-^{13}C]glutamine (CLM-1822-H-0.25; Cambridge Isotope Laboratories, Andover, MA) isotopic tracers were used for parallel isotopic labelling experiments. Glucose and glutamine stock solutions (200 mM and 40 mM, respectively) were prepared in PBS as follows: i) ^{13}C glucose and ^{12}C glutamine, ii) ^{12}C glucose and ^{13}C glutamine, and iii) ^{12}C glucose and ^{12}C glutamine. Two conditions were studied: Exponential Growth (EG) and Growth Arrest (GA). In both conditions, cells were inoculated in coated 6–well plates, in DMEM supplemented with 1% (v/v) FBS, adding up to 2 mL total volume. For Exponential Growth condition, cells were seeded at a density of 9.38×10^5 cells/well. For the Growth Arrest condition, cells were seeded at 1.66×10^6 cells/well and 24 h afterwards the medium was changed from DMEM+1% (v/v) FBS to DMEM. Growth arrest was achieved by starting with a higher cell density (1.6 million cells instead of 1 million) and serum deprivation.

Infection was performed 12 h after cell seeding in the case of EG and 36h after serum removal for the GA condition. The medium (DMEM+1%(v/v) FBS for EG cells, and DMEM for GA cells) was completely exchanged by 1.9 mL of custom DMEM, supplemented with 1.5 mM and 0.3 mM of glucose and glutamine, respectively, and 1% (v/v) FBS in the case of EG cells. Cells were infected with HAdV-5 at a MOI of 10 infection particles per cell or mock-infected (equal volume of 10 mM Tris-HCl, 2 mM $MgCl_2$ and 0.5 M trehalose, pH=8 buffer). After 4 h, 100 μl of each ^{13}C/^{12}C stock solution (i.e. to achieve a concentration of 10 mM glucose and 2 mM glutamine) were added to virus-infected and mock-infected wells, totaling 6 wells in one plate.

To completely characterize the dynamics of label incorporation two plates were harvested at the following time points: 0 min, 10 min, 30 min, 1 h, 3 h, 8 h and 24 h after label addition, approximately. For phosphoenolpyruvate (PEP) and 3-phosphoglycerate (3PG) analyses, two extra plates were harvested at 0min, 10 min, 3 h and 24 h. Metabolic quenching and extraction was performed in ^{13}C-labelled wells of virus-infected and mock-infected cells (see below). In addition, samples from all wells (triplicates of virus-infected and mock-infected cells) were collected at time points 0 h, 3 h, 8 h and 24 h, centrifuged at 200 x g for 10 min, 4°C, and stored at -20°C for extracellular metabolite analysis.

For hiPSC-CMs, [1,2-^{13}C]glucose (CLM-504-1, Cambridge Isotope Laboratories, Andover, MA) and [3-^{13}C] sodium L-lactate (201595-70-2, Sigma-Aldrich, DE) isotopic tracers were used for parallel isotopic labeling experiments. Glucose and lactate stock solutions (10 mM and 4 mM, respectively) were prepared in glucose depleted RPMI, supplemented with B27 without insulin (Invitrogen) as follows: i) ^{13}C glucose and ^{12}C sodium L-Lactate, ii) ^{12}C glucose and ^{13}C sodium L-Lactate. hiPSC-CMs were inoculated in 12-well plates at a density 0.5×10^5 cell/well. To characterize label incorporation, two timepoints were chosen: 24 h and 48 h after label addition.

3.2 Stem cells differentiation toward cardiomyocytes

3.2.1 hiPSCS differentiation toward hCMs

In this study the hPSC line DF19-9-11T.H from WiCell was used. This cell line was derived from human fibroblast cells using a non-integrating episomal vector. hiPSCs were cultured on Synthemax® II – SC Substrate (Corning) coated plates in mTESR1 medium (STEMCELL Technologies) until reaching 80% confluency. hiPSC differentiation towards CMs was performed by addition of growth factors and small molecules, using on protocols published recently (Burridge et al., 2014; Lian et al., 2012). Using this protocol monolayer cultures composed by 70-99% of hiPSC-CMs were obtained. When needed, cell population enrichment was performed by cultivation of hiPSCs-CMs in CM enrichment medium (RPMI 1640 w/o glucose (Invitrogen) supplemented with B27 (Invitrogen) and 5 mM sodium L-Lactate (Sigma-Aldrich)), during 10 days as described elsewhere ((Tohyama et al., 2013)). Cells were cultured at 37°C, in a humidified atmosphere of 5% CO_2.

3.2.2 hiPSC-CMs maturation

After differentiation, hiPSC-CMs were cultured for further 20 days (from day 15 until day 35) in three different culture media: i) standard culture medium RPMI+B27 (CM medium, CMM); ii) glucose depleted RPMI culture medium supplemented with 4 mM lactate (lactate medium, LacM), from day 15 until day 25, and standard medium RPMI+B27 (CM medium, CMM), from day 25 until day 35; iii) glucose depleted RPMI culture medium supplemented with a mixture of fatty acids (Fatty Acid Medium, FAM) from day 15 to day 35. During this culture period, hiPSC-CMs were characterized by qRT-PCR, TEM, percentage of binucleated cells and measurement of mitochondrial membrane potential.

3.2.3 Structural characterization

3.2.3.1 Immunocytochemistry

hiPSC-CMs were fixed with 4% (w/v) PFA in PBS solution for 15 min, further permeabilized and blocked with 5% (v/v) FBS, 1% (w/v) BSA, 0.3% (v/v) Triton X-100 in PBS during 1 h at room temperature. After two washes with PBS cells were incubated overnight at 4°C with primary antibodies diluted in 1% (w/v) BSA, 0.1% (w/v) TX-100 in PBS. The primary antibodies used are listed in Table 3.1. Afterwards, cells

were washed in PBS and secondary antibodies were added for 1 h at room temperature in the dark. The secondary antibodies used were: AlexaFluor 594 goat anti-mouse IgG and AlexaFluor 594 goat anti-rabbit IgG (1:500 dilution in (w/v) BSA, 0.1% (w/v) TX-100 in PBS). Cell nuclei were counterstained with Hoechst 33342 nucleic acid dye. Cells were visualized using an inverted fluorescence microscope (DMI 6000, Leica).

Table 3.1: List of primary antibodies used for immunocytochemistry and flow cytometry analysis

Analysis	Primary Antibody	Dilution	Description
Immunocytochemistry	α-sarcomeric actinin (Sigma-Aldrich)	1:200	CMs
	Titin (Santa Cruz Biotechnology)	1:100	
	troponin T (Millipore)	1:100	
	F-actin Alexa Fluors 488 dye (Life technologies)	1:100	Cytoskeletal
Flow Cytometry (intracellular antibodies)	Oct4 (Santa Cruz Biotechnology)	3 uL Ab in 50 uL WB	Pluripotency
	Nanog (R&D Systems)	1:10	
	cTNT (Thermoscientific)		CMs
Flow Cytometry (cell surface antibodies)	SSEA-1 (BD Pharmingen)	1:10	Spontaneous differentiation
	SSEA-4 (Santa Cruz Biotechnology)	3 uL Ab in 50 uL WB	Pluripotency
	Tra-1-60 (Santa Cruz Biotechnology)	3 uL Ab in 50 uL WB	
	Bry T (R&D Systems)	1:10	Mesoderm
	KDR/VEGFRα (BioLegend)	5:100	Cardiac Mesoderm
	PDGFRα (BD Pharmingen)	2:10	
	SIRPα/β (CD172a/b-PE, BioLegend)	5:100	CMs
	VCAM (BD Pharmingen)	2:10	

3.2.3.2 Flow cytometry analysis

Cells were dissociated using TrypLE™Select (Invitrogen) for 5 min and then resuspended in washing buffer (WB) solution (5% (v/v) FBS in PBS), centrifuged 300 g 5 min and washed again. Cells were incubated with the primary/conjugated antibody for 1 h at 4ºC. Afterwards, cells were washed two times in WB solution. Whenever required, cells were incubated with secondary antibody for 30 min at 4ºC. For determination of intracellular markers cells were washed two times in BD Perm/Wash (PW) solution (BD Biosceinces, diluted 1:10 in H2O MiliQ), and fixed for 20 min in BD CitoFix/Citoperm (BD Biosciences) solution at 4°C. Next, after one wash in PW solution, cells were kept 30 min in 1% (v/v) BSA solution for blocking non-specific interactions. After that, cells were washed in PW solution and then incubated with primary antibody (listed in Table 3.1) during 1 h Afterwards cells were washed twice in WB for extracellular markers and in PW for intracellular markers. Cells were incubated with secondary antibody AlexaFluor 488 goat anti-mouse IgM (1:200 in WB) for Tra-1-60, SSEA-1 and with secondary antibody AlexaFluor 488 goat anti-mouse IgG (1:200 in WB) for SSEA-4 during 30 min in dark. Cells were washed twice with WB (for extracellular markers) and with PW (for intracellular markers) and analyzed in a CyFlow® space (Partec GmbH) instrument, registering 10,000 events/sample.

3.2.3.3 Quantitative RT-PCR

Total RNA was extracted using the High Pure RNA Isolation Kit (Roche), and reverse transcription was performed with High Fidelity cDNA Synthesis Kit (Roche), following manufacturer's instructions. Relative quantification of gene expression was performed using LightCycler 480 Probes Master (Roche) in 20 µL reactions with 50 ng cDNA template and 20x concentrated TaqMan probes. The reactions were performed in 96-well plates using a LightCycler 480 Real-Time PCR System (Roche). Cycle threshold (Ct's) were determined by LightCycler 480 Software. All data was analyzed using the 2-ΔΔCt method for relative gene expression analysis. Changes in gene expression were normalized to GAPDH gene expression as internal control. The TaqMan probes used for human ISL1, KDR, GATA4, NKX2.5, TNNT2, VCAM1, MYH7, MYL2, MYL7, HCN4, CACNA1C, ACTC1, MYH6 and GAPDH genes were HS00158126_m1, HS00911699_m1, Hs00171403_m1, Hs00231763_m1, Hs00165960_m1, Hs01003372_m1, Hs01110632_m1, Hs00166405_m1 and Hs99999905_m1, Hs00221909_m1, Hs00175760_m1, Hs00167681_m1, Hs00606316_m1, Hs01101425_m1, respectively.

3.2.3.4 Transmission electron microscopy (TEM)

Monolayers and aggregates of human PSC-CMs were fixed in 2% (v/v) glutaraldehyde in 0.1 M HEPES buffer (pH 7.4) for 20 min, washed in PBS and stored in 1% (v/v) glutaraldehyde in PBS until analyses. For TEM analyses, cell aggregates were immersion fixed in a mixture of 2% glutaraldehyde and 2% paraformaldehyde in 50 mM HEPES. Subsequently, the samples were washed once in 100 mM HEPES, twice in DPBS, and twice in double-distilled water before postfixation with osmium tetroxide (1% (v/v) in water, 2 h on ice). After several washes in water, the samples were contrasted *en-bloc* with aqueous uranyl acetate (1% (w/v), 2 h on ice), washed several times in distilled water, dehydrated in a graded series of ethanol, infiltrated in epon 812 (epon/ethanol mixtures: 1:3, 1:1, 3:1, 1 h each, pure epon overnight, pure epon 6 h), and embedded in flat embedding molds. Finally, the samples were cured at 65°C in the oven. 2D-Monolayers were fixed with 2% (v/v) glutaraldehyde in 100 mM HEPES for 1 h, and washed in 100 mM HEPES and distilled water. Postfixation, *en-bloc* contrasting, dehydration, epon infiltration and curing were performed as described above. After curing, the samples were dissected into small blocks and mounted on epon dummy blocks. Ultrathin sections of aggregates and monolayers were cut on a Leica UC6 ultramicrotome using a diamond knife. Sections were collected on formvar-coated slot grids, stained with lead citrate and uranyl acetate as described in the literature(Venable and Coggeshall, 1965) and analysed on a FEI Morgagni 268 at 80 kV. Images were taken with an Olympus MegaView III using the iTEM software.

3.2.3.5 Determination of the percentage of binucleated cells

To determine percent of binucleated cells, the total number of cells in a section was determined using ImageJ software (National Institutes of Health); specifically, the total number of nuclei was counted under the Hoechst staining. Number of cells, possessing two nuclei, was divided by the total number of cells in section,

resulting in binucleated cell percentage determination. For each condition, at least 10 different section, were evaluated.

3.2.3.6 Measurement of mitochondrial membrane potential

Differences in membrane potential, were evaluated using Assay Kit MitoView™ 633 (Biotium, Inc., California, USA) following manufacturer's instructions. This kit contains the far-red fluorescent MitoView 633 mitochondrial dye for profiling changes in mitochondrial membrane potential, in intact cells. After incubation with the dye for 1 h, cells were analyzed by flow cytometry.

3.3 Culture and metabolism characterization techniques

3.3.1 Cells concentration and viability

Cell concentration and viability were determined by cell counting in a Fuchs-Rosenthal haemacytometer (Brand, Wertheim, Germany) using the trypan blue exclusion method (0.1% (v/v) solution in PBS).

3.3.2 Quantification of extracellular metabolic concentration

Concentrations of glucose, glutamate, glutamine and lactate in culture supernatants were measured in an YSI 7100 Multiparameter Bioanalytical System (YSI Life Sciences, Dayton, OH). The remaining amino acids were determined by HPLC using the Waters AcQ.Tag Amino Acid Analysis Method (Waters, Milford, MA), as described elsewhere (Carinhas et al., 2010). Ammonia concentration was measured using an enzymatic kit (Cat. No. AK00091, NZYTech, Portugal) based on the spectrophotometric detection of $NADP^+$ formed by glutamate dehydrogenase activity.

3.3.3 Extraction of intracellular metabolites

Metabolic quenching and extracting protocols were adapted from Dietmair (Dietmair et al., 2010). Firstly, culture supernatants were removed and cell monolayers were immediately washed with ice-cold 0.9% (w/v) NaCl. After the saline solution was removed, each plate was completely dipped in liquid N_2. To extract intracellular metabolites from the frozen monolayers, 2 mL of 50% (v/v) ice-cold acetonitrile were added to each well. The content of each well was transferred to tubes, snap-frozen in liquid N_2 and kept at -80°C until analysis.

3.3.4 Derivatization

Cell extract samples were thawed on ice and centrifuged at 15000g for 10 min, 4°C. The supernatants were transferred to tubes and dried by vacuum centrifugation overnight, whilst the pellets were discarded. To determine extracellular metabolite labelling enrichment, supernatant samples were also thawed and dried by vacuum centrifugation overnight. After lyophilisation, derivatization was performed according to protocols previously described (Ahn and Antoniewicz, 2011; Hofmann et al., 2008).

Amino acids, lactate and TCA intermediates were derivatized to their correspondent *tert*-butyldimethylsilyl derivatives by adding 20 µL of a 10 mg/mL O-methylhydroxylamine hydrochloride (Sigma-Aldrich, DE) solution in pyridine (Sigma-Aldrich, DE). The reaction was allowed to proceed for 2 h at 40°C in a heating block, after which 40 µL of N-methyl-N-*tert*-butyldimethylsilyl-trifluoroacetamine (MBDSTFA, Aldric, DE) were added. After 1 h at room temperature, the reaction vessel was left at 60°C for an additional 1 h (Hofmann et al., 2008). For phosphoenolpyruvate (PEP) and 3-phosphoglyceric acid (3PG), samples were incubated at room temperature with 20 µL N,O-Bis(trimethylsilyl)trifluoroacetamide (BSTFA; Supelco Analytical, DE), 10 µL Chlorotrimethylsilane (TMCS; Aldrich, DE) and 20 µL acetonitrile during 30 min (Hofmann et al., 2008). For the derivatization of glucose, a third protocol was applied: 50 µL of a 20 mg/mL O-methylhydroxylamine hydrochloride (Sigma-Aldrich, DE) solution in pyridine (Sigma-Aldrich, DE) was added. Samples were kept at 90°C for 1h. Afterwards, 100 µL of propionic anhydride were added and the reaction allowed to continue during another 30 min. Finally, samples were vacuum dried and solubilized in 100 µL ethyl acetate (Ahn and Antoniewicz, 2011). After completing the derivatization procedures, all samples were centrifuged for 1 min at 1000 x g and supernatants transferred to GC-MS glass vials.

3.3.5 GC-MS Analysis

The EI mode (70eV) mode of a QP2010 mass spectrometer (Shimadzu, Japan) was used to analyze the samples. The temperature of the ionic source and the interface connecting to the column was 250°C. GC was performed on a HP-5MS column (30 m, 0.25 mm i.d., composed of dimethylpolysiloxane with 5% phenyl groups, 0.25 mm film thickness; Agilent Technologies). Samples were injected in splitless or split (1:10, 1:15, 1:20 or 1:50, depending on the sample and the history of previous signal saturations) mode, using helium as carrier gas at an inlet pressure of 600 kPa. Automatic injections were carried out by an AOC-5000 Plus autosampler (Shimadzu, Japan), with an injection volume of 1 µL and injector temperature set at 250°C. The protocol for TCA intermediates, lactate, amino acids, PEP and 3PG consisted in starting with an oven temperature of 120°C, holding for 2 min, linearly increasing temperature at 3°C/min until 290°C, and finally holding for 3 min as described in (Neves, 1987). For glucose a different method was used: starting with an oven temperature of 80°C, holding for 2 min, linearly increasing the temperature at 15°C/min until 280°C and holding for 6 min, as described in Ahn and Antoniewicz (2011).

The obtained spectra were analyzed and integrated using GC-MS Solution software version 2.50 SU1 (Shimadz, Japan). Metabolites were identified by comparison with standard solutions prepared in water and a previously constructed metabolite library (Duarte et al., 2014). Mass Isotopomer Distributions (MID) were calculated after spectra integration and corrected for natural isotope abundance. All ions (M, M+1, M+n) were measured, where M is the mass/charge ratio of the unlabeled derivatized fragment and n is the number of labelled carbons.

3.3.6 Metabolic network and nonstationary ^{13}C-MFA

A reaction network including all major pathways of central carbon metabolism and a lumped reaction for biomass formation was built. The cell biomass composition considered is a compilation from different sources as shown in Sheikh et al 2005. A cell dry weight of 297 pg was determined, allowing to compute all metabolite coefficients included in the lumped biomass reaction. Metabolic precursor requirements for virus biomass formation were omitted based on an analysis of virus composition and virus production from infection cultures. The negligible impact of viral production in material balances of producer animal cells has been studied before (Carinhas et al., 2011).

Extracellular transport rates were considered reversible to allow equilibration with the extracellular pools, except for essential nutrients (glucose, glutamine, essential amino acids). Metabolically derived CO_2 was allowed to exchange freely with the extracellular compartment so that both labelled and unlabeled CO_2 was available for use in carboxylation reactions (Metallo et al., 2012). Cofactor balances were not considered as in common practice. Carbon atom transitions are presented at table 4.2.

To perform non-stationary ^{13}C-MFA of parallel labeling experiments, publicly availably software package for MATLAB, INCA (isotopomer network compartmental analysis) was used (Young, 2014). Mass and material balance equations are generated and simulated, based on the user-defined metabolic network structure and experimental datasets. The algorithm for flux estimation uses the "elementary metabolic unit" (EMU) method and is completely described elsewhere (Antoniewicz et al., 2007; Young et al., 2008). To find a global minimum, at least 10 restarts with random initial values were performed (Crown and Antoniewicz, 2013).

Table 3.1: Complete metabolic network model used for nonstationary ^{13}C-MFA. Coefficients in the lumped biomass formation reaction represent the nmol/10^6 cells.

	Glycolysis
R1	G6P (abcdef) ↔ F6P (abcdef)
R2	F6P (abcdef) → FBP (abcdef)
R3	FBP (abcdef) ↔ DHAP (cba) + GAP (def)
R4	DHAP (abc) ↔ GAP (abc)
R5	GAP (abc) ↔ 3PG (abc)
R6	3PG (abc) ↔ PEP (abc)
R7	PEP (abc) → Pyr.c (abc)
	Pentose-phosphate pathway
R8	G6P (abcdef) → P5P (bcdef) + CO_2 (a)
R9	P5P (abcde) + P5P (pqrst) ↔ GAP (rst) + S7P (pqabcde)
R10	S7P (abcdefg) + GAP (xyz) ↔ E4P (defg) + F6P (abcxyz)
R11	E4P (abcd) + P5P (pqrst) ↔ GAP (rst) + F6P (pqabcd)
	Lactate and alanine accumulation
R12	Pyr.c (abc) ↔ Lac (abc)

R13 Pyr.c (abc) ↔ Ala (abc)

TCA cycle and pyruvate cycling

R14 Pyr.m (abc) → AcCoA.m (bc) + CO_2 (a)

R15 Pyr.m (abc) + CO_2 (d) → OAA (abcd)

R16 OAA (abcd) + AcCoA.m (ef) → Cit (dcbfea)

R17 Cit (abcdef) ↔ AKG (abcde) + CO_2 (f)

R18 AKG (abcde) → SucCoA (bcde) + CO_2 (a)

R19 SucCoA (abcd) ↔ Suc (abcd)

R20 Suc (abcd) ↔ Fum (abcd)

R21 Fum (abcd) ↔ Mal (abcd)

R22 Mal (abcd) ↔ OAA (abcd)

R23 Mal (abcd) → Pyr.m (abc) + CO_2 (d)

Lipid precursor generation

R24 Cit (dcbfea) → OAA (abcd) + AcCoA.c (ef)

Amino acids metabolism

R25 Gln (abcde) → Glu (abcde)

R26 AKG (abcde) ↔ Glu (abcde)

R27 Asn (abcd) ↔ Asp (abcd)

R28 Asp (abcd) ↔ OAA (abcd)

R29 3PG (abc) → Ser (abc)

R30 Ser (abc) → Pyr.c (abc)

R31 Ser (abc) ↔ Gly (ab) + C1 (c)

R32 Glu (abcde) ↔ Pro (abcde)

R33 Val (abcde) + CO_2 (f) → Suc (dcef) + CO_2 (a) + CO_2 (b)

R34 Ile (abcdef) + CO_2 (g) → Suc (bcdg) + AcCoA.m (ef) + CO_2 (a)

R35 Leu (abcdef) + CO_2 (g) → AcCoA.m (bc) + AcCoA.m (de) + AcCoA.m (gf) + CO_2 (a)

R36 Thr (abcd) → AcCoA.m (cd) + Gly (ab)

R37 Phe (abcdefghi) → Tyr (abcdefghi)

R38 Tyr (abcdefghi) → Fum (defg) + AcCoA.m (bc) + AcCoA.m (hi) + CO_2 (a)

R39 Met (abcde) + Ser (fgh) + CO_2 (i) → Suc (bcdi) + Cys.snk (fgh) + CO_2 (a) + C1 (e)

R40 Lys (abcdef) → CO_2 (a) + CO_2 (f) + AcCoA.m (bc) + AcCoA.m (de)

R41 His (abcdef) → Glu (edcba) + C1 (f)

R42 Arg (abcdef) → Glu (abcde) + Urea.snk (f)

R43 Glu (abcde) + CO_2 (f) → Arg (abcdef)

Intracellular transport

R44 Pyr.c (abc) ↔ Pyr.m (abc)

Extracellular transport

R45 CO_2 (a) ↔ CO_2.ext (a)

R46 Glc.ext (abcdef) → G6P (abcdef)

R47 Lac (abc) ↔ Lac.ext (abc)

R48 Ala (abc) ↔ Ala.ext (abc)

R49 Gln.ext (abcde) → Gln (abcde)

R50 Glu (abcde) ↔ Glu.ext (abcde)

R51 Ser.ext (abc) ↔ Ser (abc)

R52 Gly (ab) ↔ Gly.ext (ab)

R53 Pro.ext (abcde) ↔ Pro (abcde)

R54 Val.ext (abcde) → Val (abcde)

R55 Ile.ext (abcdef) → Ile (abcdef)

R56 Leu.ext (abcdef) → Leu (abcdef)

R57 Thr.ext (abcd) → Thr (abcd)

R58 Phe.ext (abcdefghi) → Phe (abcdefghi)

R59 Tyr.ext (abcdefghi) → Tyr (abcdefghi)

R60 Met.ext (abcde) → Met (abcde)

R61 Lys.ext (abcdef) → Lys (abcdef)

R62 His.ext (abcdef) → His (abcdef)

R63 Arg.ext (abcdef) ↔ Arg (abcdef)

Biomass formation

R64 162.6*Ala + 104.606*Glu + 87.262*Gln + 17.34*Gly + 144.443*Ser + 154.47*Lys + 152.84*Leu + 87.8*Ile + 102.167*Arg + 127.857*Asp + 104.6*Thr + 112.736*Val + 37.398*Met + 59.349*Phe + 49.32*Tyr + 38.75*His + 84.823*Pro + 78.048*Asn + 80.216*G6P + 63.1159*P5P + 65.0942*C1 + 33.063*DHAP + 683.4620*AcCoA.c = 1 Biomass

3.4 Statistical analysis

All statistical analyses were performed using GraphPad Prism version 5 (GraphPad Software Inc.) Values are represented as mean±standard deviation. Statistical significance was evaluated using Student's t test with Welch's correction. Values of $P<0.05$ were considered statistically significant.

4. RESULTS AND DISCUSSION

4.1 Metabolic characterization of 1G3 cells for AdV production

In the first part of this thesis we studied the impact of adenovirus infection on the metabolism of 1G3 cells resorting to parallel ^{13}C tracer experiments with [1, 2-^{13}C]glucose and [U-^{13}C]glutamine. These two tracer substrates have been identified as the best combination to estimate the fluxes through central carbon metabolism of mammalian cells (Metallo et al., 2009). Cells were infected in two settings: i) during exponential growth (EG) and ii) during growth-arrested (GA) conditions, and changes in metabolism were compared to mock-infected cultures (Figure 4.1). Cells cultured in DMEM supplemented with 1% FBS at a confluency of 70% were in exponential growth (EG) before infection, while cells cultured at a confluency above 95% and kept 36 h without FBS were in growth-arrested (GA) conditions before infection. The labeled substrates were provided 4 h post infection (hpi). Immediately after the introduction of ^{13}C-labeled glucose/glutamine, a time series of samples were collected to follow the incorporation of ^{13}C from both substrates into intracellular and extracellular metabolites during 24 h by GC-MS analysis.

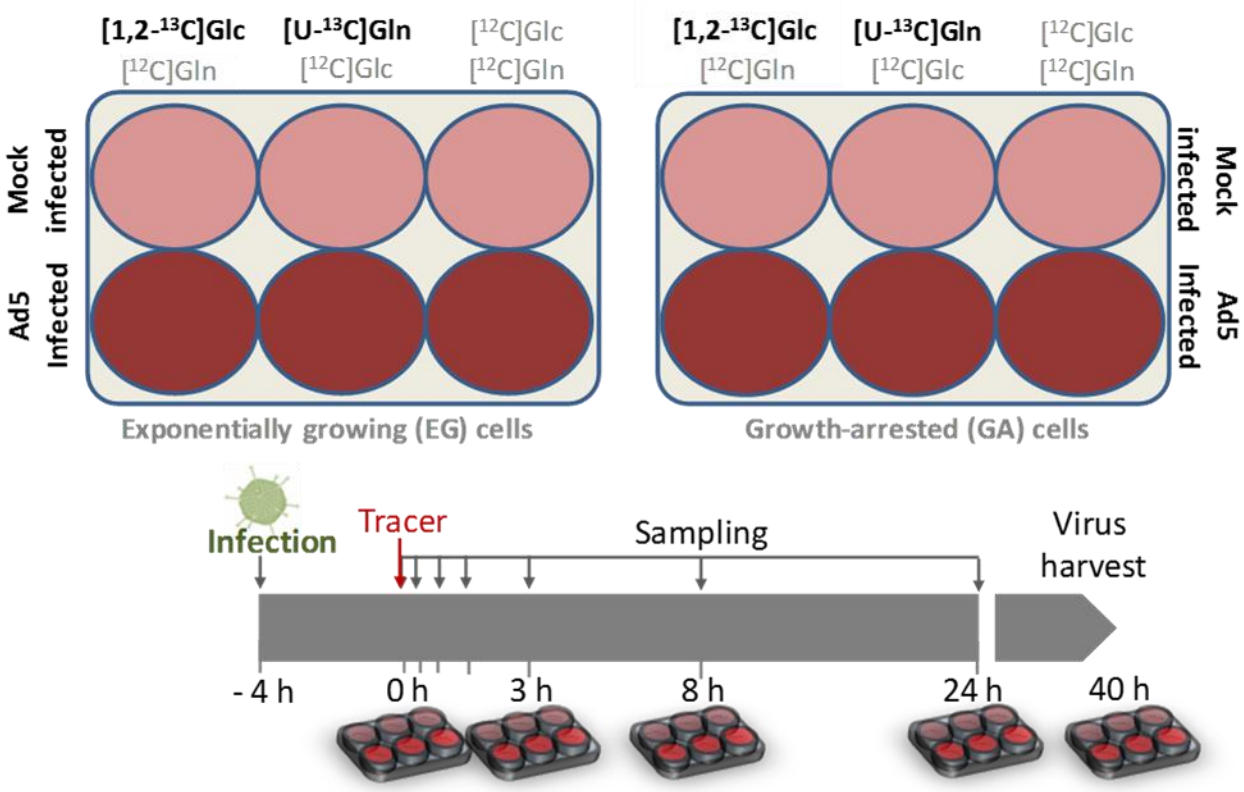

Figure 4.1: Experimental setup for ^{13}C tracer cultures of 1G3 cells infected or mock-infected with Ad5, during exponential growth or growth-arrested conditions.

4.1.1 Cell density profile and viral particles production

Figure 4.2 A shows the cell growth profiles of infected and mock-infected cultures. Mock-infected cells in the exponential growth phase had a maximum specific rate of μ_{max}= 0.014 h^{-1}, which corresponded to a doubling time of about 50 hs. Infected 1G3 cells did not grow and the cell viability started to decrease about 30 hpi. From Figure 4.2 B we can confirm that 1G3 cells were in fact growth-arrested since the cell density was maintained during the analysis time window. In these conditions, the decrease in cell viability of infected cultures occurred later (about 40 hpi) when compared to cells infected during exponential growth. This might be due to the lower replication of adenovirus in growth-arrested cultures, as the production of infectious particles per cell was 4.7 fold higher for EG than GA after 48 hpi: 1019 ± 169 versus 218 ± 49 i.p./cell, respectively (Figure 4.2 C).

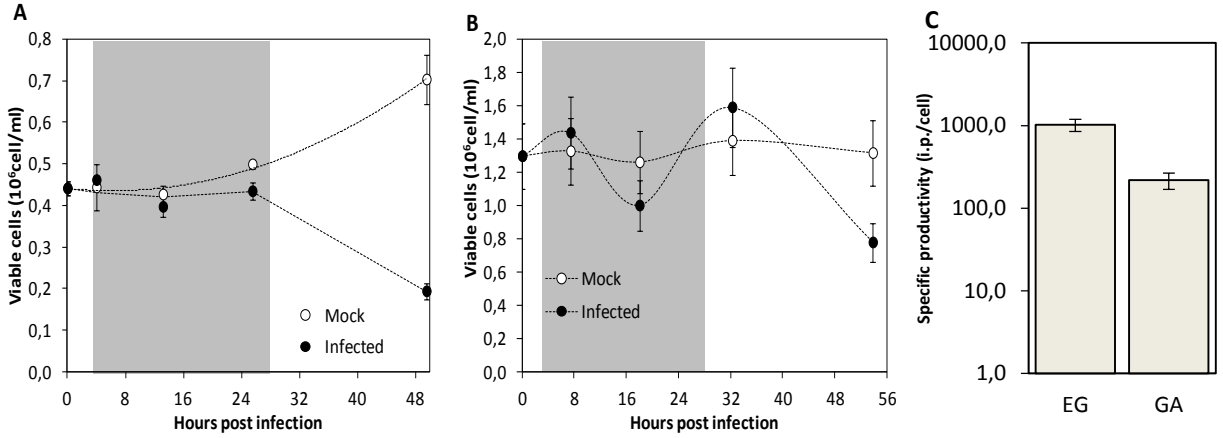

Figure 4.2: Cell growth profiles of 1G3 cells mock-infected and infected with an Ad5 viral vector. A) Exponential growth; **B)** growth arrest. The grey area corresponds to the 24h period of label monitoring; **C)** Specific viral productivity of 1G3 cell lines, under EG and GA conditions.

4.1.1.1 Metabolism characterization under Ad5 infection.

Transport rates in non-infected EG and GA cultures

The concentration profiles of metabolites in the culture supernatant were used to calculate specific consumption/production rates (Figure 4.3). In general, nutrient uptake rates were higher in EG than in GA cultures, which can be explained by the higher energy needs during exponential cell growth. In particular, glucose consumption and lactate production were 2-fold higher in EG than GA conditions. In both conditions the cells had a high lactate production to glucose consumption ratio, which was higher for EG cultures ($Y_{Lac/Glc}$=1.98; Table 4.1). This is in agreement with what has been observed for other cultured mammalian cell lines, including cancer cell lines, that can generate ATP at higher rates by increasing the glycolytic flux (despite the lower efficiency; less ATP molecules produced per glucose consumed), allowing them to divert glycolytic intermediates for biomass formation. As for the majority of mammalian cell lines

in culture, glutamine is the most consumed amino acid. Its uptake rate was also higher during exponential growth (Figure 4.3), which correlates with higher secretion rates of glutamate, alanine and ammonia compared to growth-arrested conditions. For the remaining 14 analyzed amino acids, we observed statistically significant differences in proline production and isoleucine and cysteine consumption rates, being all higher in EG.

Table 4.1: Molar ratio $Y_{Lac/Glc}$

	EG		GA	
	Mock	Inf	Mock	Inf
$Y_{Lac/Glc}$	1.98	2.08	1.68	1.85

Impact of infection on transport rates

As a major response to adenovirus infection, 1G3 cells increased the consumption of glucose and the secretion of lactate (as well as the $Y_{Lac/Glc}$ ratio) for both EG and GA conditions (Figure 4.3 and Table 4.1). Most viruses induce aerobic glycolysis (also known as the Warburg effect) in the host cell's metabolism (Delgado et al., 2010; Sanchez and Lagunoff, 2015). It was recently shown that the expression of the viral gene E4ORF1 is necessary for adenovirus induced upregulation of glycolysis by activation of Myc, allowing maximal adenovirus replication (Thai et al., 2014) Interestingly, both glucose and lactate transport rates increased more under GA than under EG conditions in relation to mock-infected cultures (Figure 4.3). In agreement, glutamine consumption increased significantly upon infection for GA but not for EG cultures, which correlates with a higher impact on alanine and ammonia production rates observed during infection of GA cultures. Glycine secretion decreased upon infection in both conditions, with a stronger effect for GA cultures. The rates of all remaining amino acids increased upon infection, with the majority of them (Ser, Thr, Arg, Cys, Val, Met, Ile, Leu, Lys) also increasing more during GA conditions. Since in GA cultures cells are not growing, all observed changes in amino acid metabolism after viral infection are caused by switching cell machinery to viral production. The virus infection impacted more the metabolism of cells in growth-arrested conditions.

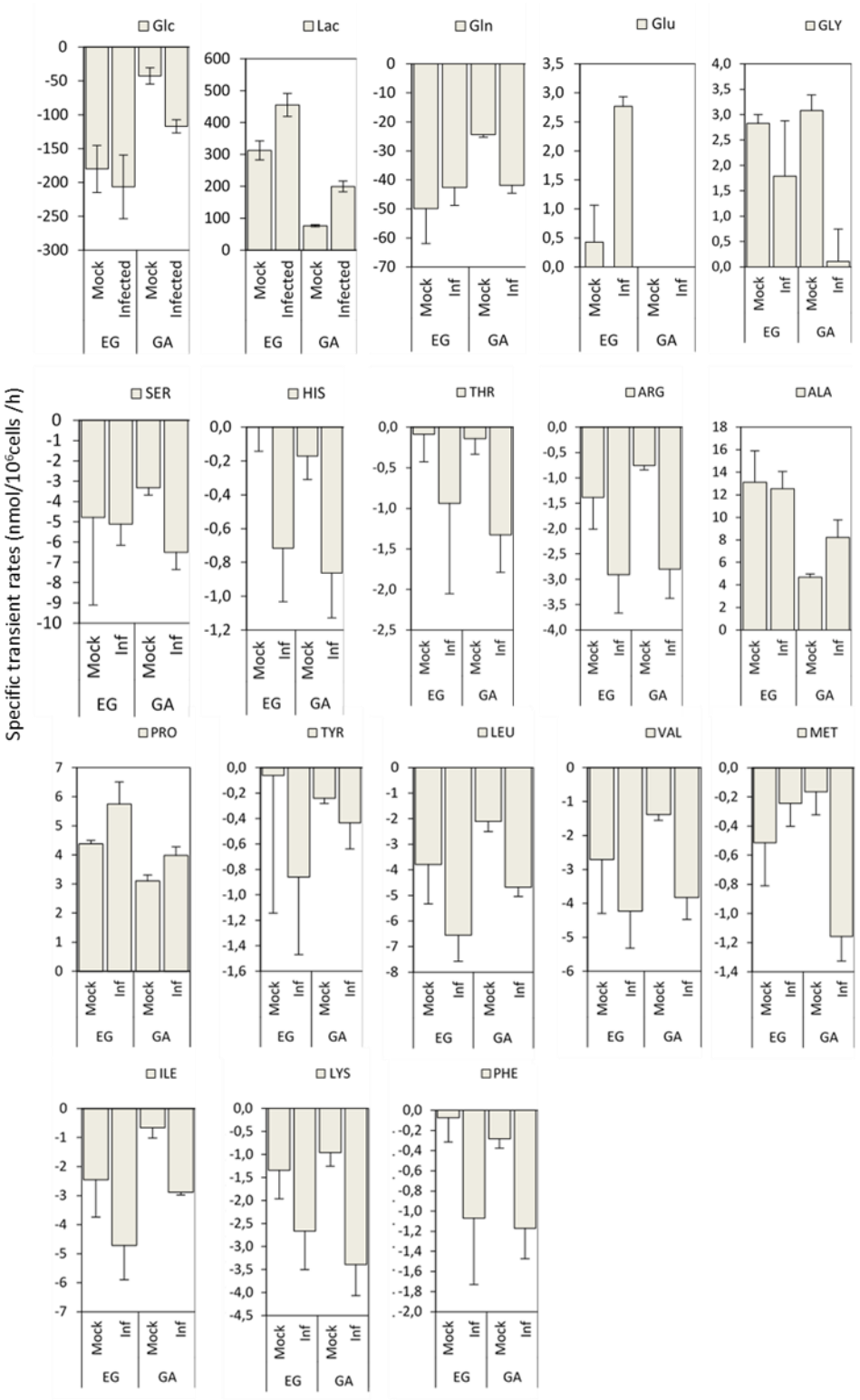

Figure 4.3: Specific uptake/secretion rates of amino acids for mock-infected and Ad5-infected 1G3 cells, under GA and EG conditions.

4.1.2 ^{13}C-Labeling dynamics of intracellular metabolites from [1, 2-^{13}C]glucose tracer

[1, 2-^{13}C]glucose is one of the best tracers for glycolysis and PPP pathway flux estimation via non-stationary ^{13}C-MFA (Ahn and Antoniewicz, 2011), and has been widely used in metabolic studies of bacterial and mammalian cells (Ahn and Antoniewicz, 2013; Leighty and Antoniewicz, 2012). For mock-infected EG cells, the dynamic profiles of ^{13}C labeling in intracellular metabolites after [1, 2-^{13}C]glucose addition are shown in Figure 4.4. Overall, the labeling patterns of intracellular metabolites under exponential growth and growth arrest, as well as after infection, were similar in these cells. In general, glycolytic intermediates displayed a higher speed of ^{13}C incorporation compared with TCA cycle intermediates, largely due to the higher metabolic rate of glycolysis and occurrence of dilution of TCA metabolites by amino acids pools (Carinhas et al., submitted). In agreement, while most metabolites did not approach isotopic steady state within 24h, the mass isotopomer distributions (MIDs) of phosphoenolpyruvate (PEP) and 3-phosphoglycerate (3PG) were relatively constant at 30min, 8h and 24 h, confirming that metabolic and isotopic steady state have been reached. The composition of glucose in the medium was 84% [1, 2-^{13}C]glucose and 16% natural glucose, corresponding to a maximum expected labeling of glycolytic intermediates of 44% which is in agreement with the measured values for PEP and 3PG. After cellular uptake, each molecule of glucose is converted to Glucose 6-phosphate (G6P), which in turn can be converted to Fructose 6-phosphate (F6P) down the glycolytic pathway, or fueled along the pentose phosphate pathway (PPP) to generate pentose phosphates, where the first ^{13}C atom is lost as CO_2 (Figure 4.6). In this way, if glucose is processed exclusively through glycolysis, only unlabeled PEP and 3PG as well as respective isotopomers with two labelled atoms will be produced, whereas an active PPP with both oxidative and nonoxidative branches will add isotopomers with one, two or three ^{13}C atoms. In this study, the very low occurrence of M1 and M3 isotopomers in glycolytic intermediates (Figure 4.4) indicates a low percentage of pentose phosphates is being recycled back to glycolysis through the nonoxidative PPP branch. This cycling activity is important to recover glycolytic intermediates when the need for reducing power (NADPH) exceeds the need for pentose precursors for nucleotide synthesis. The formation of one carbon (C1) units from serine´s decarboxylation to glycine is also a requisite for nucleotide synthesis. In the current study, 1G3 cells consumed serine from the medium and secreted glycine as part of C1 units metabolism (Figure 4.3). This behavior has been also observed previously in other studies (Carinhas et al., submitted; Carinhas et al., 2013; Duarte et al., 2014). As shown in Figure 4.4, ^{13}C incorporation in serine and glycine indicates that glucose was also a source of C1 units. While serine was composed of 6% M1 and 3% M2 isotopomers, only M1 glycine was observed in (8%), which can be explained by the fact that the third position carbon in serine, which is lost during conversion to glycine, corresponds to the first labeled carbon in glucose.

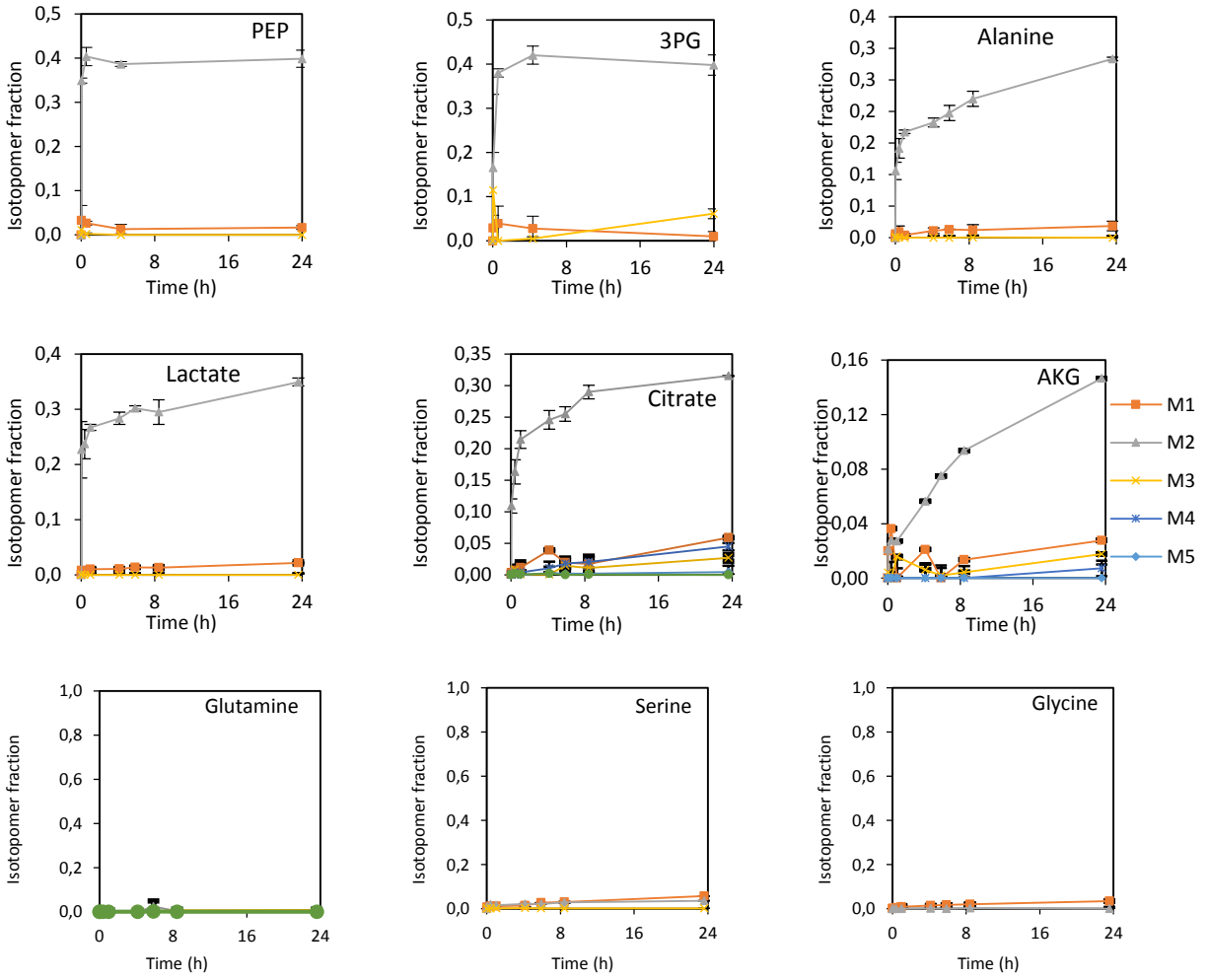

Figure 4.4: Time profiles of isotopic labeling of intracellular metabolites after the introduction of [1,2-^{13}C]glucose in mock-infected EG condition. Fractions of labeled mass isotopomers were determined from the measured mass isotopomer distribution, after correction for natural isotope abundances. The composition of glucose in the medium was 80% [1, 2- 13C]glucose and 20% natural glucose.

While AKG displayed a slow dynamics of label incorporation, citrate showed a noteworthy faster and more complete label incorporation compared with the other measured TCA cycle intermediates, indicating loss of labeled carbon from glucose from the TCA cycle (Figure 4.4). This discrepancy can be clearly seen in Figure 4.5, where the percentage of labeled intracellular metabolites from glucose is shown. Each molecule of citrate, PEP and 3PG possesses at minimum one labeled carbon atom derived from glucose. It should be also mentioned that there wasn´t ^{13}C incorporation into glutamine from [1, 2-^{13}C]glucose, indicating inactivity of glutamine synthetase.

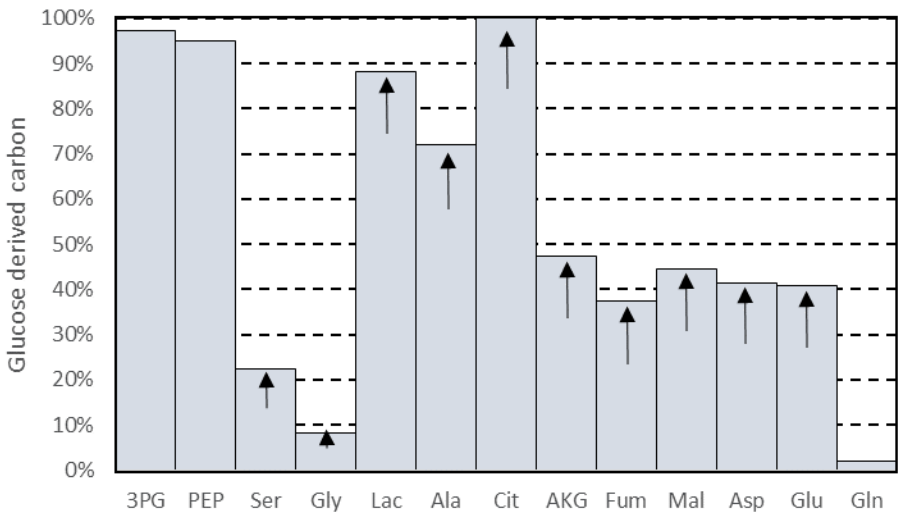

Figure 4.5: Percentage of labeled intracellular metabolites from glucose during exponential growth (mock infection) conditions. Values correspond to the sum of all mass isotopomers (excluding M0) at 24h, normalized by ^{13}C enrichment in extracellular glucose and multiplied by 2. Arrows indicate that isotopic steady-state has not been reached.

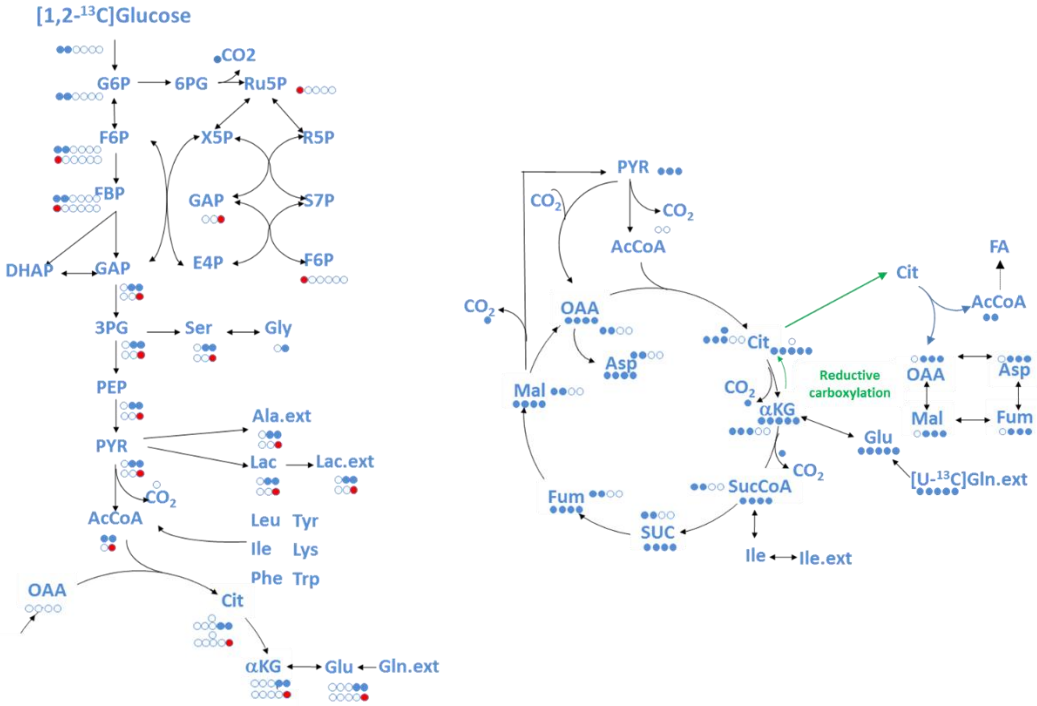

Figure 4.6: Atom transitions from [1, 2-^{13}C]glucose and [U-^{13}C]glutamine tracers. Blue atoms designate ^{13}C atoms. Red atoms designate ^{13}C atoms from one round of PPP activity. White atoms designate ^{12}C atoms.

4.1.3 ^{13}C-Labeling dynamics of intracellular metabolites from [U-^{13}C]glutamine

[U-^{13}C]glutamine was recently identified as an optimal tracer for analysis of the TCA cycle in bacterial as well as mammalian cells, by allowing a rapid incorporation of carbon atoms into TCA cycle metabolites. Figure 4.7 shows the labeling profiles of intracellular metabolites after addition of [U-^{13}C]glutamine under the exponential growth condition. Overall, the labeling patterns of intracellular metabolites under exponential growth and growth arrest, as well as after infection, were similar in these cells. The extracellular glutamine distribution was 86% [U-^{13}C]glutamine and 14% natural glutamine, which was similar to the intracellular Gln pattern, demonstrating that 1G3 cells irreversibly metabolize Gln to Glu via glutaminase (GLS) and have no glutamine synthetase activity (GS). TCA cycle intermediates and related metabolites, including glutamine (Gln), glutamate (Glu), α-ketoglutate (AKG), citrate (Cit), malate (Mal), aspartate (Asp) and fumarate (Fum) seemingly reached isotopic steady state by 8 hs after tracer addition.

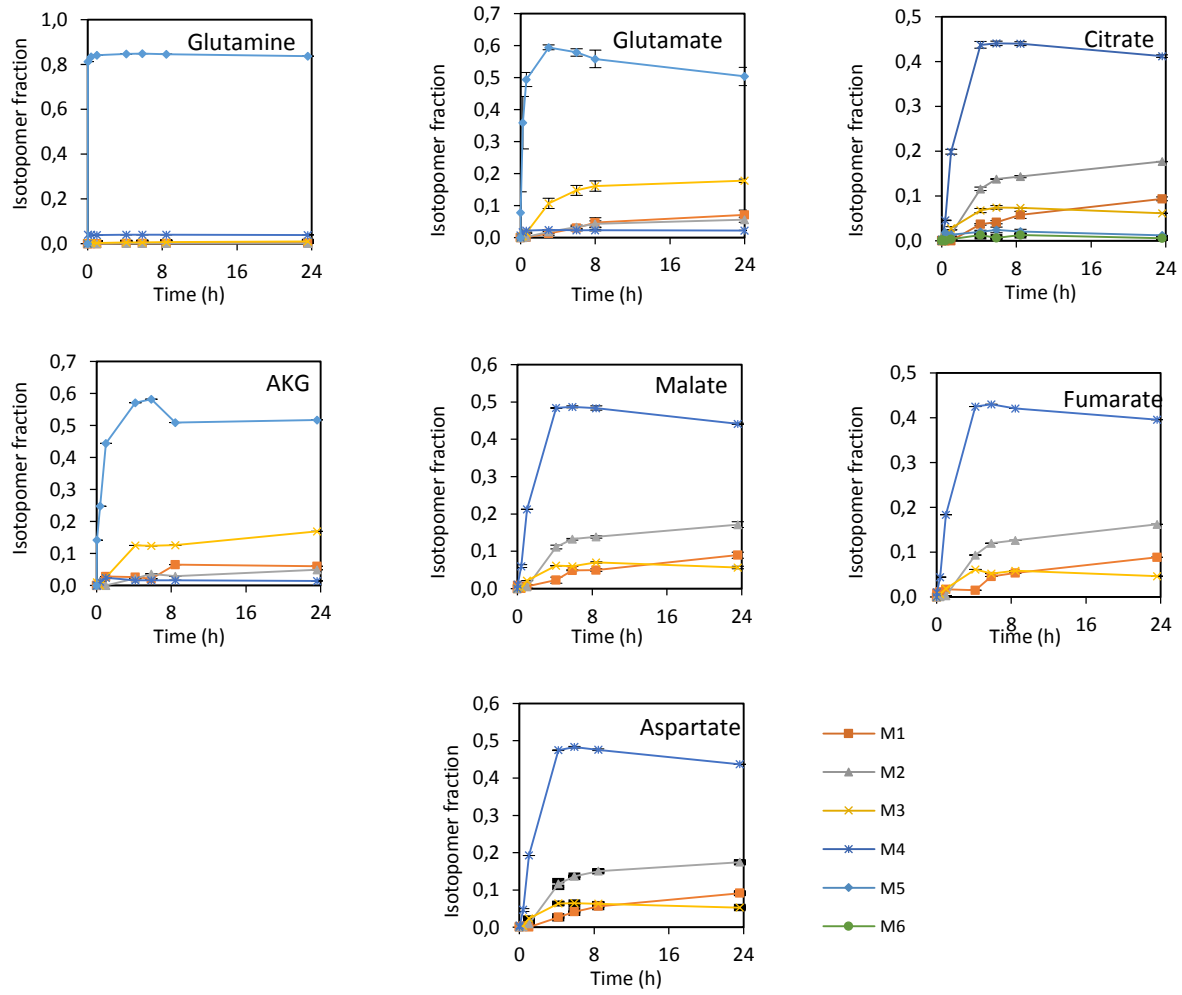

Figure 4.7: Time profiles of isotopic labeling of intercellular metabolites for mock-infected EG condition, after the introduction of [U-13C]glutamine. Fractions of labeled mass isotopomers were determined from the measured mass isotopomer distribution, after correction for natural isotope abundances. The composition of glutamine in the medium was 86% [U-^{13}C]glutamine and 14% natural glutamine.

The steady state total labeled fractions of intracellular metabolites were 1.0 for Gln, 0.94 for Glu, 0.86 for citrate, 0.92 for AKG, 0.86 for Mal, 0.78 for Fum and 0.85 for Asp (Figure 4.8). The measured percentages of labeled metabolites from glutamine for all TCA cycle intermediates except citrate were higher than the respective percentages derived from labeled glucose.

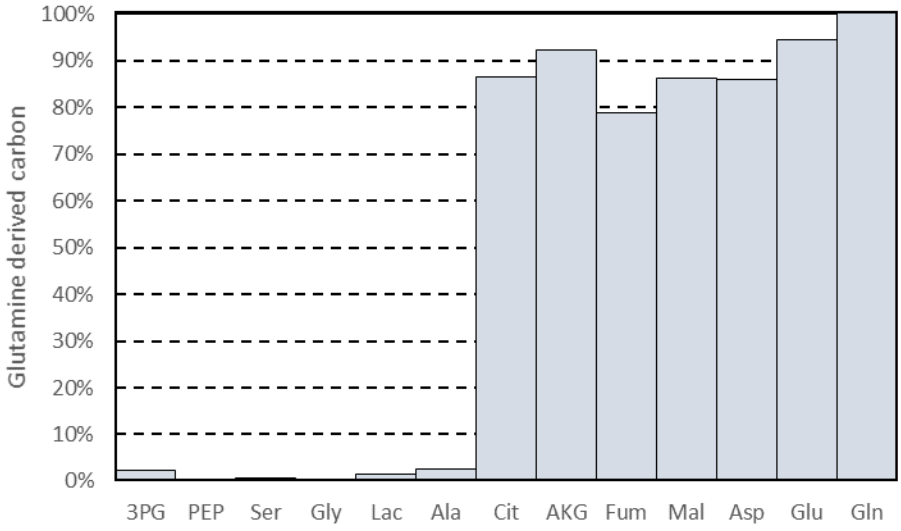

Figure 4.8: Percentage of labeled intracellular metabolites from glutamine during exponential growth (mock infection). Values correspond to the sum of all mass isotopomers (excluding M0) at 24 h, normaliazed by ^{13}C enrichement in extracellular glutamine.

The MID profiles of intracellular 3PG and PEP did not show significant labeling from [U-^{13}C]glutamine (<3%), even after 24 h, suggesting that the gluconeogenesis pathway was not active in 1G3 cells (Figure 4.9).

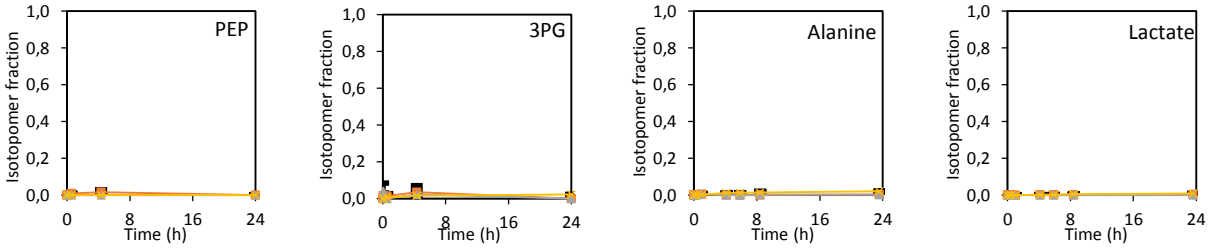

Figure 4.9: **Time profiles of isotopic labeling in PEP, 3PG, Alanine and lactate after the introduction of [U-13C]glutamine under exponential growth conditions.**

It was possible to detect M3 isotopomers of Fum, Mal and Aspartate. Appearance of M3 isotopomers in TCA cycle intermediates indicate activity of i) pyruvate cycling though ME and pyruvate carboxylase (PC), or ii) reductive carboxylation of AKG to citrate via isocitrate dehydrogenase (IDH) and aconitase, followed

by citrate transfer to the cytosol and ATP-citrate lyase (ACL) activity, which in turn generates cytosolic AcCoA for biosynthesis of fatty acids (Carinhas et al., submitted). The MID profile of citrate can help elucidate if one or both of the pathways described above are active. The observation of a low M5 fraction (around 1%) indicates low activity of reductive carboxylation in 1G3 cells. At the same time, the almost negligible percentage of the M6 isotopomer, accompanied by low alanine and lactate labeling, suggests ME is not very active. However, this is contradicted by integration of labeling data with measured influx and eflux metabolic rates, which was used to estimate the intracellular flux maps for the different conditions (see below). From this analysis, it can be seen that ME is quite active in these cells, and the low percentage of citrate M6 can be explained by an extremely large glycolytic rate compared to the anaplerotic flux from glutamine consumption, resulting in the prevalence of unlabeled pyruvate which in turn results in unlabeled lactate and alanine and incompletely labeled citrate.

4.1.4 Metabolic network, model representation and flux estimation.

Metabolic fluxes were estimated for each culture condition based on the the transport rates and combined MID data from parallel [1, 2-^{13}C]glucose and [U-^{13}C]glutamine labeling. At each timepoint, samples were collected from 2 independent wells and analyzed separately. Thus, experimental errors for MID measurements were determined and used for flux estimation. However, for some metabolites, it was not possible to correctly integrate duplicate MS spectrum. Whenever the measured error was not available or was below 1 mol%, a value of 1 mol% was used. For all scenarios, reasonable fittings were obtained (Annexes 2, Figure 7.2-7.3), but the weighted sum of squared residuals (SSR) was slightly out of the expected 95% confidence interval in all cases. This is often the case for biological experiments (Wiechert et al., 1997), particularly in complex designs involving numerous datapoints from labeling time courses. We now compare flux distributions between exponential growth (EG) and growth-arrested (GA) conditions, and particularly the impact of AdV5 infection in each case (Figure 4.10; Table 7.1). Under exponential growth condition, cells possessed higher glycolysis comparing with growth arrest condition (305.57 ± 1.52 nmol/10^6 cells/h, for EG mock-infected, and 81.4 ± 0.79 nmol/10^6 cells/h for GA). AdV5 infection caused a significant upregulation of glycolytic pathway activity in both conditions; however, while infection of EG cells led to a 30% increment, GA cells experienced a 2.6 fold increase in glycolytic activity after AdV5 infection. The oxPPP flux was extremely low under all four conditions. In parallel with the higher glycolytic flux, EG cells had a higher production of lactate (R12: 347.86 ± 1.37 nmol/10^6 cells/h) than GA cells (80.76 ± 1.74 nmol/10^6 cells/h), while AdV5 infection caused a much larger increase in lactate production in GA cultures (1.11 fold for EG and 2.75 fold for GA). Pyruvate conversion to AcCoA via PDH was also slightly in EG (R14: 23.39.67 ± 1.08 nmol/10^6 cells/h) than GA (15.5 ± 0.47 nmol/10^6 cells/h). Viral infection of

1G3 cells increased this flux in both EG and GA conditions. Anaplerosis via PC (R15) was low in EG conditions and negligible in GA conditions, and was not significantly affected by infection.

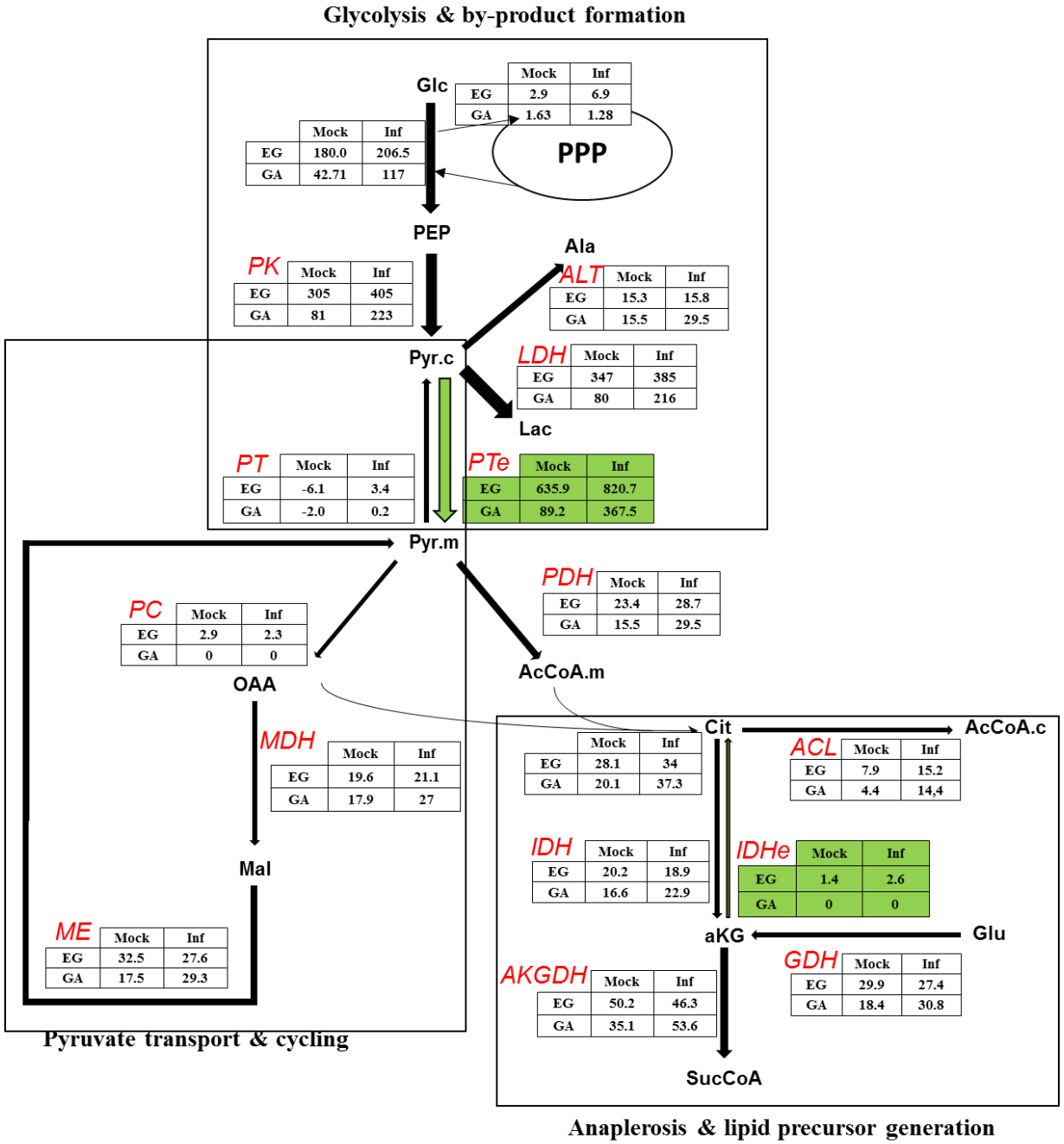

Figure 4.10: Overview of metabolic flux distributions during mock- and virus-infected 1G3 cells, under EG and GA conditions. Schematic representation of metabolic flux distributions in the highlighted reactions of central carbon metabolism, corresponding to enzymes: **ACL**, ATP citrate lyase; **AKGDH**, alpha ketoglutarate dehydrogenase; **ALT**, alanine aminotransferase; **IDH**, isocitrate dehydrogenase (lumps aconitase activity); **IDHe**, IDH exchange flux; **GDH**, glutamate dehydrogenase; **LDH**, lactate dehydrogenase; **MDH**, malate dehydrogenase; **ME**, malic enzyme; **PC**, pyruvate carboxylase; **PDH**, pyruvate dehydrogenase; **PK**, pyruvate kinase; **PT**, pyruvate transport flux; **PTe**, PT exchange flux. All fluxes represent net fluxes except for exchange fluxes, which represent the minimum of the forward and backward fluxes for a reversible reaction.

After citrate is generated in the TCA cycle, it can follow two different routes. One consists in the transfer of citrate to the cytosol and further conversion to oxaloacetate and AcCoA via ATP citrate lyase (ACL) for synthesis of fatty acids (from cytosolic AcCoA). ACL pathway activity were low in both growth conditions (EG mock-infected 7.87 ± 0.99 nmol/10^6 cells/h; GA mock-infected 4.3 ± 0.4 nmol/10^6 cells/h, R24). ACL was increased twice under AdV5 viral infection of EG Mock cells (until 15.17 ± 1 nmol/10^6 cells/h, R24), however under GA condition, cells conversely showed 3-fold increase activity of ACL flux (14.7 ± 0.71 nmol/10^6 cells/h, R24). The second route of citrate conversion is through the TCA cycle leading to αKG formation by isocitrate dehydrogenase (IDH) activity (R17), and showed a high conservation between EG mock- and virus-infected conditions, while it was increased by infection in GA.

Other TCA cycle fluxes, including ME activity, were relatively conserved in EG cultures with and without viral infection, while in GA cultures they were increased by AdV5 infection to values reasonably close to those observed in EG. Interestingly, this observation was closely matched by the glutamine consumption rate and the anaplerotic flux from glutamate toward αKG (R26), showing the importance of maintaining TCA cycle activity and glutamine anaplerosis for virus infection.

4.2. Characterization of hiPSC-CMs differentiation and maturation

4.2.1 Directed differentiation of hiPSC towards CMs

The second aim of this thesis focused on the use of metabolomics tools to study and improve the differentiation of hiPSCs towards CMs. For this purpose we used the DF19-9-11T.H hiPSC line, derived from human somatic cells using a non-integrating episomal vector. Before hiPSC differentiation, stemness of the cells was confirmed by flow cytometry analysis for the pluripotency markers SSEA-4, Tra-160, Oct4 and Nanog (Figure 4.11). More specifically, the percentage cells expressing these markers was over 90 %, of SSEA4, TRA-1-60, OCT-4 and Nanog positive cells were high (≥90 %, Figure 4.11) indicating that the majority of the cells displayed a pluripotent and undifferentiated phenotype. Additionally, the percentage of early differentiated cells (i.e. SSEA1 positive) was low (3 %, Figure 4.11).

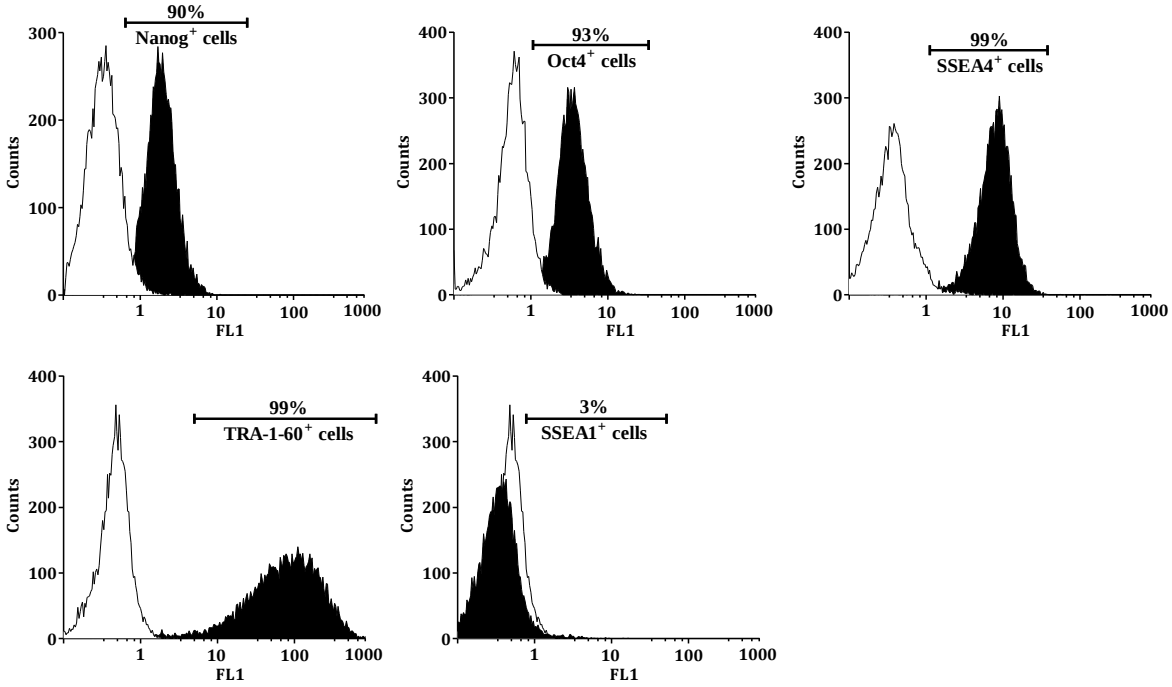

Figure 4.11: Flow cytometry analysis confirming the pluripotency state of hiPSC. The percentage of cells positive for the pluripotency markers: Nanog, Oct4, SSEA4, TRA-1-60, OCT4 and Nanog and for the spontaneous differentiation marker SSEA1 is indicated in each chart.

In order to direct the differentiation of hiPSC towards CMs we cultured the cells in differentiation medium and specific cocktails of growth factors (GFs) and small molecules (SM) were added at specific time-points. This protocol induced the differentiation of hiPSC successively towards mesoderm, cardiac mesoderm, cardiac progenitor cells and, finally, early CMs (Figure 4.12 A). To confirm that cell differentiation followed this pattern we used phase contrast microscopy, flow cytometry and qRT-PCR analyses. Upon CM differentiation induction, a decrease in the expression of the pluripotency markers Nanog and OCT4 was observed along time and become negligible by day 6 (Figure 4.12 B, C). According to Burridge et al.,

(2014b) the expression of pluripotency markers remains during the first days of differentiation and decrease progressively afterwards (Figure 4.12 B, C). The up regulation of the mesoderm marker Brachyury T (T) observed one day after CM differentiation induction, with 94 % of the cells expressing this marker (Figure 4.12 D).

After the addition of the Wnt-pathway blocking factor at day 1, cells start to differentiate from mesoderm progenitor to precardiac mesoderm cells (Burridge et al., 2012). The expression of precardiac mesoderm Bry-T started to decrease and the expression of the cardiac mesoderm markers, Mesp1 and KDR started to increase (Figure 4.12 F, G). This process lasted approximately 2 days. By day 3 of differentiation, the addition of factors induced cell differentiation towards cardiac progenitor cells. The results obtained by qRT-PCR and flow cytometry analyses clearly indicate that by day 3 onwards the expression of markers of pluripotency, mesoderm, precardiac mesoderm and cardiac mesoderm decreased whereas the expression of the cardiac progenitor markers, Nkx2.5, GATA4, SIRPA increased. By day 7 of differentiation, cells start to beat and the expression of early CM-specific genes, SIRPA, VCAM1 and cTnT increased up to day 15 of the differentiation (Figure 4.12 I, K).

After 15 days of differentiation a synchronized beating monolayer of hiPSC-CMs was obtained and cells were highly positive for the cardiac specific cell-surface markers SIRPA and VCAM1, and intracellular markers cTNNT (93%, 93% and 90%, respectively; Figure 4.12 E, I, J). The final hiPSC-CMs population was also characterized based on their structural features using immunocytochemistry tools. Figure 24 L shows that hiPSC-CMs exhibited a typical cardiac morphology, with highly organized α-actinin and cardiac troponin T (cTnT) structures.

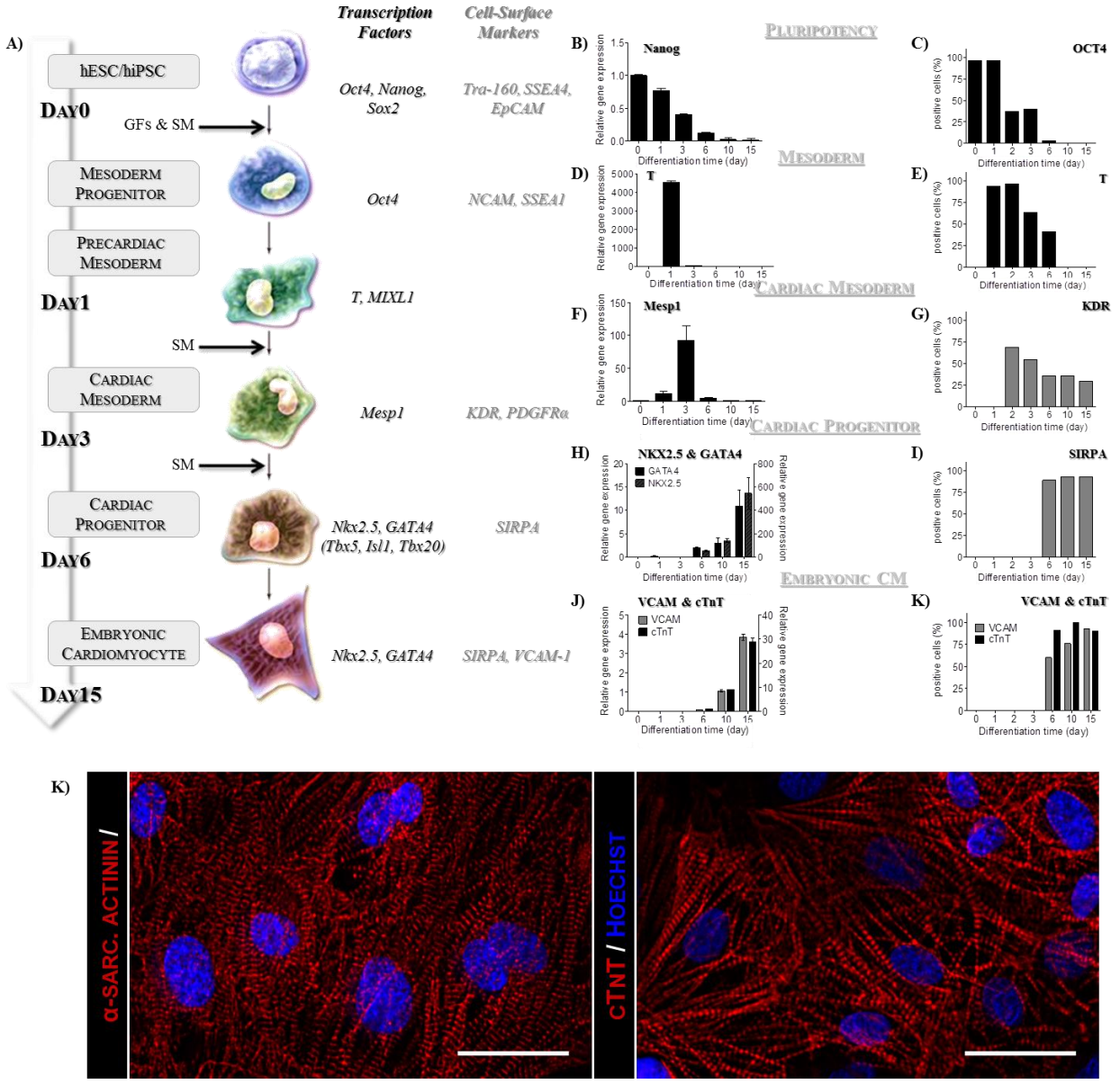

Figure 4.12: Characterization of the directed differentiation of hiPSC towards hCMs. A) Schematic representation of the differentiation process. The predominant cell population at each timepoint as well as the specific transcription factors and cell surface markers expressed each population of cells is demarked. Timepoints in which growth factors (GFs) and/or small molecules (SM) were added are also highlighted. Characterization of the differentiation process by qRT-PCR (**B**, **D**, **F**, **H**, **J**) and flow cytometry (**C**, **E**, **G**, **I**, **K**) analyses. **L)** Immunofluorescence analysis of hPSC-CMs at the end of the differentiation process (day 15) for the CM-specific markers: sarcomeric α-actinin and Troponin C (red)**.**Nuclei were counterstained with Hoescht (blue). Scale bars: 50 µm

4.2.3 Comparison of hiPSC and hiPSC-CMs in terms of growth and metabolic performance

Populations of hiPSC and their derivatives hiPSC-CMs were compared in terms of cell growth (Figure 4.13). hiPSCs had maximum specific rate of μ_{max}= 0.0217 h^{-1}, corresponding to a duplication time of $t_d = 31.8$ h. On the other hand, as expected hiPSC-CMs maintained their concentration during 9 days of culture. It is widely known that hCMs present a very low proliferation capacity (Rajala et al., 2011).

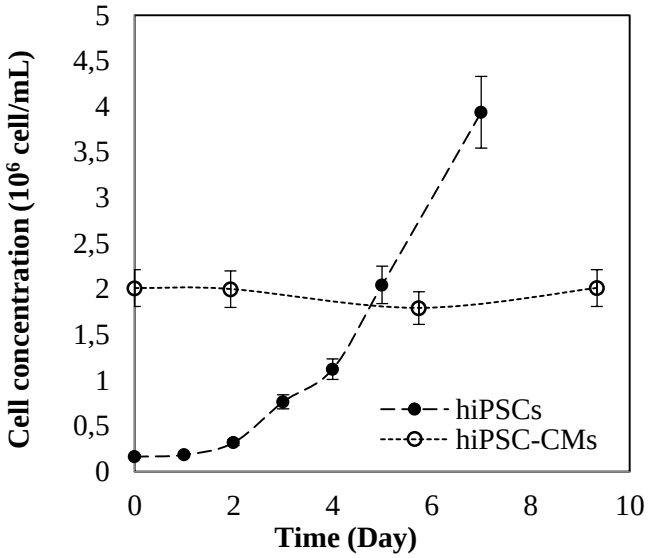

Figure 4.13: **Cell growth profiles of hiPSC-CMs and hiPSC-hCMs.**

Specific rates of glucose (q_{Glc}) and glutamine (q_{Gln}) consumption, and production of lactate (q_{LAC}), ammonia (q_{Amm}) and glutamate (q_{Glu}) were determined and compared for hiPSCs (cultivated in mTeSR1 medium) and hiPSC-CMs (cultivated in RPMI+B27 medium). Our results show that q_{Glc} and q_{Lac} were significantly lower in hiPSC-CMs when compared with hiPSCs (Figure 4.14 A, B), what correlates with other published results (qGlc = 360 ± 40 nmol/10^6 cells/h and 240 ± 20 nmol/10^6 cells/h; qLac = 630 ± 120 nmol/10^6 cells/h and 320 ± 20 nmol/10^6 cells/h for hESCs and hESC-CMs, respectively) (Lam et al., 2014). Nevertheless, the ratio $\mathbf{Y_{Lac/Glc}}$ did not changed significantly in both cell populations (1.78 ± 0.07 vs 1.68 ± 0.08 for hiPSCs vs hiPSC-CMs), indicatinc that despite early hiPSC-CMs consume less glucose than hiPSCs, they still maintain their glycolytic metabolism. The q_{Gln} and q_{Amm} did not show significant differences between hiPSCs and hiPSC-CMs (Figure 4.14 C, E). q_{Amm} values are similar to the ones obtained by Lam et al (q_{Amm} = 29 ± 3 nmol/10^6 cells/h and q_{Amm} = 23 ± 2 nmol/10^6 cells/h for HES3 and HES3-hCMs respectively; Lam et al., 2014), while q_{Gln} was about 3-fold lower than reported values for hESC-CMs (q_{Gln} = 33 ± 3 nmol/10^6 cells /h for HES3-hCMs; (Lam et al., 2014)). The q_{Glu} was very low and almost indistinguishable between hiPSCs and hiPSC-CMs (Figure 4.14 D).

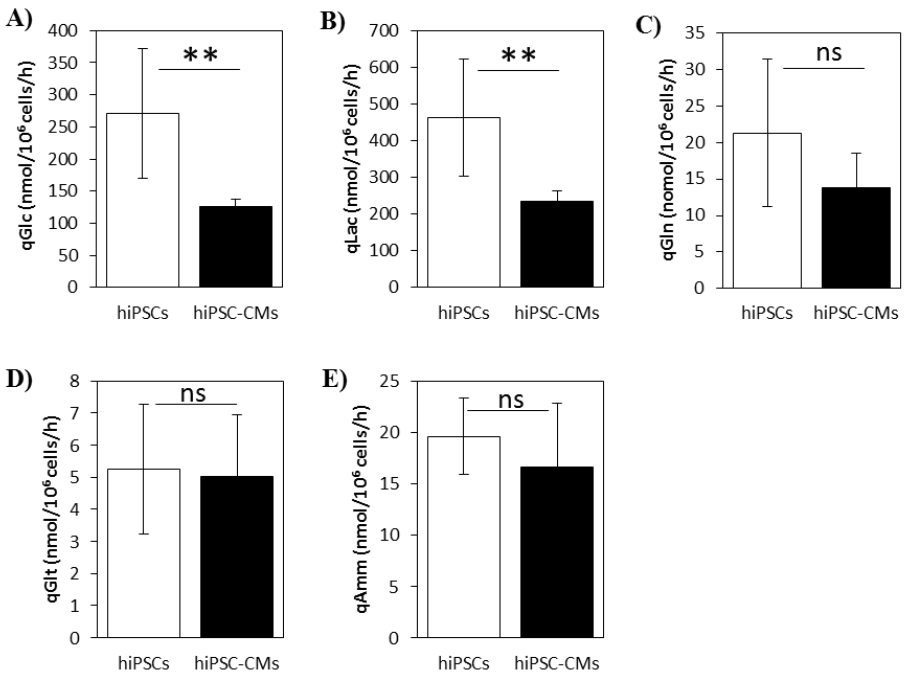

Figure 4.14: **Specific transport rates of metabolites for hiPSCs and hiPSC-CMs**. Specific consumption rate of glucose (qGlc, **A**) and glutamine (qGln, **C**) and specific production rate of lactate (qLac, **B**), glutamate (qGlu, **D**) and ammonia (qAmm, **E**). Data are presented as mean ± SD. Significantly different: $P<0.01$ (**), Not-significant (ns).

It is well known that during pluripotency and in early cardiac development, glycolysis is a major source of energy (Folmes et al., 2012). As hCMs mature and become terminally differentiated, mitochondrial oxidative capacity increases and oxidative metabolism (mainly β-oxidation of fatty acids) become a major source of energy (Lopaschuk and Jaswal, 2010; Zhu et al., 2014). The reduced qGlc by hiPSC-CMs in comparison with hiPSC can be explained by the inability of hiPSCs to obtain high amounts of ATP by oxidative phosphorylation, producing ATP almost exclusively from glycolysis. hiPSC-CMs present a higher metabolic efficiency, being able to oxidized glucose if required or metabolize other substrates to obtain energy. Thus to satisfy their energetic requirements, hiPSC might need to consume more glucose in comparison with hiPSC-CMs.

On the other hand, the similar $\mathbf{Y_{Lac/Glc}}$ by day 15 of differentiation, may suggest that hiPSC-CMs are still highly immature and still rely mainly on glycolysis as major energy source. In agreement with our results, several studies have described that hiPSC-CMs after the differentiation process are still immature compared with adult CMs in terms of structure, metabolism and electrophysiology (Blazeski et al., 2012). Also, it was reported that hiPSC-CMs rely mainly on glycolysis when cultured in glucose-containing media, even if fatty acids are available (Rana et al., 2012). In this study, after the differentiation process, hiPSC-CMs were maintained in the same culture medium (RPMI-B27) that is rich in glucose. Thus we hypothesized that hiPSC-CMs maturation could be improved if hiPSC-CMs were cultured in glucose-depleted medium

supplemented with fatty acids, the preferable carbon source used *in vivo* by adult hCMs (Yang et al., 2014a; Zhu et al., 2014).

4.2.3 Enrichment of hiPSC-CMs

Despite the addition of growth factors and small molecules, the outcome (i.e. CM purity and differentiation efficiency) from each differentiation process is still variable and highly dependent on several factors, such as, cell confluency, cell passage, growth factor lot number, etc. Previous results showed that in a total of 30 differentiation batches, CM purity achieved at day 15 may vary between 70% and 95% (Burridge et al., 2014; Tohyama et al., 2013). Tohyama et., al (2013) reported that PSC-CMs can survive in glucose depleted culture medium supplemented with lactate, but non-CMs cannot. This effect can be attributed both to the fact that PSCs and precursor cells have a lower expression of genes encoding enzymes involved in the TCA cycle and are unable to obtain large amounts of ATP by oxidative phosphorylation or by glycolysis under glucose-deprived conditions. Thus, culturing the cells in these conditions enables also the enrichment of the final differentiation population into hiPSC-CMs.

Aiming at validating/implementing this strategy, we cultured hiPSC-CM population for additional 10 days (from day 15 until day 25) in glucose-depleted RPMI culture medium supplemented with 4 mM lactate (LacM). By flow cytometry analysis (Figure 4.15A) we observed an increase in the percentage of cells positive for the CM-specific markers, SIRPA and VCAM, confirming hiPSC-CMs survival and cell death of non-hCMs. On the other hand, the population kept in control medium (CMM) during the same period, maintained constant or slightly increase the percentage of cells expressing the CM markers (Figure 4.15A).

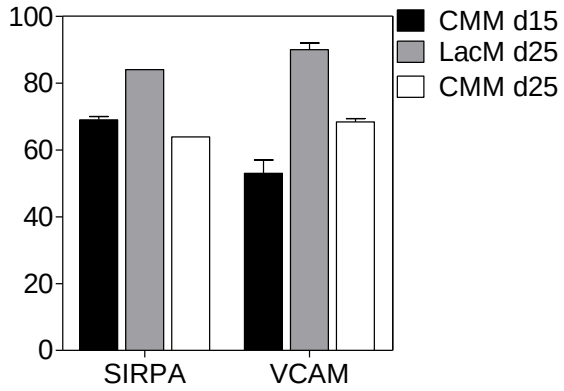

Figure 4.15: **CM enrichment after culture in glucose-depleted media supplemented with lactate.** Flow cytometry of hiPSC-CMs: Black – hiPSC-CMs at day 15, before CM enrichment; Grey- hiPSC-CMs cultivated 10 days in glucose depleted medium supplemented with 4mM sodium-L-lactate (LacM). White – hiPSC-CMs cultivated 10 days in control medium (CMM).

4.2.4 Maturation of hiPSC-CMs

The main aim of this part of the thesis was to evaluate the impact of different carbon/energy sources on hiPSC-CMs maturation. More specifically, hiPSC-CMs were cultured for 20 days (from day 15 until day

35) in three different culture media: i) standard culture medium RPMI+B27 (CM medium, CMM); ii), glucose depleted RPMI culture medium supplemented with 4 mM lactate (lactate medium, LacM), from day 15 until day 25, and standard medium RPMI+B27 (CM medium, CMM), from day 25 until day 35; iii) glucose depleted RPMI culture medium supplemented with a mixture of fatty acids (Fatty Acid Medium, FAM) from day 15 to day 35 (Figure 4.16 A).

It is known that changes in morphology, electrophysiology, calcium handling, bioenergetics and contraction force, are inherent to progression from fetal to a mature adult state (Yang et al., 2014a). Thus, to assess the effect of the different media on hiPSC-CMs maturation we evaluated and compared cell cultures in terms of cell viability, morphology, ultrastructure, gene expression and metabolism.

Immunofluoresce analyses for the CM-specific markers (α-SARC actinin, Titin, cTnT) and F-actinin showed that hPSC-CMs maintained in FAM displayed changes in morphology, namely cells presented a higher organized sarcomeric pattern, a larger size and a more oblong shape compared with hiPSC-CMs cultured in CMM and LacM (Figure 4.16 B). Also, hiPSC-CMs cultured in FAM displayed more oval nuclei and a higher degree of multi-nucleation (Figure 4.16 B). In agreement, the percentage of binucleated cells determined for the cells cultured in FAM was significantly higher at day 25 and 35 that the percentage calculated for the cells cultured in CMM and LacM (Figure 4.16 C). All these features indicate a higher level of structural maturation in hiPSC-CMs cultured in FAM comparatively to CMM and LacM.

The ultrastructure of cells cultured in FAM was also evaluated by Transmission electron microscopy (TEM) analysis (Figure 4.16 D). hiPSC-CMs cultured in this medium exhibited dense and aligned myofibrils with a sarcomeric pattern. Z bands delimiting the sarcomeres and highly specialized cell-cell junctions (intercalated disks) were identified as well as highly abundant long and slender mitochondria (Figure 4.16 D). Mitochondrial undergo structural and functional changes during heart development and *in vitro* differentiation (Porter et al., 2011; Zhu et al., 2014). In immature CMs, mitochondria distribute throughout the cytoplasm in a reticular network and only account for a small fraction of the cell volume. As development proceeds, mitochondria develop more mature lamellar cristae and, in the adult hCMs, they are regularly distributed throughout the cell (occupying ≈ 20% to 40% of the adult myocyte volume). Additionally to these structural changes, the oxidative capacity of the mitochondria increases, as reflected in a metabolic substrate switch, from glycolysis, in early cardiac development, to fatty acid β-oxidation, in mature terminally differentiated hCMs (Lopaschuk and Jaswal, 2010; Yang et al., 2014a; Zhu et al., 2014). In agreement, flow cytometry of cells stained with the fluorescent mitochondrial dye, Mitoview, revealed that the culture in FAM led to an increase in the number of CMs with high-intensity fluorescence, indicating that in this media cells presented an enhanced mitochondrial membrane potential (Figure 4.16 E). These results may also be suggestive of a more developmentally mature phenotype in cells maintained in FAM.

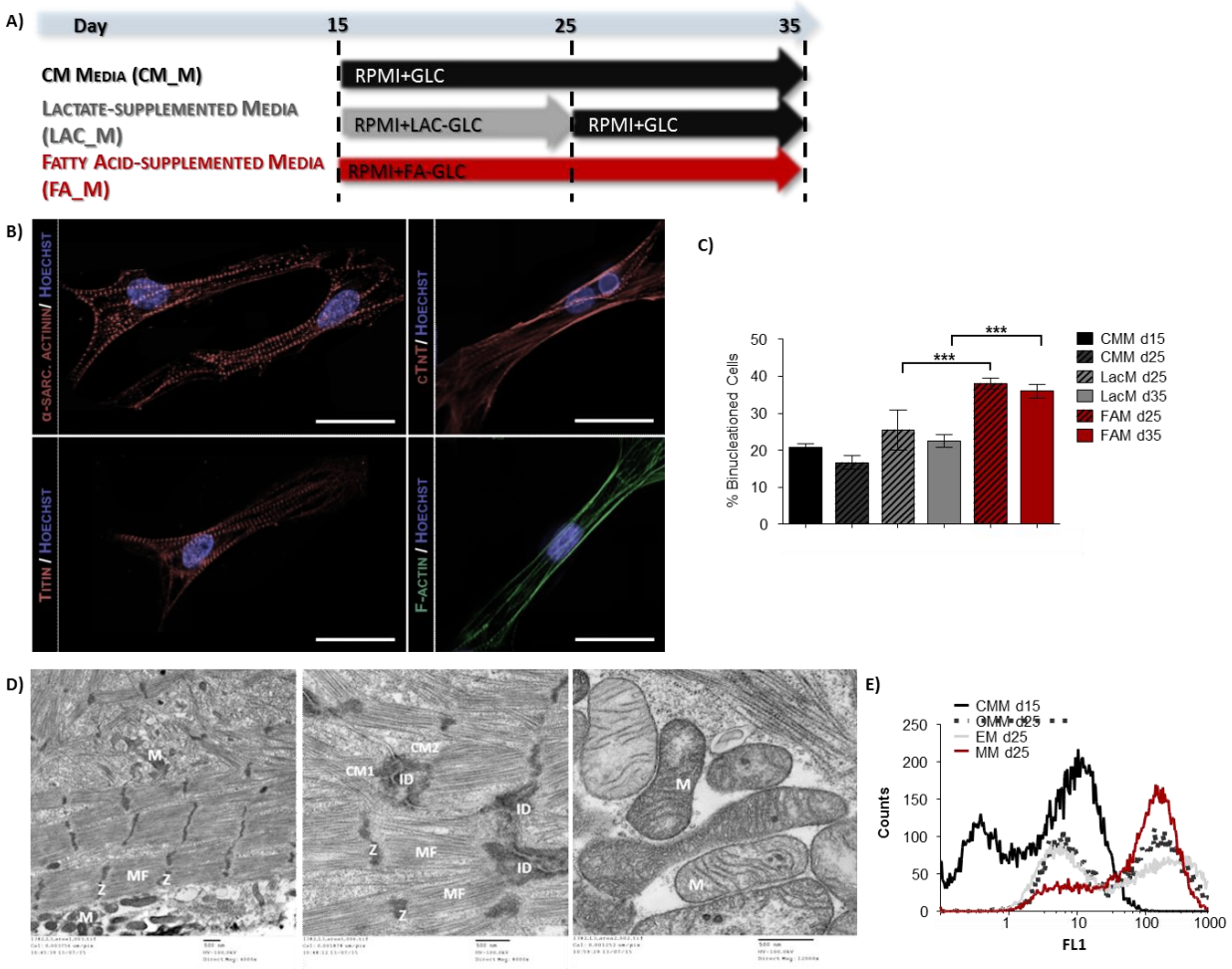

Figure 4.16: Effect of different feeding strategies on cell phenotype. A) Schematic illustration of the feeding strategies used. **B)** Immunofluorescence images of α-SARC actinin, Titin, cTnT (red) and F-actinin (green). Nuclei were labeled with Hoeschst 33432 (blue). Scale bars: 30 µm. **C)** Percentage of binucleation displayed by cells cultured in CMM, LACM and FAM. Data are presented as mean ± SD. Significantly different: P<0.05 (*), P<0.01 (**), P<0.001 (***); **D)** Transmission electron microscopy (TEM) images of hiPSC-CMs cultured in FAM. HiPSC-CMs contained many myofibrils (MF) aligned and organized in a sarcomeric pattern. Z-bands (Z) and neighbouring CMs (CM1, CM2) connected by intercalated disks (ID) were also observed. Mitochondria (M) were also highly abundant. Scale bars: 500 nm. **E)** Mitochondrial membrane potential determined by flow cytometry analysis.

Additionally, qRT-PCR reveled differences in gene expression for cells cultured in FAM medium, comparing with the ones cultured in CMM and LacM. The majority of the CM-specific genes expressed by cells cultured in both LacM and FAM were up-regulated at day 35, in comparison to CMM at day 15, suggesting that in both conditions enrichment and maturation occurred. Noteworthy, in FAM condition at day 35, several CM-specific genes were significantly higher expressed, in comparison to LacM. The majority of these genes are related with a more mature CM phenotype, such as the genes associated with sarcomeric proteins (ACTC1), calcium handling channels (SERCA2, CACNA1c), membrane ion channels (HCN2 and HCN4), and ventricular muscle (MYL2) (Figure 4.19). Connexin-43 (GJA-1), a gap junction protein highly expressed in CMs (Yang et al., 2014a) despite increased from day 15 to day 35 in both LacM

and FAM did not show significant differences between both conditions by day 35 (Figure 4.19). Yang et al. (2014a) listed the major cardiac genes upregulated (by ≥2-fold) in adult hearts compared with the immature hiPSC-CMs and among these genes are sarcomeric genes as well as genes encoding proteins for ion transport, and calcium handling. In a recent work, Ribeiro et al, reported that when cultivated in pluricyte medium (from Pluriomics BV), hiPSC-CMs showed improved electrophysiological properties, sarcomeric organization and cardiac-specific gene expression (Ribeiro et al., 2015). The medium used in this study is a glucose-rich media containing the thyroid hormone, Tri-iodo-L-thryronine (T3); it was pre-optimized for viability in culture and morphological maturation of hiPSC-CMs. Thyroid hormones have an important influence on cardiac structure, electrophysiological functions and cardiac contractility in development *in vivo* (Pascual and Aranda, 2013; Yang et al., 2014b). Therefore, T3 treatment is now one of the strategies used to enhance maturation of CMs *in vitro* (Yang et al., 2014b). In future work, comparison of pluricyte medium, should be performed, to evaluate differences between this commercial medium and FAM strategy used in our study.

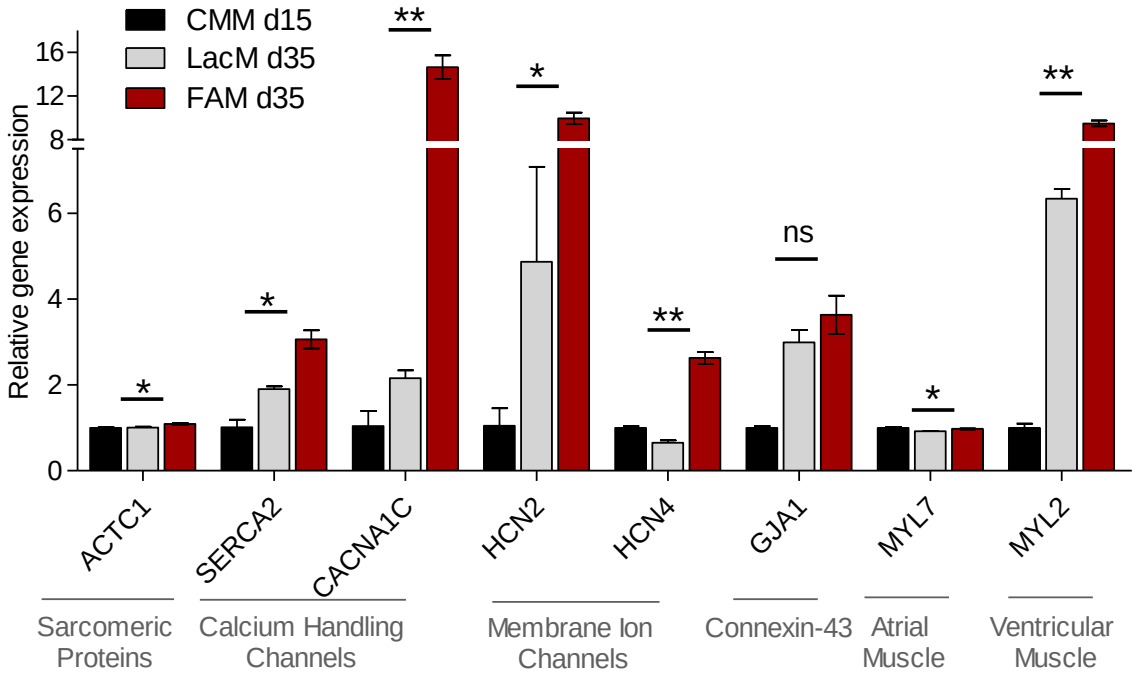

Figure 4.17: Effect of different medias on gene expression of hiPSC-CMs. qRT-PCR demonstrate relative expression of genes related to sarcomeric protein (ACTC1, TNNT2), calcium handling (SERCA2, CACNA1C), membrane ion channels (HCN2, HCN4), connexin-43 (GJA1), atrial muscle (MYL7) and ventricular muscle (MYL2) in hiPSC-CMs cultivated for 20 days in CMM, LacM and FAM in relation to hiPSC-CMs at day 15 (before maturation/enrichment). Changes in gene expression were normalized to GAPDH gene expression as internal control. Data are presented as mean ± SD. Significantly different: P<0.05 (*), P<0.01 (**), P<0.001 (***), Not-significant (ns).

The metabolic performance of hiPSC-CMs cultured in different culture media was also evaluated. Results show that when the hiPSC-CMs were cultured in standard CMM for 20 days, q_{GLC}, q_{GLN}, q_{LAC} and ratio

$Y_{Lac/Glc}$ did not change meaningfully during time (Figure 4.18 A-D), suggesting that cells do not change their metabolism, relying mainly on glycolysis.

In LacM, it was observed lactate consumption which remained constant from day 15 to day 25 (Figure 4.18 B). Noteworthy, when hiPSC-CMs returned to standard medium CMM (from day 25 to day 35), cells started to consume glucose and net production of lactate was observed (Figure 4.18 A). Also, q_{GLN} changed during time (Figure 4.18 C). When cells were cultured in media depleted of glucose and supplemented with lactate, they consume Gln at higher rates. These results suggest that in the absence of glucose, hiPSC-CMs use lactate and glutamine in the TCA cycle metabolism but rely mainly on glycolysis when cultured in glucose-containing media. Moreover, these results show that hiPSC-CMs can sudden adapt to another carbon source and shift relatively easily their metabolism. In fact, it is described that hCMs possess a metabolic plasticity highlighted by their ability to utilize glucose, lactate, ketones, and amino acids (Kolwicz and Tian, 2011). The preference in substrate utilization can change in response to altered substrate availability or altered regulation of metabolic pathways (Kolwicz and Tian, 2011). The fluctuations observed in the values of q_{GLC}, q_{LAC}, q_{GLN}, $Y_{Lac/Glc}$, after changing the media from LacM to CMM, may reflect the adaptation of the cells to another carbon source, before stabilizing their metabolism (Figure 4.18 A-D). For example, at first days after cells were returned to normal medium, the molar ratio $Y_{Lac/Glc}$, was lower, comparing with cells cultured in CMM condition. However, when cells adapted to consume glucose again, the ratio became similar with the control condition, around 2 (Figure 4.18 D), showing the same efficiency of glucose consumption as cells cultured in CMM. In FAM, neither glucose nor lactate where added to the media, thus q_{GLC} and q_{LAC} were not detected. Additionally, the values of q_{GLN} were higher when cells were cultured for 10 days in LacM and when cultivated in FAM comparatively to cells cultivated in CMM. In FAM the q_{GLN} were also higher than in LacM. Glutamine can be converted to glutamate that can be converted to AKG, a TCA cycle intermediate. This anaplerotic reaction contributes to the increase in TCA cycle intermediates and consequently to the maintenance of oxidative capacity.

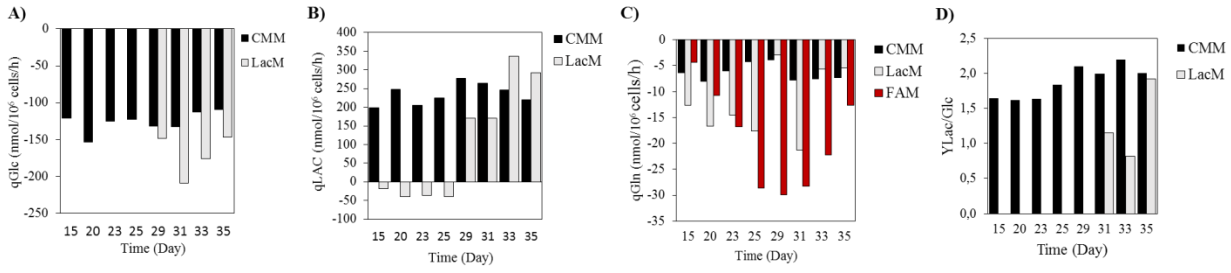

Figure 4.18: Specific metabolite transport rates and ratio Lac/Glc in hiPSC-CMs cultured in CMM, LacM and FAM, from day 15 until day 35. Specific consumption rate of glucose (qGlc, **A**) and glutamine (qGln, **C**) and specific production rate of lactate (qLac, **B**). Molar ratio of lactate production per glucose consumption (YLac/Glc).

This result reflects the ability of hiPSC-CMs to easily shift their metabolism when glucose is absence in the medium. In the presence of glucose, glutamine metabolism is not meaningful (Figure 4.18 C). To confirm if hiPSC-CMs consume the fatty acids present in the media we used a Fatty Acid Quantification Kit, a sensitive enzyme-based method that enables the detection of long-chain free fatty acids (FA). The results show that when cultured in FAM (in the absence of glucose), hiPSC-CMs consume fatty acids (Figure 4.19 A). Specific consumption rate of fatty acid (q_{FA}) varied from 0.5 to 0.3 nmol/10^6 cells/h during time (Figure 4.19 A). Also, it was observed a significant increase in the expression of genes related with fatty acids uptake and metabolism (ACADL and PPARA) when the cells were cultured in FAM (Figure 4.19 B)

It is important to note that even in CMM (rich in glucose) a slight consumption of fatty acids was observed, mainly at day 35. CMM is composed by RPMI supplemented with B27, which contains linoleic acid and linolenic acid. The increased interest for fatty acid consumption even in the presence of glucose may suggest that hiPSC-CMs underwent a slight metabolic maturation when maintain in standard culture media. In fact, several studies have reported that prolonged *in vitro* culture of hESC- and hiPSC-derived CMs result in the maturation of their structural and contractile properties to a more adult-like phenotype (Lundy et al., 2013).

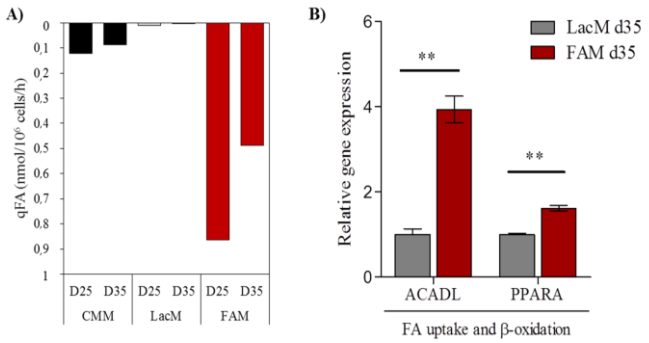

Figure 4.19: Effect of the presence of fatty acids in medium on hiPSC-CM metabolism and on the expression of genes related with fatty acid metabolism. A) Specific consumption rate of FA in CMM, LacM and FAM. **B)** Relative expression of genes related with fatty acid uptake and ß-oxidation: ACADL (Acyl-CoA Dehydrogenase, Long Chain) and PPARA (Peroxisome proliferator-activated receptor alpha).

Further metabolic characterization of hiPSC-CMs maturation, was performed by analysis of amino acid consumption and production rates by HPLC. Our results suggest that there are differences in the consumption and production of certain amino acids in cells cultured in different media. Alanine is produced from pyruvate that is formed during glycolysis. Alanine production was lower in LacM and FAM at days 25 and 35, comparatively to cells at d15 when cultured in CMM. This result, also confirms that cells rely less on glycolysis when cultured in these two media for prolonged periods of time (Figure 4.20). The specific rate of alanine production did not decrease in control condition (CMM), again reflecting that glycolysis is the predominant energy pathway in this culture condition. Interestingly, it was observed an increase in the consumption of glutamate, glutamine, arginine, valine and tyrosine when the cells were cultured in FAM and LacM (for 10 days) comparatively to day 15 and cells cultured in CMM. These amino acids can be

readily converted to AcCoA or to TCA intermediates (Annex, Figure 7.1) presenting an anaplerosis contribution to TCA (Drake et al., 2012). In the absence of glucose hiPSC-CMs are forced to consume the other available substrates mainly lactate and fatty acids. The oxidation of these substrates increases the need for the maintenance of the TCA intermediate levels, which may justify the increase in amino acid metabolism in these media comparing to CMM. It should be noted that in generally the consumption of the referred amino acids decreased in FAM medium at day 35 comparatively to day 25.

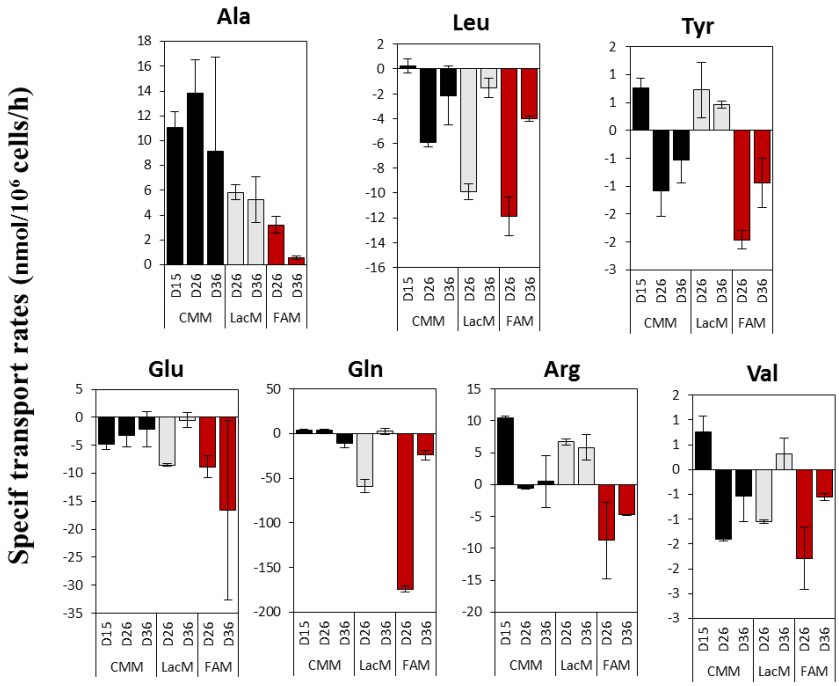

Figure 4.20: Specific transport rates of amino acids determined by HPLC. Specific consumption/production rate of Alanine (Ala), Leucine (Leu), Tyrosine (Tyr), Glutamate (Glu), Glutamine (Gln), Arginine (Arg) and Valine (Val).

This may suggest that at this timepoint cells do not rely so much in amino acid metabolism because other substrates, mainly AcCoA resulting from β-oxidation of fatty acids, can actively contribute to maintain overall TCA cycle function.

4.2.5 Labeling experiment in hiPSC-CMs maturation

To better reveal the metabolic changes that occurred during time in different culture media we cultured the cells in the presence of labelled substrates. Specifically, we compared the metabolism of hiPSC-CMs cultivated in CMM and LACM, from day 15 to day 35, using [1, 2-^{13}C]glucose and [3-^{13}C]lactate tracers.

4.2.5.1 ^{13}C-Labeling dynamics of intracellular metabolites from [1, 2-^{13}C]glucose tracer

Cells were cultured in RPMI+B27 medium supplemented with [1, 2-^{13}C]glucose at days 15, 26 and 36 of culture, and samples were collected 24 and 48 hs after ^{13}C-labeled addition. The incorporation of ^{13}C into

intracellular metabolites was evaluated by GC-MS analysis. Analysis of MIDs of different intracellular metabolites showed that for hiPSC-CMs cultured in CMM, the speed of incorporation of ^{13}C in glycolysis and TCA metabolites was slightly higher at day 26 and 36 comparing with day 15 (Figure 4.21). This can be concluded due to higher percentage of M2 isotopomers in glycolysis related metabolites (Ala and Lac) and TCA metabolites (Cit, Glu, Asp, Mal) at day 26, comparing with day 15, at timepoint 24h (Figure 4.21 and Figure 4.22). Nevertheless, the final percentage of M2 isotopomers in these TCA metabolites is very similar at day 15, 26 and 36. Also, MIDs profiles of metabolites at day 26 and day 36, did not show detectable pattern difference. Incorporation of ^{13}C in lactate was very high (≥80%) during time (Figure 4.23). However, it should be noted that 13C labeled TCA intermediates were also identified suggesting that oxidation of glucose in TCA cycle may also occur. The differences in the speed of incorporation may suggest that the velocity of some pathways that generate these metabolites may increase during time in culture, possibly due to enhanced expression of some of the enzymes that catalyze these reactions.

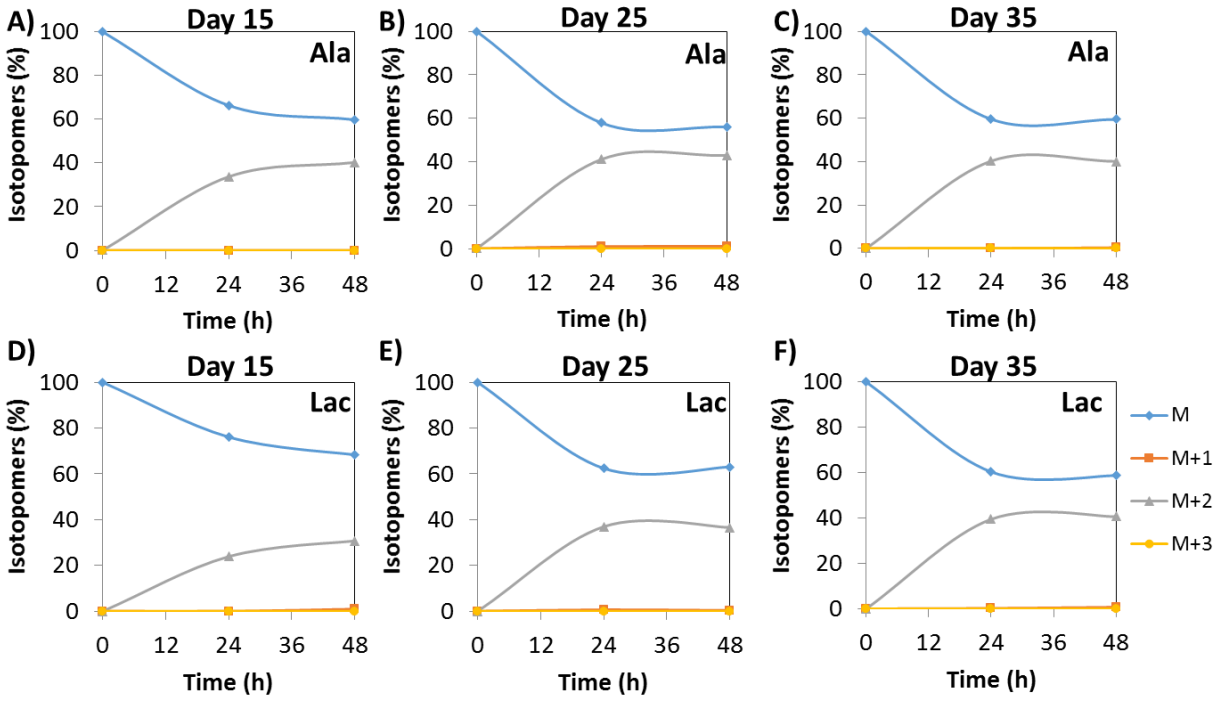

Figure 4.21: Time profiles of isotopic labeling of glycolysis metabolites after the introduction of [1, 2-^{13}C]glucose. Fractions of labeled mass isotopomers were determined from the measured mass isotopomer distribution, after correction for natural isotope abundances. Alanine (**A, B, C**) and Lactate (**D, E, F)** day15, day 25 and day 35 of hiPSC-CMs after start of differentiation. The composition of glucose in the medium was 100% [1, 2- 13C]glucose.

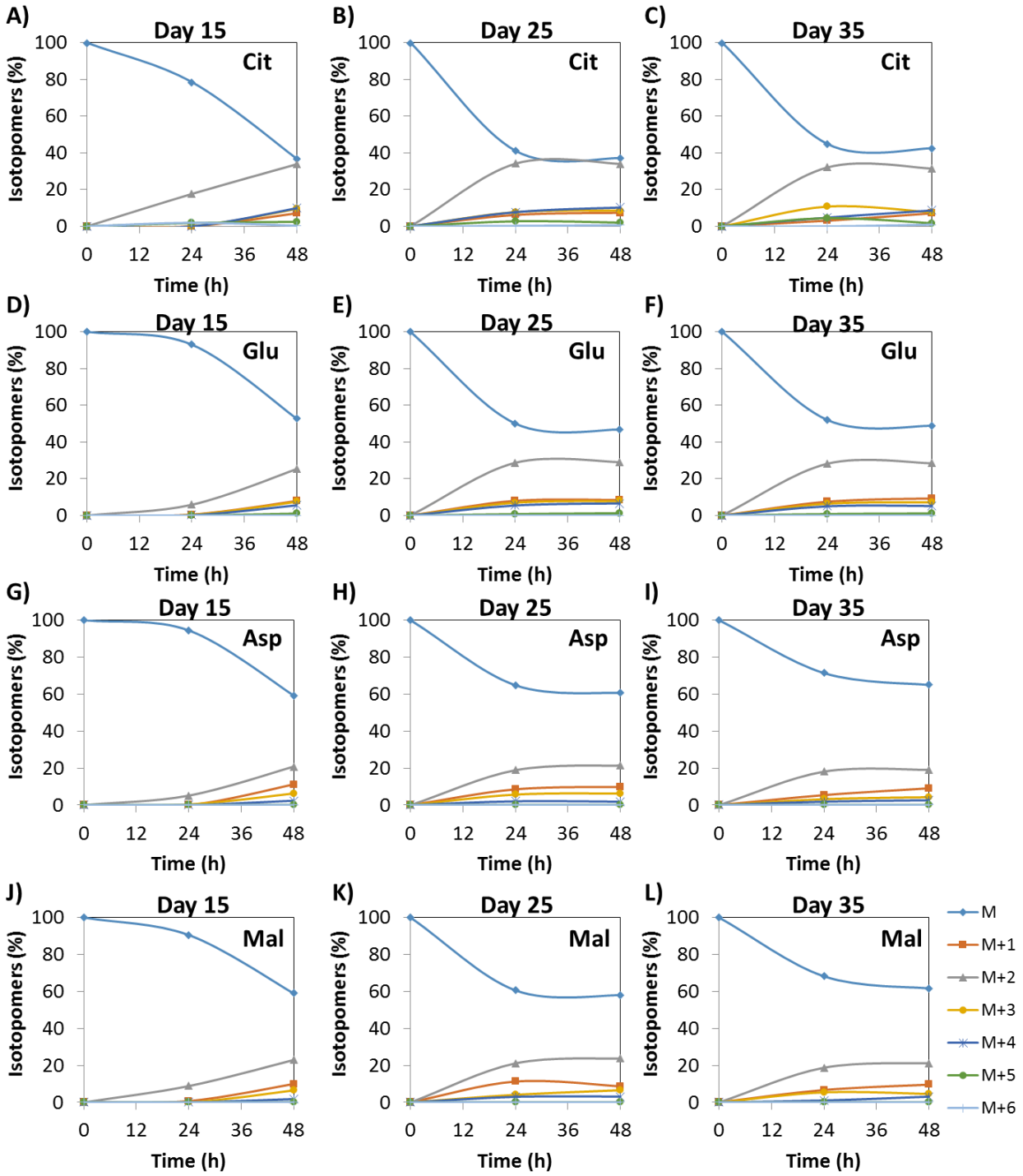

Figure 4.22: **Time profiles of isotopic labeling of TCA metabolites after the introduction of [1, 2-^{13}C]glucose.** Fractions of labeled mass isotopomers were determined from the measured mass isotopomer distribution, after correction for natural isotope abundances. Cit, Glu, Asp, Mal at day 15 (**A,D,G,J**), day 25 (**B, E, H, K**) and day 35 (**C, F, I, L**) of hiPSC-CMs after start of differentiation. The composition of glucose in the medium was 100% [1, 2- 13C]glucose

However, in line with what was mentioned before these results confirmed that no changes in the preferred carbon source and in the metabolic efficiency in processing glucose occurred when hiPSC-CMs are maintained in CMM.

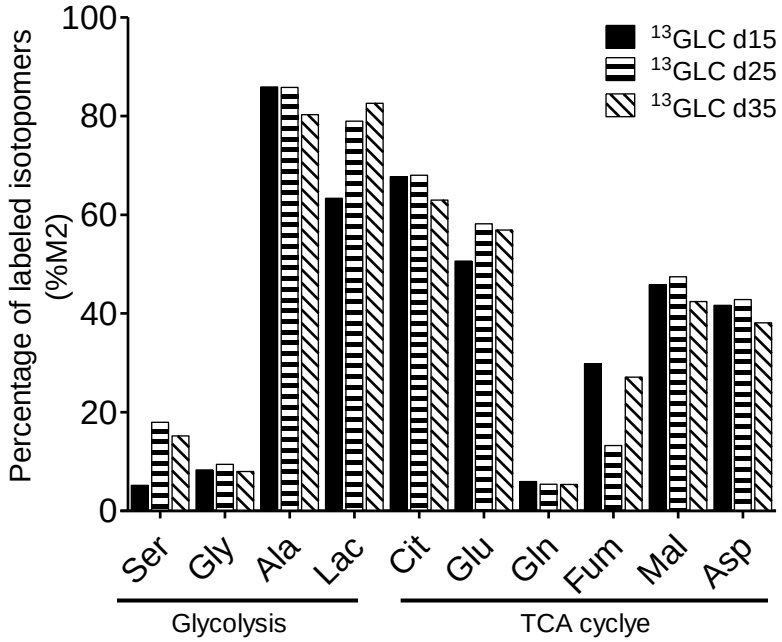

Figure 4.23: Percentage of labeled intracellular metabolites from glucose. Values correspond to the M2 isotopomers.

4.2.5.2 ^{13}C-Labeling dynamics of intracellular metabolites from [3-^{13}C]lactate tracer

In this experiment, cells were maintained in glucose depleted medium RPMI+B27, with addition of 4 mM [3-^{13}C]lactate as alternative carbon source. Cells were collected 24 and 48 hs after ^{13}C-labeled tracer introduction and incorporation of ^{13}C were evaluated by GC-MS analysis at day 15 and day 25. Differences in MID profiles were observed for several metabolites at day 15 and 25. For example at day 15, the speed of ^{13}C incorporation in TCA metabolites (Glu, Gln, Asp, Mal, Fum) is slower and the total percentage of incorporation is lower, comparatively to day 25 (Figure 4.24 and Figure 4.25). This can be explained by the fact that cells were only cultivated in medium depleted in glucose supplemented with lactate from day 15 onwards. It is known that cells need some time to adapt to new carbon sources, thus at day 15, hiPSC-CM are probably not yet capable to consume lactate at maximum efficiency. In fact, a high ^{13}C incorporation in Alanine was also observed (Figure 4.25) suggesting that a meaningful quantity of lactate is still being converted to Alanine instead of being fully oxidized in TCA. Nevertheless, the ^{13}C incorporation in TCA metabolites by day 26 reveals that by this time-point hiPSC-CM are already capable to efficiently oxidize acetyl lactate by the TCA cycle. Lactate tracer has been used to elucidate differences in metabolism between PSC and CMs (Tohyama et al., 2013). Tohyama et al. (2013) observed higher level of ^{13}C-labeled

intracellular metabolites of TCA cycle in CMs, comparing with PSCs, indicating higher usage of TCA cycle in CMs, comparing with PSCs.

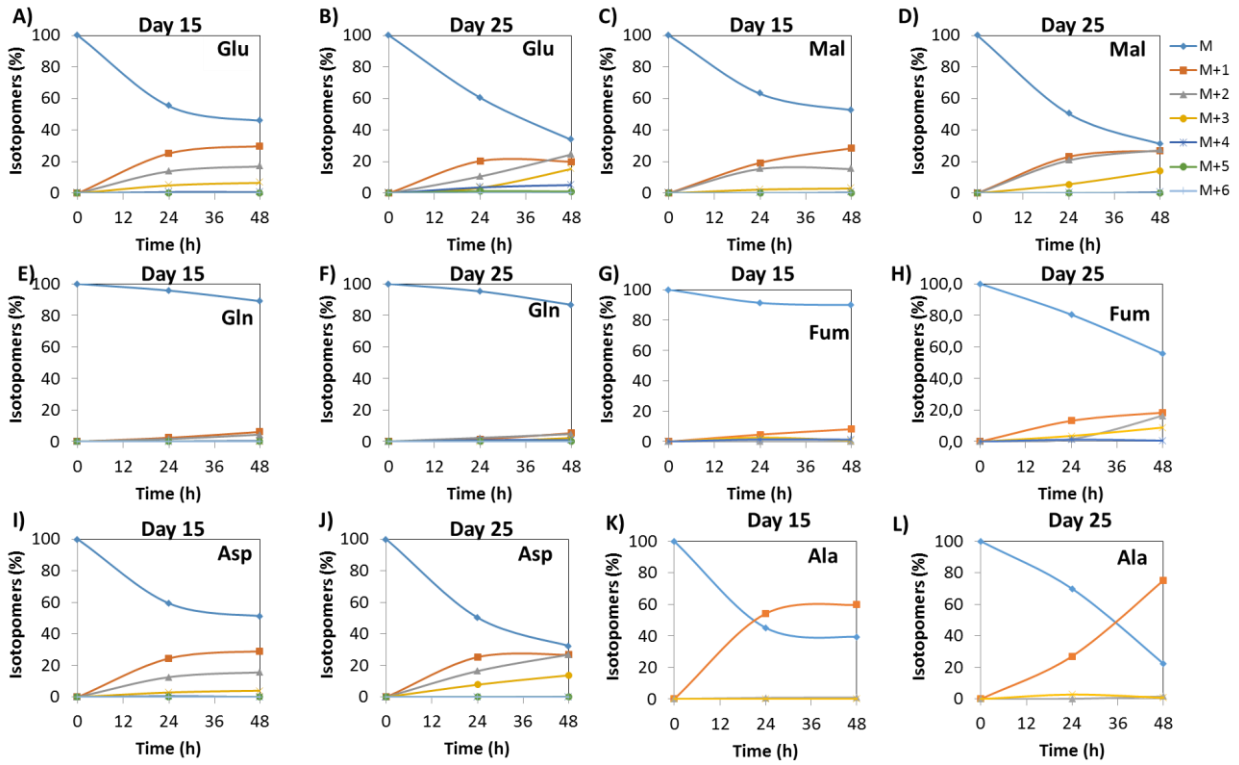

Figure 4.24: Time profiles of isotopic labeling of TCA metabolites after the introduction of [3-^{13}C]lactate. Percentage of labeled mass isotopomers were determined from the measured mass isotopomer distribution, after correction for natural isotope abundances. Glu (**A, B**), Mal (**C, D**), Gln (**E, F**), Fum (**G, H**), Asp (**I, J**) day 15 and day 25 of hiPSC-CMs after start of differentiation. The composition of lactate in the medium was 100% [3- ^{13}C] lactate.

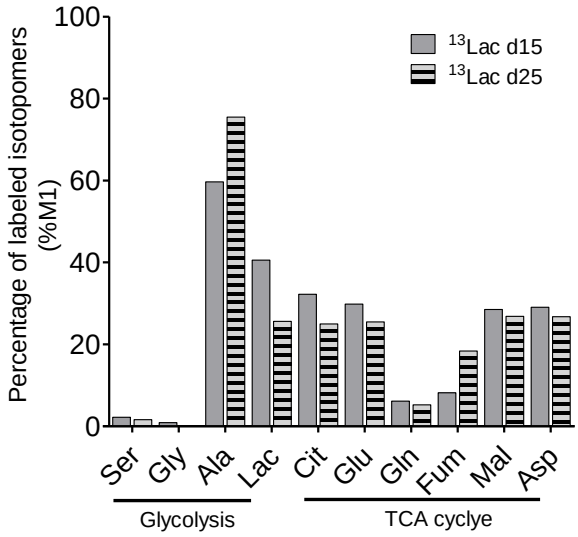

Figure 4.25: Percentage of labeled intracellular metabolites from lactate at day 15 and day 25 of culture. Values correspond to the M1 isotopomer.

However, there are still no examples of using of labeling tracer to study metabolism shift during hiPSC-CMs maturation. Overall the results presented in this section suggest that cells cultured in glucose depleted medium supplemented with fatty acids exhibit a more mature structure, ultrastructure, gene expression profiles and a metabolic performance more similar to adult CMs. Thus, replacing glucose in the culture medium by fatty acids showed to be a promising method to improve maturation of hPSC-CM *in vitro*.

5. CONCLUSION

In this work, a detailed biological characterization of two promising therapeutic products, AdV for gene delivery and hiPSC-CMs for cardiac cell-based therapies, was performed.

In the first part of this thesis, using parallel labelling experiments with [1,2-^{13}C]glucose and [U-^{13}C]glutamine, followed by non-stationary metabolic flux analysis, we revealed important metabolic changes that occur in the production cell line, 1G3, under viral infection. First, we showed that after FBS removal there is absence of cell growth, confirming that the cells were in GA conditions. The results obtained from metabolomic profiling and ^{13}C-MFA indicate that 1G3 cells possess a generally higher metabolic activity under exponential growth conditions compared to growth arrested cultures, particularly the fluxes of glycolysis and by-product formation, TCA cycle, glutamine anaplerosis and lipid generation. Moreover, the cellular response to viral infection was quantitatively very different. In EG conditions, cells increased glycolytic activity and lipid generation in a significant way, while maintaining glutamine consumption and TCA cycle activity. On the other hand, under GA conditions, the increase in metabolic activity was much more pronounced and complete. These results indicate that exponentially growing cells provide a better metabolic environment for establishment of infection and viral replication, which is corroborated by the higher AdV5 productivities obtained in these cultures.

In the second part of the thesis, a detailed phenotypic, structural and metabolic characterization was performed during CM differentiation and maturation processes. We showed that cells present typical gene and protein expression profiles throughout cardiomyocyte differentiation time. Moreover, our results demonstrated that the metabolism of early differentiated hiPSC-CMs do not significantly differ from hiPSC, when both were cultured in glucose-rich medium, both relying on glycolysis. Nonetheless, hiPSC-CMs displayed metabolic plasticity being able to consume not only glucose but also lactate and fatty acids. Noteworthy, when cultured in glucose-depleted medium supplemented with fatty acids, hiPSC-CMs showed a more mature structure and ultrastructure; displayed higher expression of genes responsible for contraction, calcium handling and electrophysiology; and used fatty acid as energy source, a typical feature of adult CMs. Future work, will be focused on parallel labeling experiment and intracellular flux map determination using stationary MFA during hiPSC-CMs maturation.

6. BIBLIOGRAPHY

Ahn WS, Antoniewicz MR. 2011. Metabolic flux analysis of CHO cells at growth and non-growth phases using isotopic tracers and mass spectrometry. *Metab. Eng.* **13**:598–609.

Ahn WS, Antoniewicz MR. 2013. Parallel labeling experiments with [1,2-(13)C]glucose and [U-(13)C]glutamine provide new insights into CHO cell metabolism. *Metab. Eng.* **15**:34–47.

Aiuti A, Slavin S, Aker M, Ficara F, Deola S, Mortellaro A, Morecki S, Andolfi G, Tabucchi A, Carlucci F, Marinello E, Cattaneo F, Vai S, Servida P, Miniero R, Roncarolo MG, Bordignon C. 2002. Correction of ADA-SCID by stem cell gene therapy combined with nonmyeloablative conditioning. *Science* **296**:2410–2413.

Améen C, Strehl R, Björquist P, Lindahl A, Hyllner J, Sartipy P. 2008. Human embryonic stem cells: current technologies and emerging industrial applications. *Crit. Rev. Oncol. Hematol.* **65**:54–80.

Antoniewicz MR, Kelleher JK, Stephanopoulos G. 2007. Elementary metabolite units (EMU): a novel framework for modeling isotopic distributions. *Metab. Eng.* **9**:68–86.

Armstrong L, Tilgner K, Saretzki G, Atkinson SP, Stojkovic M, Moreno R, Przyborski S, Lako M. 2010. Human induced pluripotent stem cell lines show stress defense mechanisms and mitochondrial regulation similar to those of human embryonic stem cells. *Stem Cells* **28**:661–73.

Baines CP. 2014. How and when do myocytes die during ischemia and reperfusion: the late phase. *J. Cardiovasc. Pharmacol. Ther.* **16**:239–43.

Bier DM. 1987. 3 The use of stable isotopes in metabolic investigation. *Baillieres. Clin. Endocrinol. Metab.* **1**:817–836.

Bil-lula I, Ussowicz M. 2010. Adenoviral Infection – Common Complication Following Hematopoietic Stem Cell Transplantation. In: . *New Adv. Stem Cell Transplant.*, pp. 533–556.

Birbrair A, Zhang T, Wang Z-M, Messi ML, Olson JD, Mintz A, Delbono O. 2014. Type-2 pericytes participate in normal and tumoral angiogenesis. *Am. J. Physiol. Cell Physiol.* **307**:C25–38.

Blazeski A, Zhu R, Hunter DW, Weinberg SH, Boheler KR, Zambidis ET, Tung L. 2012. Electrophysiological and contractile function of cardiomyocytes derived from human embryonic stem cells. *Prog. Biophys. Mol. Biol.* **110**:178–195.

Bloom DE, Cafiero ET, Jané-Llopis E, Abrahams-Gessel S, Bloom LR, Fathima S, Feigl AB, Gaziano T, Mowafi M, Pandya A, Prettner K, Rosenberg L, Seligman B, Stein AZ, Weinstein C, Bloom DE, Cafiero ET, Jané-Llopis EC. 2011. The Global Economic Burden of Non-communicable Diseases. *Glob. Econ. Burd. Noncommunicable Dis. Geneva World Econ. Forum* 5-45 p.

Blumenthal R, Seth P, Willingham MC, Pastan I. 1986. pH-dependent lysis of liposomes by adenovirus. *Biochemistry* **25**:2231–2237.

de Bolster MWG. 1997a. Glossary of Terms Used in Bioinorganic Chemistry: Catabolism. *Int. Union Pure Appl. Chem. Retrieved 2007-10-30*.

de Bolster MWG. 1997b. Glossary of Terms Used in Bioinorganic Chemistry: Anabolism. *Int. Union Pure Appl. Chem. Arch. from Orig. 30 Oct. 2007*.

Bongso A, Tan S. 2005. Human Blastocyst Culture and Derivation of Embryonic Stem Cell Lines. *Stem Cell Rev.* **05**:87–98.

Bouard D, Alazard-Dany D, Cosset F-L. 2009. Viral vectors: from virology to transgene expression. *Br. J. Pharmacol.* **157**:153–165.

Brennan J, Lu CC, Norris DP, Rodriguez T a, Beddington RS, Robertson EJ. 2001. Nodal signalling in the epiblast patterns the early mouse embryo. *Nature* **411**:965–969.

Burridge PW, Keller G, Gold JD, Wu JC. 2012. Production of de novo cardiomyocytes: human pluripotent stem cell differentiation and direct reprogramming. *Cell Stem Cell* **10**:16–28.

Burridge PW, Matsa E, Shukla P, Lin ZC, Churko JM, Ebert AD, Lan F, Diecke S, Huber B, Mordwinkin NM, Plews JR, Abilez OJ, Cui B, Gold JD, Wu JC. 2014. Chemically defined generation of human cardiomyocytes. *Nat. Methods* **11**:855–860.

Carinhas N, Bernal V, Monteiro F, Carrondo MJT, Oliveira R, Alves PM. 2010. Improving baculovirus production at high cell density through manipulation of energy metabolism. *Metab. Eng.* **12**:39–52.

Carinhas N, Bernal V, Teixeira AP, Carrondo MJT, Alves PM, Oliveira R. 2011. Hybrid metabolic flux analysis : combining stoichiometric and statistical constraints to model the formation of complex recombinant products. *BMC Syst. Biol.* **5**:34.

Carinhas N, Duarte TM, Barreiro LC, Alves PM, Teixeira AP. 2013. Metabolic signatures of GS CHO cell clones associated with butyrate treatment and culture phase transition. *Biotechnol. Bioeng.* **110**:3244–3257.

Carinhas N, Pais DA, Koshkin A, Fernandes P, Coroadinha AS, Carrondo MJ, Alves PM, P TA. Parallel 13C labeling and isotopic nonstationary metabolic flux analysis of MDCK cells during growth and canine adenovirus vector production. *Biotechnol. Bioeng.*

Chang A, Towbin J. 2006. Heart Failure in Children and Young Adults: From molecular mechanisms to medical and surgical strategies. Saunders. Elsevier; 828 p.

Chen EC, Yagi S, Kelly KR, Mendoza SP, Maninger N, Rosenthal A, Spinner A, Bales KL, Schnurr DP, Lerche NW, Chiu CY. 2011. Cross-species transmission of a novel adenovirus associated with a fulminant pneumonia outbreak in a new world monkey colony. *PLoS Pathog.* **7**:e1002155.

Chinnadurai G. 1998. Control of Apoptosis by Human Adenovirus Genes. *Semin. Virol.* **8**:399–408.

Coura S, Nardi NB. 2008. A role for adeno-associated viral vectors in gene therapy. *Genet. Mol. Biol.* **11**:1–11.

Crown SB, Antoniewicz MR. 2013. Parallel labeling experiments and metabolic flux analysis: Past, present and future methodologies. *Metab. Eng.* **16**:21–32.

DeBerardinis RJ, Lum JJ, Hatzivassiliou G, Thompson CB. 2008. The biology of cancer: metabolic reprogramming fuels cell growth and proliferation. *Cell Metab.* **7**:11–20.

Delgado T, Carroll P a, Punjabi AS, Margineantu D, Hockenbery DM, Lagunoff M. 2010. Induction of the Warburg effect by Kaposi's sarcoma herpesvirus is required for the maintenance of latently infected endothelial cells. *Proc. Natl. Acad. Sci. U. S. A.* **107**:10696–10701.

Dierickx P, Doevendans P a., Geijsen N, Van Laake LW. 2012. Embryonic template-based generation and purification of pluripotent stem cell-derived cardiomyocytes for heart repair. *J. Cardiovasc. Transl. Res.* **5**:566–580.

Dietmair S, Timmins NE, Gray PP, Nielsen LK, Krömer JO. 2010. Towards quantitative metabolomics of mammalian cells : Development of a metabolite extraction protocol. *Anal. Biochem.* **404**:155–164.

Dormond E, Perrier M, Kamen a. 2009. From the first to the third generation adenoviral vector: What parameters are governing the production yield? *Biotechnol. Adv.* **27**:133–144.

Dowell JD, Rubart M, Pasumarthi KBS, Soonpaa MH, Field LJ. 2003. Myocyte and myogenic stem cell transplantation in the heart **58**:336–350.

Drake KJ, Sidorov VY, McGuinness OP, Wasserman DH, Wikswo JP. 2012. Amino acids as metabolic substrates during cardiac ischemia. *Exp. Biol. Med. (Maywood).* **237**:1369–78.

Duarte TM, Carinhas N, Barreiro LC, Carrondo MJT, Alves PM, Teixeira AP. 2014. Metabolic Responses of CHO Cells to Limitation of Key Amino Acids. *Biotechnol. Bioeng.* **111**:2095–2106.

Eefting F, Rensing B, Wigman J, Pannekoek WJ, Liu WM, Cramer MJ, Lips DJ, Doevendans P a. 2004. Role of apoptosis in reperfusion injury. *Cardiovasc. Res.* **61**:414–26.

Facucho-Oliveira JM, St John JC. 2009. The relationship between pluripotency and mitochondrial DNA proliferation during early embryo development and embryonic stem cell differentiation. *Stem Cell Rev.* **5**:140–58.

Fallaux F, Bout A, Velde I, Wollenberg D, Hehir K, J K, Auger C, Cramer S, HV O, EB A, Valerio D, Hoeben R. 1998. New Helper Cells and Matched Early 1-Deleted Adenovirus Vectors Prevent Generation of Replication-Competent Adenoviruses. *Hum. Gene Ther.* **9**:1909–1917.

Farson D, Tao L, Ko D, Li Q, Brignetti D, Segawa K, Mittelstaedt D, Harding T, Yu DC, Li Y. 2006. Development of Novel E1-Complementary Cells for Adenoviral Production Free of Replication-Competent Adenovirus. *Mol. Ther.* **14**:305–311.

Ferreira TB, Perdigão R, Silva AC, Zhang C, Aunins JG, Carrondo MJT, Alves PM. 2009. 293 Cell cycle synchronisation in adenovirus vector production. *Biotechnol. Prog.* **25**:235–243.

Filipczyk a a, Passier R, Rochat a, Mummery CL. 2007. Regulation of cardiomyocyte differentiation of embryonic stem cells by extracellular signalling. *Cell. Mol. Life Sci.* **64**:704–18.

Fisher DJ, Heymann M a, Rudolph a M. 1981. Myocardial consumption of oxygen and carbohydrates in newborn sheep. *Pediatr. Res.* **15**:843–846.

Folmes CDL, Dzeja PP, Nelson TJ, Terzic A. 2012. Metabolic plasticity in stem cell homeostasis and differentiation. *Cell Stem Cell* **11**:596–606.

Folmes CDL, Nelson TJ, Martinez-Fernandez A, Arrell DK, Lindor JZ, Dzeja PP, Ikeda Y, Perez-Terzic C,

Terzic A. 2011. Somatic oxidative bioenergetics transitions into pluripotency-dependent glycolysis to facilitate nuclear reprogramming. *Cell Metab.* **14**:264–71.

Garbern JC, Mummery CL, Lee RT. 2013. Model systems for cardiovascular regenerative biology. *Cold Spring Harb. Perspect. Med.* **3**:a014019.

Gibbs M, Horecker BL. 1954. The mechanism of pentose phosphate conversion to hexose monophosphate. II. With pea leaf and pea root preparations. *J. Biol. Chem.* **208**:813–820.

Gómez-Navarro J, Curiel DT. 2000. Conditionally replicative adenoviral vectors for cancer gene therapy. *Lancet Oncol.* **1**:148–158.

Graham FL, Smiley J, Russell WC, Nairn R. 1977. Characteristics of a human cell line transformed by DNA from human adenovirus type 5. *J. Gen. Virol.* **36**:59–74.

Greber UF, Webster P, Weber J, Helenius a. 1996. The role of the adenovirus protease on virus entry into cells. *EMBO J.* **15**:1766–1777.

Habib M, Caspi O, Gepstein L. 2008. Human embryonic stem cells for cardiomyogenesis. *J. Mol. Cell. Cardiol.* **45**:462–74.

Heart Federation. 2011. Global Atlas on cardiovascular disease prevention and control 1-153 p.

Hehir KM, Armentano D, Cardoza LM, Choquette TL, Berthelette PB, White G a, Couture L a, Everton MB, Keegan J, Martin JM, Pratt D a, Smith MP, Smith a E, Wadsworth SC. 1996. Molecular characterization of replication-competent variants of adenovirus vectors and genome modifications to prevent their occurrence. *J. Virol.* **70**:8459–8467.

Hofmann U, Maier K, Niebel A, Vacun G, Reuss M, Mauch K. 2008. Identification of metabolic fluxes in hepatic cells from transient 13C-labeling experiments: Part I. Experimental observations. *Biotechnol. Bioeng.* **100**:344–54.

Huangfu D, Maehr R, Guo W, Eijkelenboom A, Snitow M, Chen AE, Melton D a. 2008. Induction of pluripotent stem cells by defined factors is greatly improved by small-molecule compounds. *Nat. Biotechnol.* **26**:795–7.

J.K. Raty, J.T . Pikkarainen TW and SY-H. 2008. Gene Therapy: The First Approved Gene-Based Medicines, Molecular Mechanisms and Clinical Indications. *Curr. Mol. Pharmacol.* **1**:13–23.

Jawetz E. 1959. The Story of Shipyard Eye*. *Br. Med. J.* **1**:873–876.

Jennings R, Steenbergen C. 1985. Nucleotide metabolism and cellular damage in myocardial ischemia. *Ann. Rev. Physiol* **47**:727–49.

Johnson MT, Mahmood S, Patel MS. 2003. Intermediary metabolism and energetics during murine early embryogenesis. *J. Biol. Chem.* **278**:31457–60.

Kattman SJ, Witty AD, Gagliardi M, Dubois NC, Niapour M, Hotta A, Ellis J, Keller G. 2011. Stage-specific optimization of activin/nodal and BMP signaling promotes cardiac differentiation of mouse and human pluripotent stem cell lines. *Cell Stem Cell* **8**:228–40.

Kelleher JK. 2001. Flux Estimation Using Isotopic Tracers : Common Ground for Metabolic Physiology and Metabolic Engineering. *Metab. Eng.* **3**:100–110.

Kelleher JK. 2004. Probing metabolic pathways with isotopic tracers: insights from mammalian metabolic physiology. *Metab. Eng.* **6**:1–5.

Kolwicz SC, Tian R. 2011. Glucose metabolism and cardiac hypertrophy. *Cardiovasc. Res.* **90**:194–201.

Kovesdi I, Hedley SJ. 2010. Adenoviral producer cells. *Viruses* **2**:1681–1703.

Laflamme M a, Chen KY, Naumova A V, Muskheli V, Fugate J a, Dupras SK, Reinecke H, Xu C, Hassanipour M, Police S, O'Sullivan C, Collins L, Chen Y, Minami E, Gill E a, Ueno S, Yuan C, Gold J, Murry CE. 2007. Cardiomyocytes derived from human embryonic stem cells in pro-survival factors enhance function of infarcted rat hearts. *Nat. Biotechnol.* **25**:1015–24.

Lam AT-L, Chen AK-L, Li J, Birch WR, Reuveny S, Oh SK-W. 2014. Conjoint propagation and differentiation of human embryonic stem cells to cardiomyocytes in a defined microcarrier spinner culture. *Stem Cell Res. Ther.* **5**:110.

Landry DW, Zucker H a. 2004. Embryonic death and the creation of human embryonic stem cells. *J. Clin. Invest.* **114**:1184–1186.

Leighty RW, Antoniewicz MR. 2012. Parallel labeling experiments with [U-13C]glucose validate E. coli metabolic network model for 13C metabolic flux analysis. *Metab. Eng.* **14**:533–41.

Leri A, Kajstura J, Anversa P. 2011. Role of cardiac stem cells in cardiac pathophysiology: a paradigm shift in human myocardial biology. *Circ. Res.* **109**:941–61.

Lian X, Hsiao C, Wilson G, Zhu K, Hazeltine LB, Azarin SM, Raval KK, Zhang J, Kamp TJ, Palecek SP. 2012. Robust cardiomyocyte differentiation from human pluripotent stem cells via temporal modulation of canonical Wnt signaling. *Proc. Natl. Acad. Sci. U. S. A.* **109**:E1848–57.

Lopaschuk GD, Jaswal JS. 2010. Energy metabolic phenotype of the cardiomyocyte during development, differentiation, and postnatal maturation. *J. Cardiovasc. Pharmacol.* **56**:130–140.

Lundy SD, Zhu W-Z, Regnier M, Laflamme MA. 2013. Structural and functional maturation of cardiomyocytes derived from human pluripotent stem cells. *Stem Cells Dev.* **22**:1991–2002.

Marvin MJ, Di Rocco G, Gardiner a, Bush SM, Lassar a B. 2001. Inhibition of Wnt activity induces heart formation from posterior mesoderm. *Genes Dev.* **15**:316–27.

Meier O, Greber UF. 2003. Adenovirus endocytosis. *J. Gene Med.* **5**:451–462.

Mercola M, Ruiz-Lozano P, Schneider MD. 2011. Cardiac muscle regeneration: Lessons from development. *Genes Dev.* **25**:299–309.

Metallo CM, Gameiro PA, Bell EL, Mattaini KR, Yang J, Hiller K, Jewell CM, Johnson ZR, Irvine DJ, Guarente L, Kelleher JK, Vander MG. 2012. Reductive glutaminemetabolismby IDH1 mediates lipogenesis under hypoxia. *Nature* **481**:380–384.

Metallo CM, Walther JL, Stephanopoulos G. 2009. Evaluation of 13C isotopic tracers for metabolic flux

analysis in mammalian cells. *J. Biotechnol.* **144**:167–74.

Mima T, Fischman DA. 1995. Fibroblast growth factor receptor is required for in vivo cardiac myocyte proliferation at early embryonic stages of heart development. **92**:467–471.

Mummery CL, Zhang J, Ng ES, Elliott D a, Elefanty AG, Kamp TJ. 2012. Differentiation of human embryonic stem cells and induced pluripotent stem cells to cardiomyocytes: a methods overview. *Circ. Res.* **111**:344–58.

Murry CE, Keller G. 2008. Differentiation of embryonic stem cells to clinically relevant populations: lessons from embryonic development. *Cell* **132**:661–80.

Musunuru K, Domian I, Chien K. 2010. Stem Cell Models of Cardiac Development and Disease. *Annu Rev Cell Dev Biol.* **26**:667–687.

Nakagawa M, Koyanagi M, Tanabe K, Takahashi K, Ichisaka T, Aoi T, Okita K, Mochiduki Y, Takizawa N, Yamanaka S. 2008. Generation of induced pluripotent stem cells without Myc from mouse and human fibroblasts. *Nat. Biotechnol.* **26**:101–6.

Neves D. 1987. Capillary gas chromatography of amino acids, including asparagine and glutamine: Sensitive gas chromatographic-mass spectrometric and selected ion monitoring gas chromatographic-mass spectrometric detection of the N,O (S)-tert-butyldimethylsilyl derivativ **392**:249–258.

Nielsen J. 2003. It Is All about Metabolic Fluxes GUEST COMMENTARY It Is All about Metabolic Fluxes. *J. Bacteriol.* **185**:7031–7035.

Nöh K, Wiechert W. 2011. The benefits of being transient: isotope-based metabolic flux analysis at the short time scale. *Appl. Microbiol. Biotechnol.* **91**:1247–65.

Nussbaum J, Minami E, Laflamme M a, Virag J a I, Ware CB, Masino A, Muskheli V, Pabon L, Reinecke H, Murry CE. 2007. Transplantation of undifferentiated murine embryonic stem cells in the heart: teratoma formation and immune response. *FASEB J.* **21**:1345–57.

O'Malley J, Woltjen K, Kaji K. 2009. New strategies to generate induced pluripotent stem cells. *Curr. Opin. Biotechnol.* **20**:516–21.

Oldiges M, Lütz S, Pflug S, Schroer K, Stein N, Wiendahl C. 2007. Metabolomics: current state and evolving methodologies and tools. *Appl. Microbiol. Biotechnol.* **76**:495–511.

Orlic D. 2005. BM stem cells and cardiac repair: Where do we stand in 2004? *Cytotherapy* **7**:3–15.

Paige SL, Osugi T, Afanasiev OK, Pabon L, Reinecke H, Murry CE. 2010. Endogenous Wnt/beta-catenin signaling is required for cardiac differentiation in human embryonic stem cells. *PLoS One* **5**:e11134.

Pantaleon M, Kaye PL. 1998. Glucose transporters in preimplantation development. *Rev. Reprod.* **3**:77–81.

Parks R, Evelegh C, Graham F. 1999. Use of helper-dependent adenoviral vectors of alternative serotypes permits repeat vector administration. *Gene Ther.* **6**:1565–1573.

Pascual A, Aranda A. 2013. Thyroid hormone receptors, cell growth and differentiation. *Biochim. Biophys. Acta* **1830**:3908–16.

Patterson S, Russell WC. 1983. Ultrastructural and immunofluorescence studies of early events in adenovirus-HeLa cell interactions. *J. Gen. Virol.* **64**:1091–1099.

Porter G a., Hom JR, Hoffman DL, Quintanilla R a., Bentley KLDM, Sheu SS. 2011. Bioenergetics, mitochondria, and cardiac myocyte differentiation. *Prog. Pediatr. Cardiol.* **31**:75–81.

Price ND, Papin JA, Schilling CH, Palsson BO. 2003. Genome-scale microbial in silico models: the constraints-based approach. *Trends Biotechnol.* **21**:162–9.

Prigione A, Fauler B, Lurz R, Lehrach H, Adjaye J. 2010. The senescence-related mitochondrial/oxidative stress pathway is repressed in human induced pluripotent stem cells. *Stem Cells* **28**:721–33.

Qin C, Yang YH, May L, Gao X, Stewart A, Tu Y, Woodman OL, Ritchie RH. 2014. Cardioprotective potential of annexin-A1 mimetics in myocardial infarction. *Pharmacol. Ther.* **148**:47–65.

Rajala K, Pekkanen-Mattila M, Aalto-Setälä K. 2011. Cardiac differentiation of pluripotent stem cells. *Stem Cells Int.* **2011**:383709.

Rana P, Anson B, Engle S, Will Y. 2012. Characterization of Human Induced Pluripotent Stem Cell Derived Cardiomyocytes : Bioenergetics and Utilization in Safety Screening Characterization of Human Induced Pluripotent Stem Cell Derived Cardiomyocytes : Bioenergetics and Utilization in Safety Scr. *Toxicol. Sci.* **130**:117–31.

Räty JK, Lesch HP, Wirth T, Ylä-Herttuala S. 2008. Improving safety of gene therapy. *Curr. Drug Saf.* **3**:46–53.

Rekosh R. 1977. Identification of a protein linked to the Ends of Adenovirus DNA. *Virology* **11**:293–295.

Ribeiro MC, Tertoolen LG, Guadix JA, Bellin M, Kosmidis G, D'Aniello C, Monshouwer-Kloots J, Goumans M-J, Wang Y, Feinberg AW, Mummery CL, Passier R. 2015. Functional maturation of human pluripotent stem cell derived cardiomyocytes in vitro – Correlation between contraction force and electrophysiology. *Biomaterials* **51**:138–150.

Robertson C, Tran DD, George SC. 2013. Concise review: Maturation phases of human pluripotent stem cell-derived cardiomyocytes. *Stem Cells* **31**:829–837.

Robinton DA, Daley GQ. 2012. The promise of induced pluripotent stem cells in research and therapy. *Nature* **481**:295–305.

Rowe W, Huebner R, Gilmore L, Parrott R, Ward T. 1953. Isolation of a cytopathogenic agent from human adenoids undergoing spontaneous degeneration in tissue culture. *Proc Soc Exp Biol Med* **84**:570–573.

Russell WC. 2000. Update on adenovirus and its vectors General properties of adenoviruses. *J. Gen. Virol.* **81**:2573–2604.

Russell WC. 2009. Adenoviruses: Update on structure and function. *J. Gen. Virol.* **90**:1–20.

Sanchez EL, Lagunoff M. 2015. Viral activation of cellular metabolism. *Virology* **479-480**:609–618.

Saphire a C, Guan T, Schirmer EC, Nemerow GR, Gerace L. 2000. Nuclear import of adenovirus DNA in vitro involve the nuclear protin import pathway and Hsc70. *J. Biol. Chem.* **275**:4298–4304.

Schiedner G, Hertel S, Kochanek S. 2000. Efficient transformation of primary human amniocytes by E1 functions of Ad5: generation of new cell lines for adenoviral vector production. *Hum. Gene Ther.* **11**:2105–2116.

Segers VFM, Lee RT. 2008. Stem-cell therapy for cardiac disease. *Nature* **451**:937–42.

Shyh-Chang N, Daley GQ, Cantley LC. 2013. Stem cell metabolism in tissue development and aging. *Development* **140**:2535–47.

Silva AC, Simão D, Küppers C, Lucas T, Sousa MFQ, Cruz P, Carrondo MJT, Kochanek S, Alves PM. 2015. Human amniocyte-derived cells are a promising cell host for adenoviral vector production under serum-free conditions. *Biotechnol. J.* **10**:760–771.

Smith C a, Want EJ, O'Maille G, Abagyan R, Siuzdak G. 2006. XCMS: processing mass spectrometry data for metabolite profiling using nonlinear peak alignment, matching, and identification. *Anal. Chem.* **78**:779–87.

Sreekumar A, Poisson LM, Rajendiran TM, Khan AP, Cao Q, Yu J, Laxman B, Mehra R, Lonigro RJ, Li Y, Nyati MK, Ahsan A, Kalyana-Sundaram S, Han B, Cao X, Byun J, Omenn GS, Ghosh D, Pennathur S, Alexander DC, Berger A, Shuster JR, Wei JT, Varambally S, Beecher C, Chinnaiyan AM. 2009. Metabolomic profiles delineate potential role for sarcosine in prostate cancer progression. *Nature* **457**:910–4.

Srivastava D. 2006. Making or breaking the heart: from lineage determination to morphogenesis. *Cell* **126**:1037–48.

Suomalainen M, Nakano MY, Keller S, Boucke K, Stidwill RP, Greber UF. 1999. Microtubule-dependent plus- and minus end-directed motilities are competing processes for nuclear targeting of adenovirus. *J. Cell Biol.* **144**:657–672.

Takahashi K, Tanabe K, Ohnuki M, Narita M, Ichisaka T, Tomoda K, Yamanaka S. 2007. Induction of pluripotent stem cells from adult human fibroblasts by defined factors. *Cell* **131**:861–72.

Tatsis N, Ertl HC. 2004. Adenoviruses as vaccine vectors. *Mol. Ther.* **10**:616–629.

Thai M, Graham NA, Braas D, Nehil M, Komisopoulou E, Kurdistani SK, McCormick F, Graeber TG, Christofk HR. 2014. Adenovirus E4ORF1-induced MYC activation promotes host cell anabolic glucose metabolism and virus replication. *Cell Metab.* **19**:694–701.

Thomas CE, Ehrhardt A, Kay MA. 2003. Progress and problems with the use of viral vectors for gene therapy. *Nat. Rev. Genet.* **4**:346–358.

Thomson JA, Itskovitz-eldor J, Shapiro S, Waknitz MA, Swiergiel JJ, Jones JM. 1998. Embryonic Stem Cell Lines Derived from Human Blastocysts **282**:1145–1147.

Tirziu D, Giordano FJ, Simons M. 2010. Cell communications in the heart. *Circulation* **122**:928–37.

Tohyama S, Hattori F, Sano M, Hishiki T, Nagahata Y, Matsuura T, Hashimoto H, Suzuki T, Yamashita H, Satoh Y, Egashira T, Seki T, Muraoka N, Yamakawa H, Ohgino Y, Tanaka T, Yoichi M, Yuasa S, Murata M, Suematsu M, Fukuda K. 2013. Distinct metabolic flow enables large-scale purification of

mouse and human pluripotent stem cell-derived cardiomyocytes. *Cell Stem Cell* **12**:127–37.

Univer- JG. 1995. Bone mor hogenetic protein-4 Is reqmrea for mesoderm formation and patterning in the mouse. *Genes Dev.*:2105–2116.

Vacanti NM, Metallo CM. 2013. Exploring metabolic pathways that contribute to the stem cell phenotype. *Biochim. Biophys. Acta* **1830**:2361–9.

Venable JH, Coggeshall R. 1965. A simplified lead citrate stain for use in electron microscopy. *J. Cell Biol.* **25**:407–408.

Walker JM, Ditor SEE. 2004. Gene Delivery to Mammalian Cells. In: . *Methods Mol. Biol.*, pp. 1–559.

Wang K, Huang S, Kapoor-Munshi a, Nemerow G. 1998. Adenovirus internalization and infection require dynamin. *J. Virol.* **72**:3455–3458.

World Health Organization. 2011. Global status report on noncommunicable diseases.

World Health Organization. 2015. The top 10 causes of death. *Fact Sheet N 310*. http://www.who.int/mediacentre/factsheets/fs310/en/index2.html.

Xu C. 2012. Differentiation and enrichment of cardiomyocytes from human pluripotent stem cells. *J. Mol. Cell. Cardiol.* **52**:1203–1212.

Yang L, Soonpaa MH, Adler ED, Roepke TK, Kattman SJ, Kennedy M, Henckaerts E, Bonham K, Abbott GW, Linden RM, Field LJ, Keller GM. 2008. Human cardiovascular progenitor cells develop from a KDR+ embryonic-stem-cell-derived population. *Nature* **453**:524–8.

Yang X, Pabon L, Murry CE. 2014a. Engineering adolescence: Maturation of human pluripotent stem cell-derived cardiomyocytes. *Circ. Res.* **114**:511–523.

Yang X, Rodriguez M, Pabon L, Fischer KA, Reinecke H, Regnier M, Sniadecki NJ, Ruohola-Baker H, Murry CE. 2014b. Tri-iodo-l-thyronine promotes the maturation of human cardiomyocytes-derived from induced pluripotent stem cells. *J. Mol. Cell. Cardiol.* **72**:296–304.

Ylä-Herttuala S AK. 2003. Gene transfer as a tool to induce therapeutic vascular growth. tle. *Nat Med.*:694–701.

Young JD. 2014. Systems biology INCA : A computational platform for isotopically nonstationary metabolic flux analysis. *Bioinformatics* **30**:1333–5.

Young JD, Walther JL, Antoniewicz MR, Yoo H, Stephanopoulos G. 2008. An elementary metabolite unit (EMU) based method of isotopically nonstationary flux analysis. *Biotechnol. Bioeng.* **99**:686–99.

Yu J, Vodyanik M a, Smuga-Otto K, Antosiewicz-Bourget J, Frane JL, Tian S, Nie J, Jonsdottir G a, Ruotti V, Stewart R, Slukvin II, Thomson J a. 2007. Induced pluripotent stem cell lines derived from human somatic cells. *Science* **318**:1917–20.

Zhang J, Wilson GF, Soerens AG, Koonce CH, Yu J, Palecek SP, Thomson J a, Kamp TJ. 2009. Functional cardiomyocytes derived from human induced pluripotent stem cells. *Circ. Res.* **104**:e30–41.

Zhang J, Nuebel E, Daley GQ, Koehler CM, Teitell M a. 2012. Metabolic regulation in pluripotent stem

cells during reprogramming and self-renewal. *Cell Stem Cell* **11**:589–95.

Zhu R, Blazeski A, Poon E, Costa KD, Tung L, Boheler KR. 2014. Physical developmental cues for the maturation of human pluripotent stem cell-derived cardiomyocytes. *Stem Cell Res. Ther.* **5**:117.

Zimmermann W-H, Didié M, Döker S, Melnychenko I, Naito H, Rogge C, Tiburcy M, Eschenhagen T. 2006. Heart muscle engineering: an update on cardiac muscle replacement therapy. *Cardiovasc. Res.* **71**:419–29.

Zwi-Dantsis L, Gepstein L. 2012. Induced pluripotent stem cells for cardiac repair. *Cell. Mol. Life Sci.* **69**:3285–3299.

7. ANNEXES

Annex 1

Table 7.1: Metabolic flux analysis for mock- and virus-infected cells results using combined 13C-MFA of [1,2-^{13}C]glucose and [U-^{13}C]glutamine parallel labeling experiments at the exponential phase. Shown are the estimated net and exchange fluxes (nmol/10^{6}cell/h)

		EG Mock-infected		EG virus-infected	
		nmol/10^{6}cells/h	SD	nmol/10^{6}cells/h	SD
G6P <-> F6P	R1 net	176.10	31.01	197.76	39.39
G6P <-> F6P	R1 exch	0.00	862.87	0.00	432.95
F6P -> FBP	R2	177.62	10.30	201.48	13.11
FBP <-> DHAP + GAP	R3 net	177.62	10.30	201.48	13.11
FBP <-> DHAP + GAP	R3 exch	72.17	862.32	115.03	431.16
DHAP <-> GAP	R4 net	177.24	10.29	200.75	13.11
DHAP <-> GAP	R4 exch	14708.00	862.32	215550.00	431.16
GAP <-> 3PG	R5 net	355.61	10.24	404.08	13.09
GAP <-> 3PG	R5 exch	105.84	862.32	0.00	431.16
3PG <-> PEP	R6 net	305.57	9.37	403.52	1.18
3PG <-> PEP	R6 exch	305.93	862.32	0.17	431.16
PEP -> Pyr.c	R7	305.57	9.37	403.52	1.18
Pyr.c <-> Pyr.m	R44 net	-6.17	1.54	3.42	1.62
Pyr.c <-> Pyr.m	R44 exch	635.97	429.04	820.77	431.16
G6P -> P5P + CO2	R8	3.00	31.04	6.97	39.41
P5P + P5P <-> GAP + S7P	R9 net	0.76	10.35	1.86	13.14
P5P + P5P <-> GAP + S7P	R9 exch	25.67	2.05	93486.00	431.16
S7P + GAP <-> E4P + F6P	R10 net	0.76	10.35	1.86	13.14
S7P + GAP <-> E4P + F6P	R10 exch	0.00	862.32	0.00	431.16
E4P + P5P <-> GAP + F6P	R11 net	0.76	10.35	1.86	13.14
E4P + P5P <-> GAP + F6P	R11 exch	41469.00	862.32	25375.00	431.16
Pyr.c <-> Lac	R12 net	347.86	9.63	385.20	13.77
Pyr.c <-> Lac	R12 exch	784.31	862.37	0.00	431.38
Pyr.c <-> Ala	R13 net	15.31	1.53	15.83	5.55
Pyr.c <-> Ala	R13 exch	0.00	398.58	469.40	20.01
Pyr.m -> AcCoA.m + CO2	R14	23.40	0.68	28.66	0.87
OAA + AcCoA.m -> Cit	R16	28.08	0.83	34.06	1.13
Cit <-> AKG + CO2	R17 net	20.20	0.75	18.90	0.77
Cit <-> AKG + CO2	R17 exch	1.43	0.24	2.68	0.28
AKG -> SucCoA + CO2	R18	50.19	1.38	46.26	2.22
SucCoA <-> Suc	R19 net	50.19	1.38	46.26	2.22
SucCoA <-> Suc	R19 exch	19565.00	862.32	0.00	431.16
Suc <-> Fum	R20 net	52.15	1.64	48.70	1.47
Suc <-> Fum	R20 exch	57693.00	862.32	0.00	431.16
Fum <-> Mal	R21 net	52.15	1.62	48.70	1.38

Fum <-> Mal	R21 exch	34026.00	862.32	314.96	101.97
Mal <-> OAA	R22 net	19.63	0.86	21.11	1.07
Mal <-> OAA	R22 exch	282.46	862.32	2936.70	431.16
Mal -> Pyr.m + CO2	R23	32.52	1.19	27.59	1.13
Pyr.m + CO2 -> OAA	R15	2.94	0.53	2.35	0.51
Gln -> Glu	R25	39.42	0.13	40.64	0.13
AKG <-> Glu	R26 net	-29.98	0.80	-27.37	1.55
AKG <-> Glu	R26 exch	249.56	25.61	519.91	431.16
Asn <-> Asp	R27 net	-0.90	0.11	-1.73	0.11
Asn <-> Asp	R27 exch	0.49	0.74	4.69	431.16
3PG -> Ser	R29	50.04	6.94	0.56	13.12
Ser -> Pyr.c	R30	51.42	6.45	0.94	13.06
Ser <-> Gly + C1	R31 net	0.75	0.38	1.44	0.31
Ser <-> Gly + C1	R31 exch	263.34	77.67	5.23	1.23
Glu <-> Pro	R32 net	5.77	0.18	8.22	0.51
Glu <-> Pro	R32 exch	20884.00	862.32	315.06	33.52
Val + CO2 -> Suc + CO2 + CO2	R33	0.81	0.74	1.14	0.58
Ile + CO2 -> Suc + AcCoA.m + CO2	R34	1.15	0.84	1.30	1.36
Leu + CO2 -> AcCoA.m + AcCoA.m + AcCoA.m + CO2	R35	0.34	0.57	1.37	0.71
Thr -> AcCoA.m + Gly	R36	2.51	0.36	0.00	0.56
Phe -> Tyr	R37	0.00	0.31	0.01	0.43
Tyr -> Fum + AcCoA.m + AcCoA.m + CO2	R38	0.00	0.53	0.00	0.54
Met + Ser + CO2 -> Suc + Cys.snk + CO2 + C1	R39	0.00	0.34	0.00	0.12
Lys -> CO2 + CO2 + AcCoA.m + AcCoA.m	R40	0.00	0.64	0.00	0.54
His -> Glu + C1	R41	0.00	0.14	0.00	0.22
Arg -> Glu + Urea.snk	R42	0.02	0.93	0.06	431.61
Glu + CO2 -> Arg	R43	1.34	0.91	0.00	431.61
162.6*Ala + 104.6*Glu + 87.26*Gln + 17.34*Gly + 144.4*Ser + 154.5*Lys + 152.8*Leu + 87.8*Ile + 102.2*Arg + 127.9*Asp + 104.6*Thr + 112.7*Val + 37.4*Met + 59.35*Phe + 49.32*Tyr + 38.75*His + 84.82*Pro + 78.05*Asn + 80.22*G6P + 63.12*P5P + 65.09*C1 + 33.06*DHAP + 683.5*AcCoA.c -> Biomass	R64	0.01	0.00	0.02	0.00
Glc.ext -> G6P	R46	180.03	0.00	206.52	0.00
Lac <-> Lac.ext	R47 net	347.86	9.63	385.20	13.77
Lac <-> Lac.ext	R47 exch	0.00	862.32	0.00	431.16
Ala <-> Ala.ext	R48 net	13.43	1.51	12.22	5.54
Ala <-> Ala.ext	R48 exch	5.58	145.54	52.54	4.60
Gln.ext -> Gln	R49	40.43	0.00	42.58	0.00
Glu <-> Glu.ext	R50 net	1.15	0.35	2.80	0.12
Glu <-> Glu.ext	R50 exch	1.85	1.33	1.79	1.91

Ser.ext <-> Ser	R51 net	3.79	2.37	5.02	0.74
Ser.ext <-> Ser	R51 exch	2.34	862.32	0.00	431.16
Gly <-> Gly.ext	R52 net	3.06	0.19	1.06	0.56
Gly <-> Gly.ext	R52 exch	281.24	119.33	0.00	431.16
Pro.ext <-> Pro	R53 net	-4.79	0.14	-6.34	0.51
Pro.ext <-> Pro	R53 exch	0.00	1.54	0.00	1.96
Val.ext -> Val	R54	2.11	0.73	3.64	0.57
Ile.ext -> Ile	R55	2.16	0.86	3.25	1.37
Leu.ext -> Leu	R56	2.10	0.67	4.76	0.77
Thr.ext -> Thr	R57	3.71	0.33	2.32	0.56
Phe.ext -> Phe	R58	0.68	0.30	1.33	0.44
Tyr.ext -> Tyr	R59	0.57	0.46	1.08	0.41
Met.ext -> Met	R60	0.43	0.34	0.83	0.11
Lys.ext -> Lys	R61	1.78	0.64	3.43	0.56
His.ext -> His	R62	0.45	0.12	0.86	0.22
Arg.ext <-> Arg	R63 net	-0.14	0.44	2.33	1.41
Arg.ext <-> Arg	R63 exch	456.39	862.32	154.28	431.16
Asp <-> OAA	R28 net	-2.37	0.30	-4.57	0.30
Asp <-> OAA	R28 exch	0.69	862.32	0.00	431.16
Cit -> OAA + AcCoA.c	R24	7.87	0.99	15.17	1.00
CO2 <-> CO2.ext	R45 net	125.84	32.06	127.17	431.62
CO2 <-> CO2.ext	R45 exch	0.00	31.29	0.00	431.61

Table 7.2: Metabolic flux analysis for mock- and virus-infected cells results using combined 13C-MFA of [1,2-^{13}C]glucose and [U-^{13}C]glutamine parallel labeling experiments at the growth arrest phase. Shown are the estimated net and exchange fluxes (nmol/10^{6}cell/h)

		GA Mock-infected		GA infected	
		nmol/10^{6}cells/h	SD	nmol/10^{6}cells/h	SD
G6P <-> F6P	R1 net	40.56	5.25	114.10	10.92
G6P <-> F6P	R1 exch	0.00	218.07	32704.00	308.50
F6P -> FBP	R2	41.38	1.73	114.08	3.64
FBP <-> DHAP + GAP	R3 net	41.38	1.73	114.08	3.64
FBP <-> DHAP + GAP	R3 exch	0.00	218.01	50288.00	308.31
DHAP <-> GAP	R4 net	41.17	1.73	113.38	3.64
DHAP <-> GAP	R4 exch	0.00	218.01	36112.00	308.31
GAP <-> 3PG	R5 net	82.97	1.70	227.44	3.66
GAP <-> 3PG	R5 exch	5203.90	218.01	1143.60	308.31
3PG <-> PEP	R6 net	81.40	0.80	223.88	1.93
3PG <-> PEP	R6 exch	7744.80	218.01	5927.60	308.31
PEP -> Pyr.c	R7	81.40	0.80	223.88	1.93

Pyr.c <-> Pyr.m	R44 net	-2.04	0.88	0.25	1.60
Pyr.c <-> Pyr.m	R44 exch	89.29	13.34	367.56	104.13
G6P -> P5P + CO2	R8	1.64	5.26	1.29	10.92
P5P + P5P <-> GAP + S7P	R9 net	0.41	1.76	-0.01	3.64
P5P + P5P <-> GAP + S7P	R9 exch	0.00	218.01	8932.20	308.33
S7P + GAP <-> E4P + F6P	R10 net	0.41	1.76	-0.01	3.64
S7P + GAP <-> E4P + F6P	R10 exch	2.91	0.76	14.74	3.92
E4P + P5P <-> GAP + F6P	R11 net	0.41	1.76	-0.01	3.64
E4P + P5P <-> GAP + F6P	R11 exch	6.10	218.01	0.00	308.33
Pyr.c <-> Lac	R12 net	80.76	1.74	216.80	4.41
Pyr.c <-> Lac	R12 exch	1407.00	218.02	31418.00	308.34
Pyr.c <-> Ala	R13 net	5.77	0.22	11.79	1.10
Pyr.c <-> Ala	R13 exch	0.00	329.16	0.00	847.88
Pyr.m -> AcCoA.m + CO2	R14	15.51	0.47	29.52	0.81
OAA + AcCoA.m -> Cit	R16	20.98	0.86	37.26	1.38
Cit <-> AKG + CO2	R17 net	16.60	0.94	22.90	1.60
Cit <-> AKG + CO2	R17 exch	0.00	0.70	0.00	1.23
AKG -> SucCoA + CO2	R18	35.07	1.05	53.69	1.83
SucCoA <-> Suc	R19 net	35.07	1.05	53.69	1.83
SucCoA <-> Suc	R19 exch	0.00	218.01	1752.00	308.31
Suc <-> Fum	R20 net	35.46	1.18	56.50	2.05
Suc <-> Fum	R20 exch	120.79	218.01	80.38	308.31
Fum <-> Mal	R21 net	35.46	1.22	56.50	2.15
Fum <-> Mal	R21 exch	27607.00	218.01	31727.00	308.31
Mal <-> OAA	R22 net	17.91	0.85	27.23	0.89
Mal <-> OAA	R22 exch	20013.00	218.01	90.31	308.31
Mal -> Pyr.m + CO2	R23	17.54	0.73	29.27	1.61
Pyr.m + CO2 -> OAA	R15	0.00	0.76	0.00	1.26
Gln -> Glu	R25	23.81	0.05	40.06	0.10
AKG <-> Glu	R26 net	-18.47	0.31	-30.78	0.60
AKG <-> Glu	R26 exch	184.82	31.32	445.07	139.53
Asn <-> Asp	R27 net	-0.50	0.05	-1.64	0.09
Asn <-> Asp	R27 exch	2.64	0.51	0.02	0.03
3PG -> Ser	R29	1.57	2.41	3.57	4.96
Ser -> Pyr.c	R30	3.09	2.35	4.95	4.92
Ser <-> Gly + C1	R31 net	0.42	0.16	1.20	0.26
Ser <-> Gly + C1	R31 exch	10.70	6.72	26.46	18.24
Glu <-> Pro	R32 net	4.27	0.15	6.17	0.22
Glu <-> Pro	R32 exch	201.30	30.55	332.54	42.10
Val + CO2 -> Suc + CO2 + CO2	R33	0.39	0.13	1.59	0.46
Ile + CO2 -> Suc + AcCoA.m + CO2	R34	0.00	0.25	1.06	0.12
Leu + CO2 -> AcCoA.m + AcCoA.m + AcCoA.m + CO2	R35	1.58	0.22	1.93	0.25
Thr -> AcCoA.m + Gly	R36	0.72	0.13	0.62	0.27

Phe -> Tyr	R37	0.05	0.07	0.39	0.21
Tyr -> Fum + AcCoA.m + AcCoA.m + CO2	R38	0.00	0.09	0.00	0.26
Met + Ser + CO2 -> Suc + Cys.snk + CO2 + C1	R39	0.00	0.11	0.17	0.13
Lys -> CO2 + CO2 + AcCoA.m + AcCoA.m	R40	0.01	0.20	0.14	0.42
His -> Glu + C1	R41	0.00	0.10	0.00	0.18
Arg -> Glu + Urea.snk	R42	0.02	5.61	0.09	0.98
Glu + CO2 -> Arg	R43	0.03	5.58	0.97	0.92
162.6*Ala + 104.6*Glu + 87.26*Gln + 17.34*Gly + 144.4*Ser + 154.5*Lys + 152.8*Leu + 87.8*Ile + 102.2*Arg + 127.9*Asp + 104.6*Thr + 112.7*Val + 37.4*Met + 59.35*Phe + 49.32*Tyr + 38.75*His + 84.82*Pro + 78.05*Asn + 80.22*G6P + 63.12*P5P + 65.09*C1 + 33.06*DHAP + 683.5*AcCoA.c -> Biomass	R64	0.00	0.00	0.01	0.00
Glc.ext -> G6P	R46	42.71	0.00	117.07	0.00
Lac <-> Lac.ext	R47 net	80.76	1.74	216.80	4.41
Lac <-> Lac.ext	R47 exch	0.00	218.01	0.00	308.31
Ala <-> Ala.ext	R48 net	4.73	0.20	8.37	1.09
Ala <-> Ala.ext	R48 exch	3.82	218.01	4.29	308.31
Gln.ext -> Gln	R49	24.37	0.00	41.89	0.00
Glu <-> Glu.ext	R50 net	0.40	0.12	0.02	0.05
Glu <-> Glu.ext	R50 exch	0.00	0.27	0.04	308.31
Ser.ext <-> Ser	R51 net	2.87	0.26	5.79	0.61
Ser.ext <-> Ser	R51 exch	0.00	218.01	0.00	308.31
Gly <-> Gly.ext	R52 net	-0.01	0.16	-1.92	0.31
Gly <-> Gly.ext	R52 exch	19.14	12.28	0.00	308.31
Pro.ext <-> Pro	R53 net	-3.72	0.15	-4.39	0.21
Pro.ext <-> Pro	R53 exch	0.00	0.74	0.00	1.08
Val.ext -> Val	R54	1.11	0.12	3.96	0.45
Ile.ext -> Ile	R55	0.56	0.25	2.90	0.07
Leu.ext -> Leu	R56	2.56	0.25	5.14	0.25
Thr.ext -> Thr	R57	1.39	0.12	2.82	0.28
Phe.ext -> Phe	R58	0.43	0.07	1.64	0.21
Tyr.ext -> Tyr	R59	0.27	0.03	0.65	0.14
Met.ext -> Met	R60	0.24	0.10	0.95	0.12
Lys.ext -> Lys	R61	1.00	0.20	3.38	0.47
His.ext -> His	R62	0.25	0.09	0.81	0.18
Arg.ext <-> Arg	R63 net	0.65	0.06	1.26	0.40
Arg.ext <-> Arg	R63 exch	0.00	218.01	4.39	308.31
Asp <-> OAA	R28 net	-1.32	0.12	-4.33	0.22
Asp <-> OAA	R28 exch	5897.90	218.01	0.01	308.31
Cit -> OAA + AcCoA.c	R24	4.38	0.40	14.36	0.75
CO2 <-> CO2.ext	R45 net	86.73	2.09	137.56	11.54

CO2 <-> CO2.ext	R45 exch	109.36	39.56	0.00	10.48

Annex 2

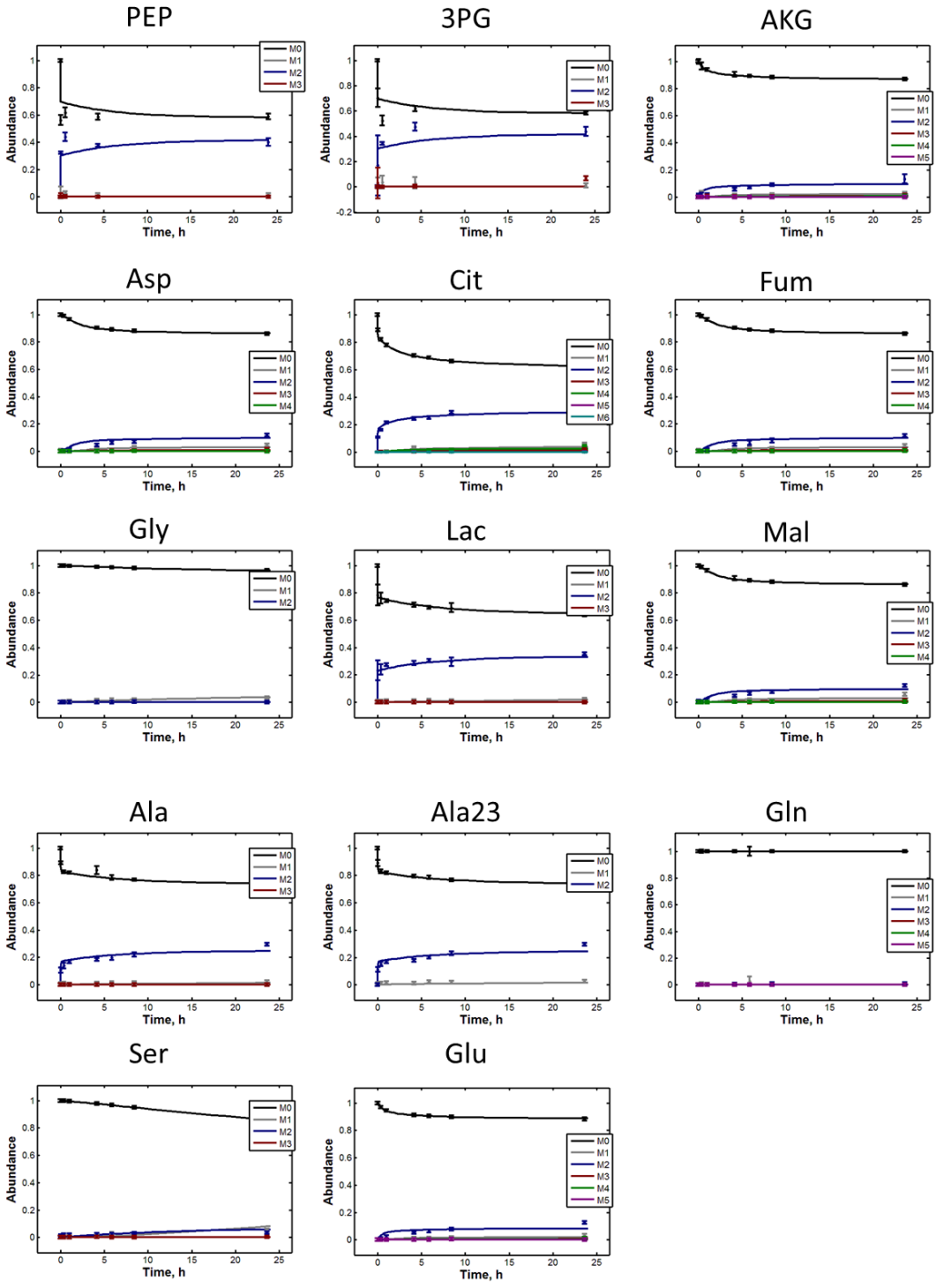

Figure 7.1: Intracellular ^{13}C-labelling dynamics during growth (mock infection) from [1,2-^{13}C]glucose. Symbols correspond to GC-MS measurements. Lines correspond to fitted MIDs from nonstationary ^{13}C-MFA flux estimation of parallel labelling experiments.

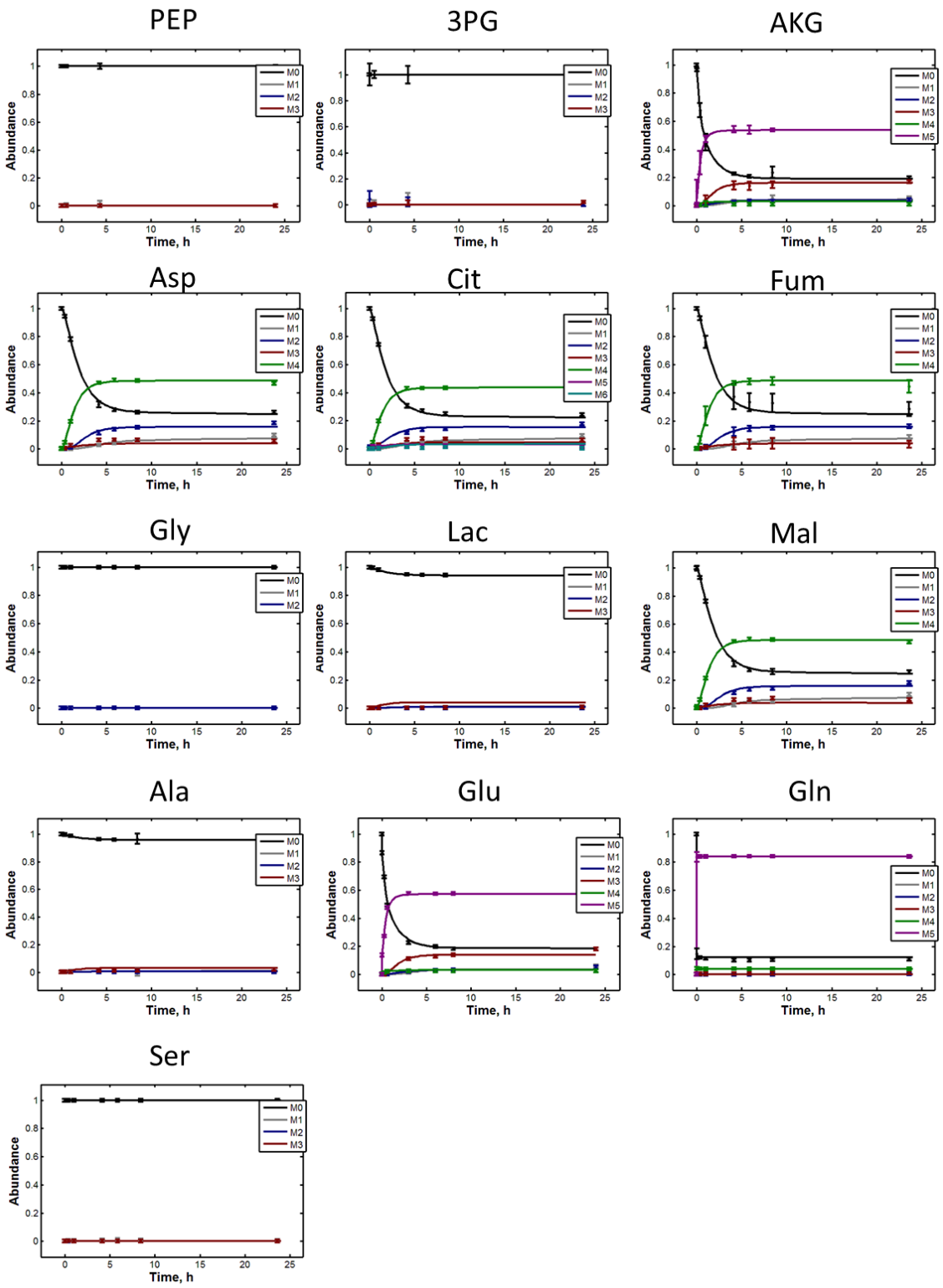

Figure 7.2: Intracellular ^{13}C labelling dynamics during growth (mock infection) from [U-13C]glutamine. Symbols correspond to GC-MS measurements. Lines correspond to fitted MIDs from nonstationary ^{13}C-MFA flux estimation of parallel labelling experiments.

Annex 3

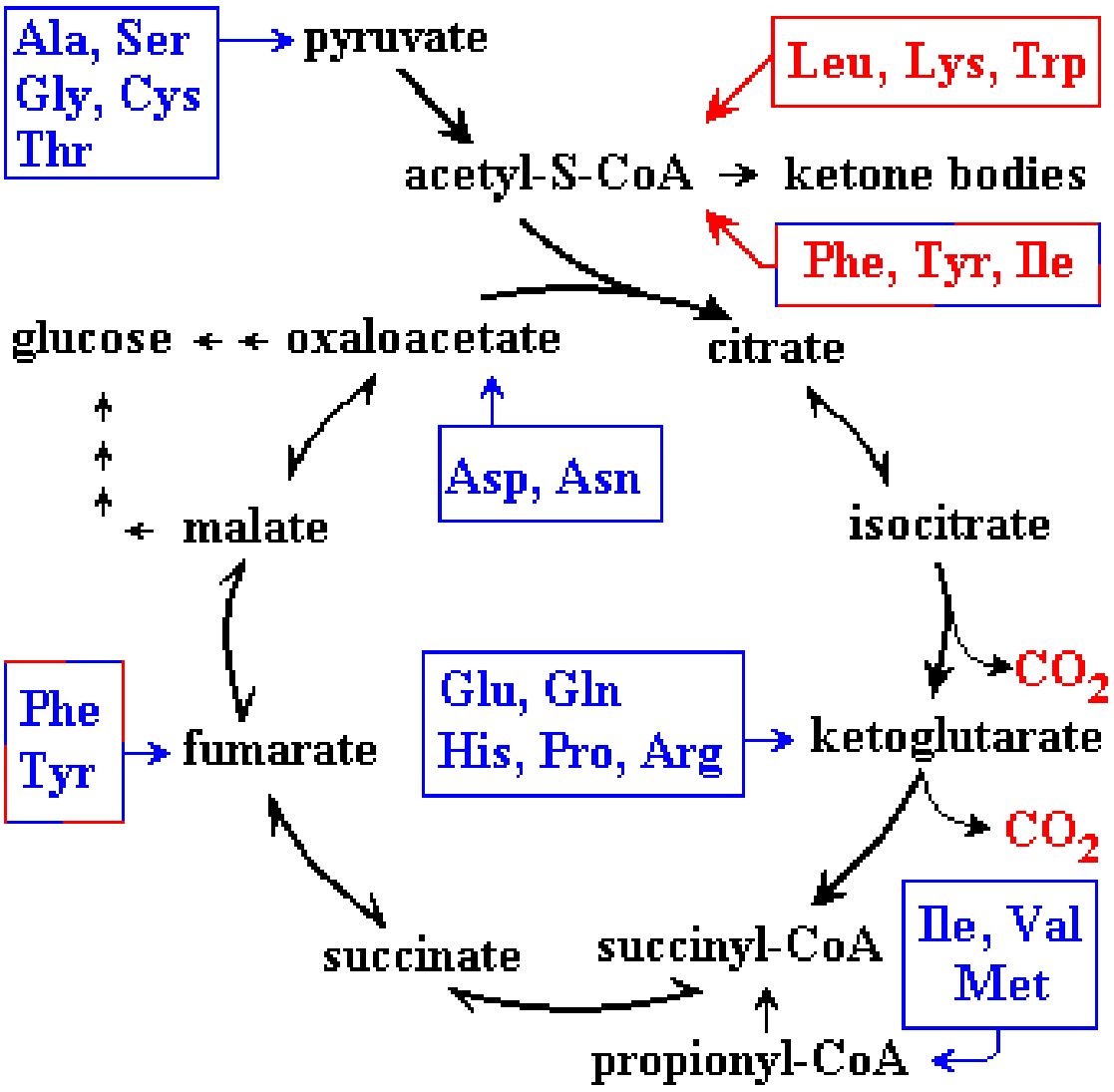

Figure 7.3: TCA cycle metabolism, with aminoacid, participating in formation of intermediates of the cycle.